INSTITUT FÜR BAUSTOFFE, MASSIVBAU UND BRANDSCHUTZ

MATERIALPRÜFANSTALT FÜR DAS BAUWESEN - MPA BRAUNSCHWEIG

iBMB

TU BRAUNSCHWEIG

Bericht

Früher Zwang in massigen Sohlplatten

em. Prof. Dr.-Ing. Dr.-Ing. E.h. F. S. Rostásy

Dipl.-Math. M. Krauß

Dr.-Ing. A. W. Gutsch

Forschungsprojekt der europäischen Gemeinschaft:

Brite Euram BE96-3843

IPACS - Improved Production of Advanced Concrete Structures

Heft 157 **BRAUNSCHWEIG** **2001**

ISBN 3 – 89288 – 138 – 3

Improved Production of Advanced Concrete Structures -IPACS

REPORT BE96-3843/2001:59-1

Engineering Models for the Assessment of Restraint of Slabs by Soil and Piles During Early Age of Concrete

Ferdinand S. Rostásy[1] *Matias Krauß*[2]
Alexander-W. Gutsch[3]

[1,2,3] *Institut für Baustoffe, Massivbau und Brandschutz, Technische Universität Braunschweig*

Published by
Department of Civil & Mining Engineering
Division of Structural Engineering

ISBN 91 - 89580 – 59 – 1 • 2001:59-1 • SE

LULEÅ UNIVERSITY OF TECHNOLOGY

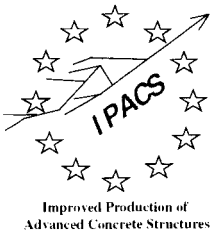

Engineering Models for the Assessment of Restraint of Slabs by Soil and Piles During Early Age of Concrete

Report N°: 2001:59-1

Author	**Ferdinand S. Rostásy[1]**	**f.rostasy@tu-bs.de**
Author	**Matias Krauß[2]**	**m.krauss@tu-bs.de**
Author	**Alexander-W. Gutsch[3]**	**a.gutsch@tu-bs.de**
Address[1,2,3]	**IBMB, TU Braunschweig** **Beethovenstraße 52** **38106 Braunschweig, Germany**	

Task/Subtask	**T 4**
	Brite EuRam Contract No. BRPR-CT97-0437
Project n°:	**Brite EuRam Proposal No. BE96-3843**
Project title:	**IPACS - IMPROVED PRODUCTION OF ADVANCED CONCRETE STRUCTURES**
Project co-ordinator:	**Betongindustri AB, Dr Mats Emborg**
Partners:	**Betongindustri AB** **Cementa AB** **Selmer ASA** **Technical University of Delft** **ENEL** **Technical University of Luleå** **NCC AB** **Skanska Teknik AB** **Technical University of Braunschweig** **Ismes** **Norwegian Public Roads Directorate** **Elkem AS** **Norcem AS** **Technical University of Trondheim**

Date of issue of this report: **November 1999**

Revised date: **December 2000**

Project funded by the European Community under the Industrial & Materials Technologies Programme (Brite-EuRam III)

IMPROVED PRODUCTION OF ADVANCED CONCRETE STRUCTURES - IPACS

Background
Research and practical experience show that the quality and lifetime of concrete structures largely depend on the curing conditions in the concrete's early life, as inadequate curing leads to malfunction and cracking. A major source of deleterious cracking already in the construction stage is the occurrence of stresses in the hardening concrete due to restrained volume change related to hydration temperatures and shrinkage phenomena. It is thus of utmost importance, especially regarding new high performance concrete, that the proper execution conditions are maintained throughout the construction period by avoiding the premature cracking.

Objective of project
Main goal of IPACS is to evaluate, integrate and extend the existing knowledge about early age concrete crack prediction in engineering practice yielding the following benefits:
Contractors and designers will have new and more reliable engineering instruments enabling them to predict and to optimise the technical effect and cost of alternative designs and execution procedures - all in the process of fulfilling the quality requirements set up by the owners or the community (codes).
Reduced costs because of the present tendency to specify costly but unnecessarily rigorous crack criteria will be avoided. Owners will have access to improved means of specifying and controlling desired quality requirements regarding serviceability and service life of their structures.
Reduced maintenance costs and increase of service lifetime.

Main tasks and investigations in IPACS and output from the project:
Hydration and volume changes – To acquire data for the modelling of properties of a number of currently used concrete types.
Mechanical properties - Testing and modelling of mechanical properties.
Behaviour of structures - Computer modelling of structural behaviour.
Field tests - To check and improve the models of the previous tasks in full-scale tests.
Expert System.

The *Expert System* synthesises the results from the project into a robust engineering tool for planning and control of the production of concrete structures. It contains modules of varying simplicity, which can be used in all the phases of a construction project from pre-design to maintenance

Project Partners:
See earlier page

Project Co-ordinator:
Dr Mats Emborg – Betongindustri AB (Heidelberger Zement North Europe) (SE)
Dr Hans-Erik Gram/Mr Mats Öberg – Cementa AB (Heidelberger Zement North Europe) (SE)

Disclaimer

Editorial/production supervision:	Prof. Lennart Elfgren
Cover design:	Hans Hedlund
Prepress material:	By report authors
Printed and published by	Luleå University of Technology, Department of Civil and Mining Engineering, Division of Structural Engineering SE-971 87 Luleå, Sweden

CONTENTS

NOTATIONS AND SYMBOLS

Roman Capital Letters

A	aggregate content [kg/m^3]
A_c	cross-section [m^2]
B	total binder content [kg/m^3]
C	cement content [kg/m^3]
C_{cr}	crack ratio
E_a	activation energy
E_{ct}	Young's modulus in tension
E	mean E-modulus
E_e	mean effective E-modulus
E_v	activation energy of visco-elastic deformation
FA	fly-ash content [kg/m^3]
G_F	fracture energy
I_{cr}	thermal cracking index
M	bending moment
N	normal force
P_{1c}, P_{2c}	creep parameter
P_{1r}, P_{2r}	relaxation parameter
SF	content of silica [M-% of C]
SL	content of ground blast furnace slag [M-% of C]
T_{c0}	temperature of fresh concrete
T_{a0}	mean daily air temperature
V	coefficient of variation

Roman Lower Case Letters

a	distance
b	width, breadth
c	specific heat
cal	calculated
c_1	parameter of degree of hydration [-]
d	height, thickness
f	strength of concrete
f_c	mean compressive strength
f_{ct}	mean axial tensile strength
f_{cte}	mean effective tensile strength
f_{cts}	mean splitting tensile strength
h	height, thickness
j	general coordinate
ℓ	length
ℓ_{pr}	width of fracture process zone
obs	observed
meas	measured
t	age, general
t_1	age at on-set of strength formation ($\cong \alpha_0$)
t_c	normalizer, 1 [h]
t_e	effective age
t_{e0}	effective age at on-set of strength formation ($\cong \alpha_0$)
t_i	age at on-set of strain step i
t_k	parameter of degree of hydration [h]
t_n	age

t_{N1}	first zero-stress age ($\cong t_1$)
t_{N2}	second zero-stress age
v	relative displacement
w	crack opening
x, y, z	coordinates

Greek letters

α	degree of hydration, general
α_0	degree of hydration at on-set of strength formation
α_i	degree of hydration at age t_i
α_T	linear thermal expansion coefficient
Δ	difference, differential
δ	integer
ε	strain, general
ε_{as}	autogenous shrinkage strain
ε_{cr}	creep strain
ε_{ctu}	strain at f_{ct}
ε_{el}	elastic strain
ε_e	effective strain
ε_{fr}	free strain
η	integer
φ	creep function
κ	curvature
λ	coefficient of heat conduction
μ_f	friction coefficient
ρ	density, general; coefficient of relaxation
ρ_c	density of concrete
τ	shear stress
ω_e	reduction factor of tensile strength
ψ	relaxation function

Subscripts

0	zero
A	aggregate
ad	adiabatic
as	autogenous shrinkage
C	cement
c	concrete, compression
cr	related to cracking
crit	critical
e	effective
el	elastic, elevated
FA	fly-ash
i	on-set of strain step at t_i
k	characteristic
m	mean
p	probability
pot	potential
r	micro-cracking
R	resultant, resistance
SF	silica fume
sh	drying shrinkage
SL	ground blast furnace slag
T	thermal
w	water

x, y, z coordinates

Conversions

1 J (Joule)	= 1 Ws
1 kJ	= $2.778 \cdot 10^{-4}$ kWh
1 cal (calory)	= 4.186 J
1 kcal	= 4.186 kJ
860 kcal	= 1 kWh
1 kW	= 860 kcal/h

PREFACE

Slabs cast on ground or additionally supported by piles are subjected to restraint. The motor of restraint are the free thermal deformations in conjunction with autogenous shrinkage. Such restraint may lead to cracks at early age. Practice deals with restraint in widely differing ways, especially with respect of the assumptions regarding the type and magnitude of restraint. Usually, the present methods and computational softwares do not accurately take the young concrete's rapid hardening into account.

It is the aim of this report to present the usual models for the assessment of restraint, to validate and modify them. Improved models have to be developed. In the focus of this report are engineering models with adequate accuracy to assess the restraint in the phases of pre-design, design and execution.

This report was written in conjunction of iBMB's partnership in the Brite Euram Project IPACS (Improved Production of Advanced Concrete Structures). The comments and advise of partners in the EC research project IPACS is greatly appreciated. The authors are also indebted for the valuable discussions with Prof. W. Rodatz, Institute of Geotechnical Engineering and Prof. H. Ahrens, Institute for Structural Analysis, both from the Technical University of Braunschweig. Cordial acknowledgement is due to Claudia Gerdau, Ria Köser and Tanja Kohl for their excellent drawing work and untiring engagement.

F. S. Rostásy

1 INTRODUCTION

1.1 Parameters of Restraint and Stiffness

A slab cast on ground is more or less restrained. Restraint will commence in the early age of concrete and may continue also into the service life of structure. Restraint is caused by the simultaneous occurrence of

- free thermal, autogenous and hygral volume change of concrete and by the
- hindrance of these volume changes due to the interaction of the slab with the soil.

The magnitude of restraint can be expressed as a function of the stiffness of soil and slab. The main parameters of the stiffness are:

Parameters of soil

- type of soil
- stiffness of soil, E_s
- angle of shear friction φ
- cohesion c
- compactness D (bedding density)
- grain size, uniformity of soil
- water content
- stratification etc.

Parameters of slab

- dimensions d_c, b_c, ℓ
- dead and live loads
- mechanical properties of concrete as functions of age etc.
- volume changes
- depth of slab in soil etc.

1.2 Free Deformations and Restraint

Restraint is associated with stresses in the slab and may cause cracks. Because the free strains in the hardening concrete member are not uniformly distributed over the slab's depth d_c, the following components of deformation have to be distinguished with respect to their contribution to stresses (Fig. 1.1):

- Mean free strain ε_{0m} and free curvature κ_0 are the linear components, which lead to the restraint actions N and M.

- The differences between the strains $\varepsilon_0(z, t)$ and the linear components $\text{lin}\,\varepsilon_0(z, t)$ - described by strain compensation plane - are associated with eigenstresses. Eigenstresses self-equilibrate and hence do not contribute to N and M.

For very young concrete the separate assessment of stresses caused by these deformational components is inadmissible because of the concrete's varying visco-elastic behaviour over the depth d_c. As hydration progresses, the separate assessment may lead to reasonably correct restraint actions. In practice, the non-linear strain components and stresses are often neglected, only stresses caused by the actions N and M are considered. Such procedure may underestimate the crack risk. It should be noted that for early age concrete, drying shrinkage may be disregarded as cause for restraint stresses and cracks. However, at later age drying shrinkage may become an important cause for cracking. Hence, one should keep in mind that the early age of concrete describes only a segment of the structure's life.

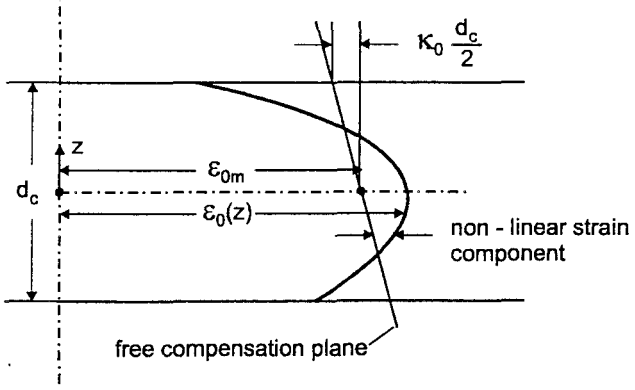

Fig. 1.1 Components of Free Deformations Across Slab's Depth

1.3 Basic Approaches for the Description of Interaction

The interaction between a foundation slab and the ground is dealt with in numerous publications. In most of the latter, emphasis is put on the structural design of the slab, loaded by its self-weight and the actions of the rising structure [8]. In this report, the early age of the slab is in the focus. In this period, it is pre-supposed that only the slab's self-weight is acting as ground pressure. This ground pressure will, however, be super-imposed by restraint reaction stresses caused by the free deformation of the hardening concrete. This kind of interaction has also been dealt with though to a lesser extent than the load-induced interaction [5, 7, 9, 10]. Especially, the effects of the rapidly changing mechanical properties of young concrete have not yet been taken into consideration satisfactorily.

The approaches to describe interaction can be generally categorized with respect to the material laws of concrete and soil as well as to the mode of coupling of slab to soil. The restraint of the slab's free axial deformation is commonly described by shear-friction or others contact elements: horizontal interaction.

The restraint of the slab's free curvature can be described in several ways: vertical interaction. In practice, often either the stiffness modulus or the subgrade reaction modulus method is used. Thereby, only the restraint moments can be assessed.

The separate treatment of axial and bending restraint and the superposition of reactions resp. are mechanically unsound. In long slabs there exists an inner region in which the slab is elastically coupled - without differential slip - to the ground. The restraint reactions can be assessed by the so-called multi-layer method, which renders simultaneously the axial and bending restraint reaction. By this method the slab and soil over its interactive depth form a package for which the plane strain condition is assumed. However, this method also exhibits certain shortcomings. Therefore in this report a rational combination of methods will be developed.

It is the aim of this report not only to present the existing and new engineering models but also to validate their suitability with respect to interaction. In this report, reinforced slabs with a thickness $d_c > 50$ cm are treated. Slabs on rock are not dealt with in this report.

Axial restraint can be mitigated by sliding layers between slab and soil. Restraint may be enhanced by stiff piles impeding the slab's free deformations etc.

2 GEOMETRY OF SLAB ON SOIL AND FREE DEFORMATIONS

It is pre-supposed that the interaction of a slab with the soil can be idealized by a linear cut-out from the large rectangular slab dc x b x ℓ. Fig. 2.1 shows a particular solution with a sliding layer (e.g. bituminous layer, PE-foils etc.) to break or to mitigate the friction interaction with subsoil. Commonly, a 10 to 20 cm thick compacted gravel layer (capillary breaker) and a about 5 to 10 cm thick blinding of concrete (for levelling and clean placement of reinforcement) are placed on the natural soil. Emphasis is put here on the most common solution in practice in which a sliding layer is omitted. In this case, the slab is cast on the blinding. In a later section, the efficiency of sliding layers will be discussed.

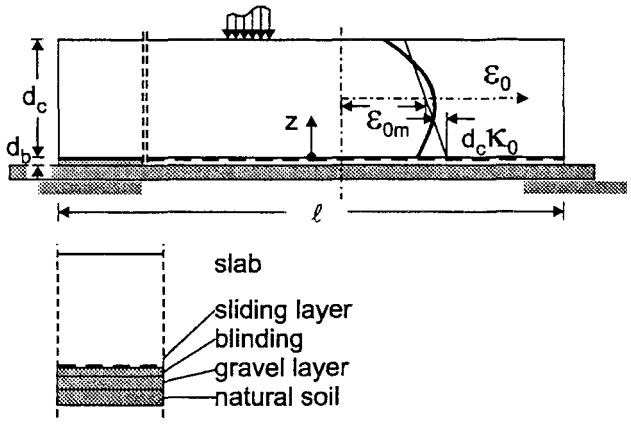

Fig. 2.1: Geometry of Slab and Free Deformations

In Fig. 2.1 the free deformations ε_0 (z, t) of slab are also depicted. Their linear components ε_{0m} (mean free strain) and κ_0 (free curvature) lead to the expansion and contraction of concrete as well as to the curvature of varying sign of slab. The free deformations will be impeded by the dead weight of slab and interaction with soil. More to these aspects can be found in section 4 and 5.

3 MECHANICAL BEHAVIOUR OF SOIL WITH RESPECT TO INTERACTION

3.1 Problem and Intentions

For the assessment of interaction between slab and ground the relevant mechanical properties of cohesive and non-cohesive soil must be formulated. Within the framework of this report, natural soils with a stiffness modulus $E_s \leq 200$ N/mm^2 are dealt with. Soil is regarded as an elastic, non-tension material under shear and compressive stress. Material behaviour of soil will be modelled. Besides that, the basic engineering models of interaction will be outlined.

3.2 Shear Behaviour of Soils

Horizontal interaction between slab and soil is influenced by the response of soil under the combination of shear stress τ and normal stress σ_n. Internal friction forces and deformations arise. Frictional sliding, particle re-orientation and dilatancy are activated.

In **non-cohesive soil** (cohesion c = 0; sand, gravel, natural crushed stone) the following parameters determine the shear-strength and deformation:

- compactness D
- coefficient of uniformity $U = d_{gr60\%} / d_{gr10\%}$
- grain size d_{gr} and shape of grains
- normal stress σ_n

The compactness D expresses the difference between maximum and the actual natural pore volume of soil. It is hence a measure of the natural density of soil (D = 0.3: loose; D = 0.50: medium; D = 0.70: dense). Fig. 3.1 schematically shows the relationship between the shear-stress and the local displacement. The upper line is valid for a high, the lower one for a low compactness D (bedding density). The shear-strength τ_{shu} can be expressed by

$$\tau_{shu} = \sigma_n \tan \varphi \qquad (3.1)$$

with σ_n, normal pressure and φ, angle of internal friction of soil.

Table 3.1 contains data on soil parameters from different sources [6].

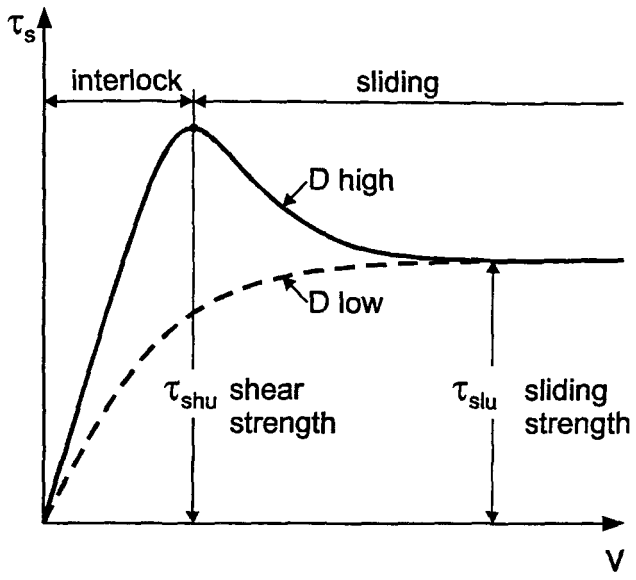

Fig. 3.1: Relationship Between Shear-Stress τ_s and Displacement v of Soil (Schematic)

For **cohesive soil** (clay, loam, boulder clay, silt etc.) the following soil parameters are important:

- consistency
- water content
- grain size distribution
- over-consolidation etc.

The shear behaviour of soil as shown in Fig. 3.1 is also valid for cohesive soil. In Fig. 3.2 the relationship τ_{shu} vs. σ_n is plotted. It can be expressed by

$$\tau_{shu} = c + \sigma_n \tan \varphi \qquad (3.2)$$

with c, cohesion. Table 3.2 contains soil data from various sources.

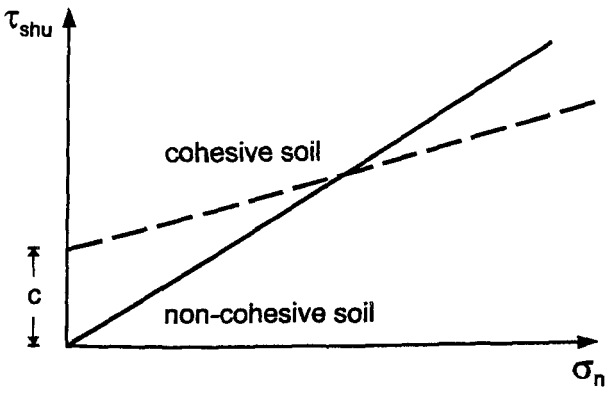

Fig. 3.2: Shear Strength of Soil vs. Normal Stress for Cohesive and Non-Cohesive Soil

Table 3.1: Properties of Non-Cohesive Soils (Mean Approximate Values)

type of soil	density of moist soil ρ_{sm}	buoyant density of soil ρ_{sb}	angle of internal friction φ	constrained (stiffness) modulus E_s
[-]	[kN/m^3]	[kN/m^3]	[°]	[MN/m^2]
sand, loose, round	18	10	30	20 - 50
sand, loose, angular	18	10	32,5	40 - 80
sand, dense, round	19	11	32,5	50 - 100
sand, dense, angular	19	11	35	80 - 150
sand, very dense, angular	19	11	37,5	150 - 250
gravel without sand	16	10	37,5	100 - 200
natural crushed stone	18	11	40	150 - 300

Table 3.2: Properties of Cohesive Soils (Mean Approximate Values)

type of soil	density of wet soil ρ_{sm}	buoyant density of soil ρ_{sb}	angle of internal friction φ	cohesion c	constrained (stiffness) modulus E_s
[-]	[kN/m^3]	[kN/m^3]	[°]	[kN/m^2]	[MN/m^2]
clay, semi-solid	19	9	25	25	5 - 10
clay, stiff	18	8	20	20	2,5 - 5
clay, soft	17	7	17,5	10	1 - 2,5
boulder clay	22	12	30	25	30 - 100
loam, semi-solid	21	11	27,5	10	5 - 20
loam, soft	19	9	27,5	-	4 - 8
silty soil	18	8	27,5	-	3 - 10

3.3 Model of Shear-Friction Interaction for Non-Cohesive Soil

Comprehensive sliding tests with concrete slabs on various substrates by [4], [5] and others show that the base friction behaviour, Fig. 3.3 a, follows the relationship depicted in Fig. 3.1. In [4] an analytical relationship τ_{fr} - v was developed, Fig. 3.3 a. Besides the angle of internal friction, other parameters such as the roughness of the intermediate contact plane, compactness, coefficient of uniformity etc. influence the behaviour. The maximum shear stress can be expressed by

$$\tau_{fu} = \mu_f \cdot \sigma_n \tag{3.3}$$

with μ_f, friction coefficient; σ_n, normal pressure. It was found that the friction coefficient exceeds tan φ:

$$\mu_f = f\,(U, D, \sigma_n \ldots) \geq \tan \varphi. \tag{3.4}$$

For the slab on ground and during early age of concrete, the normal stress is caused by the slab's dead weight:

$$\sigma_n = d_c\, \rho_c \quad [kN/m^2] \tag{3.5}$$

with ρ_c, density of concrete ($\approx$ 25 kN/m^3). For sand 0/2 mm, Eq. (3.4) can approximated by

$$\mu_f \approx 0.6 + 0.56\, D - 0.11\, \ln (\sigma_n / 100) \tag{3.6}$$

and for a sand-gravel soil 0/16 mm by

$$\mu_f \approx 0.7 + 0.56\, D - 0.11\, \ln (\sigma_n / 100). \tag{3.7}$$

In Table 3.3 values of the friction coefficient - calculated with Eq. (3.6) and (3.7) - for a 1 m thick slab on the before mentioned soils are presented. These values can be compared with internal friction of the soil. The value tan φ of internal friction of sand 0/2 mm is in the range of 0.58 to 0.77 and for sandy gravel about 0.77. It should be pointed out, that the pressure σ_n may increase as construction progresses.

Table 3.3 Approximate Values of Friction Coefficient for a 1 m Thick Slab on Non-Cohesive Soils

relative density	compactness D	proctor density	sand μ_f	sand-gravel μ_f
[-]	[-]	[%]	[-]	[-]
low	≥ 0.3	≥ 95	0.9	1.0
dense	≥ 0.5	≥ 98	1.0	1.1
medium	≥ 0.45	≥ 98	0.9	1.0
very dense	≥ 0.65	≥ 100	1.1	1.2

It is believed that values of μ_f - calculated with Eq. (3.6) and (3.7) - represent upper boundary values (sup μ_f) which should be used when assessing axial restraint of slab.

The Eq. (3.6) and (3.7) pre-suppose that the deformations v and sliding occur in the soil. If however a layer of compacted gravel or sand-gravel is placed on the soil, the relative displacement of slab may occur in this layer and not in the natural soil. This mechanism will happen if the compactness $D_{layer} < D_{soil}$.

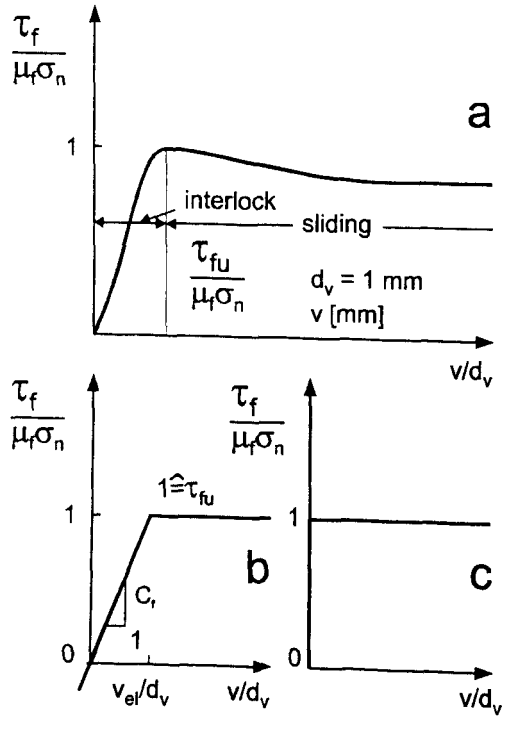

Fig. 3.3: Normalized Relationship of Shear-Friction Stress vs. Relative Displacement and Idealized Models for Non-Cohesive Soil

For the assessment of restraint, the τ_f-v-relationship of Fig. 3.3 a can be simplified. Fig. 3.3 b shows an elasto-plastic model. The elastic branch was described in [7]:

$$\tau_f = \sqrt{D}\mu_f \cdot \sigma_n \frac{v}{d_v} \leq \tau_{fu} \tag{3.8}$$

with the slope C_f in MN/m^3 :

$$C_f = \frac{\sqrt{D}}{d_v}\mu_f \sigma_n \tag{3.9}$$

with σ_n in MN/m^3 and $d_V = 0.001$ m. For sand-gravel soil the following values for C_f $[MN/m^3]$ dependent on the soil's density are reasonable: 13 d_c (low), 16 d_c (medium) and 19 d_c (high); d_C in m.

C_f can be interpreted as the stiffness of a horizontal spring or as a shear modulus. Elastic behaviour ends at displacement

$$v_{el} = d_v / \sqrt{D} \quad [mm], \tag{3.10}$$

with $d_v = 1$ mm. If $v > v_{el}$, sliding motion occurs. In long slabs, a region around the axis of symmetry may not perform sliding motion. Elastic interlock prevails there. Fig. 3.3 c shows the rigid-plastic model, which represents the simplest approach.

3.4 Model of Shear Friction Interaction for Cohesive Soil

The relationship for the shear-strength of soil is given by Eq. (3.2), viz. Fig. 3.1 and Fig. 3.2. There is little information to be found in literature as to shear-friction interaction of slabs with cohesive soil. It is proposed to proceed as for non-cohesive soil:

$$\tau_{fu} = c + \mu_f \sigma_n \tag{3.11}$$

with c, cohesion, Table 2; μ_f as described by Eq. (3.6) and (3.7). It must be mentioned that the density of cohesive soil is measured in-situ in different ways as for non-cohesive soil (e.g. penetration tests). The elasto-plastic description of the relationship τ_f - v in the elastic branch is:

$$\tau_f = c + \sqrt{D}\mu_f \cdot \sigma_n \frac{v}{d_v} \leq \tau_{fu} \tag{3.12}$$

for $v \leq v_{el} = d_v / \sqrt{D}$.

If the slip v exceeds v_{el}, Eq. (3.11) is valid. If a sand or sand-gravel blinding is placed on soil, then the relevant resistance has to be determined by comparative calculation with Eq. (3.8) and (3.11).

3.5 Models of Elastic Bedding of Slab on Soil

Besides complex models several engineering approaches have been developed to assess the bending restraint of a slab on ground. These approaches comprise the stiffness modulus method and the subgrade reaction modulus method, which are widely applied and for which commercial software exists. In addition to these common methods, the so-called three-layer method has been developed. All these methods take the deformability of soil over an interacting depth d_S into account. For the sake of simplicity, the soil is regarded as an elastic material. This is a conservative assumption, because the inclusion of time-dependent deformation of soil leads to the relaxation of soil stresses and hence to a lower restraint of slab.

The above-mentioned engineering methods are here briefly described. It is often argued that the stiffness modulus method is physically superior to the less complex subgrade reaction modulus method. In view of the numerous uncertainties in the models and material parameters it is acceptable to opt for the subgrade reaction modulus method.

- **Subgrade reaction modulus method**

Thereby, the compressibility of soil below the slab and over the depth d_s are modelled by elastic springs as shown in Fig. 3.4. In the spring constant, called modulus of subgrade reaction SRM, the elasticity of soil and the depth d_s are incorporated.

The modulus of subgrade reaction is defined by

$$k_s = \frac{\sigma_n}{s}, \tag{3.13}$$

with σ_n, ground pressure and s, mean settlement, both directly below slab. The mean settlement is expressed by

$$s = \frac{\sigma_n\, b}{E_S} \cdot f = \frac{\sigma_n\, d_S}{E_S} \cdot f\, \frac{b}{d_S}. \tag{3.14}$$

By inserting Eq. (3.13) into Eq. (3.12) we obtain

$$k_s = \frac{E_S}{b\, f}, \tag{3.15}$$

with E_s, mean stiffness modulus of soil layer d_s (viz. Table 3.2 and Table 3.3); b, breadth of slab with $b \leq \ell$; f [-], parameter dependent on the ratios d_S/b and ℓ/b. Fig. 3.5 shows the dependence of f on certain values of ℓ/b and on d_s/b. For other values reference is made to [1].

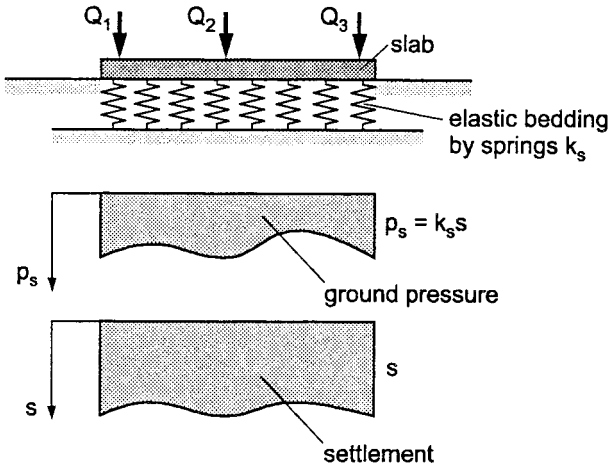

Fig. 3.4: Method of Subgrade Reaction Modulus

Returning to Eq. (3.13), the settlement can be interpreted as vertical deformation of the soil column with the height d_s with $f(\ell/b, d_s/b)$ being a correction factor. In Fig. 3.4 the dependence of the modulus k_s for e.g. the depth d_s = 10 m is shown for the several values of E_s and ℓ/b. The lower E_s, the lesser the influence of ℓ and ℓ/b.

For the determination of the subgrade reaction modulus k_s in the pre-design phase, appropriate values of E_s and d_s must be assumed. The parameter f is then - for given dimensions of slab ℓ and b - determined from graphs (e.g. [1]). For more concise investigations - e.g. in the design phase with contract awarded etc. - E_s and d_s can be based on test results of soil mechanical investigations.

The modulus of subgrade reaction is not a true material property of ground and is connected with several uncertainties. If its determination can not be based on the results of preceding geotechnical investigations, it will be a rather unprecise value. It was however found that this inexactness does not significantly influence the restraint actions. More to this will follow in chapter 5.

With the subgrade reaction modulus method only the restraint moments dependent on slab's length and several other parameters can be derived. The axial restraint force must be independently calculated with the shear friction method and be superimposed. The taking into account of aging and visco-elasticity of young concrete is difficult. In contrast to this, bending and axial restraint of slab as well as the physical non-linearity of concrete can be simultaneously taken into consideration with the so-called three-layer method.

- **Three-layer method TLM**

This method pre-supposes that the inner region of slab - on both sides of axis of symmetry - may be elastically interlocked with the soil which interacts over an effective depth d_S of soil with the slab. Slab, blinding and soil layer form a three-layer system which is treated with the postulate of "plane sections remain plane". Consequently, neither shear stresses nor relative displacements occur in the inner region. If the mean free strain ε_{0m} is large enough, the sliding shear strength τ_{fu} of soil may be overcome in the outer regions of slab (ends of slab). Consequently, the length of the elastically blocked zone must be known in order to combine the TLM with the shear friction method and to develop an physically overall acceptable depiction of restraint. More to this will follow in section 5.

- **Deformations and support conditions**

In Fig. 3.7 the free deformations of slab are depicted. During heating-up caused by hydration the slab tends to expand. The expansion phase is then followed by the contraction phase in course of cooling. The free curvature κ_0 is for slabs on ground generally negative. The slab, hence, has the tendency to curl-up at ends. Due to restraint, the residual (i.e. final) deformations commonly fall below the free deformations because the latter will be more or less impeded by the deformations caused by the restraint actions.

The residual deformations and eventual bending cracks are schematically shown by Fig. 3.8. Restraint is highest in the region around the axis of symmetry. Depending on length and depth of slab and stiffness modulus of soil etc. the slab's end may lift off from ground.

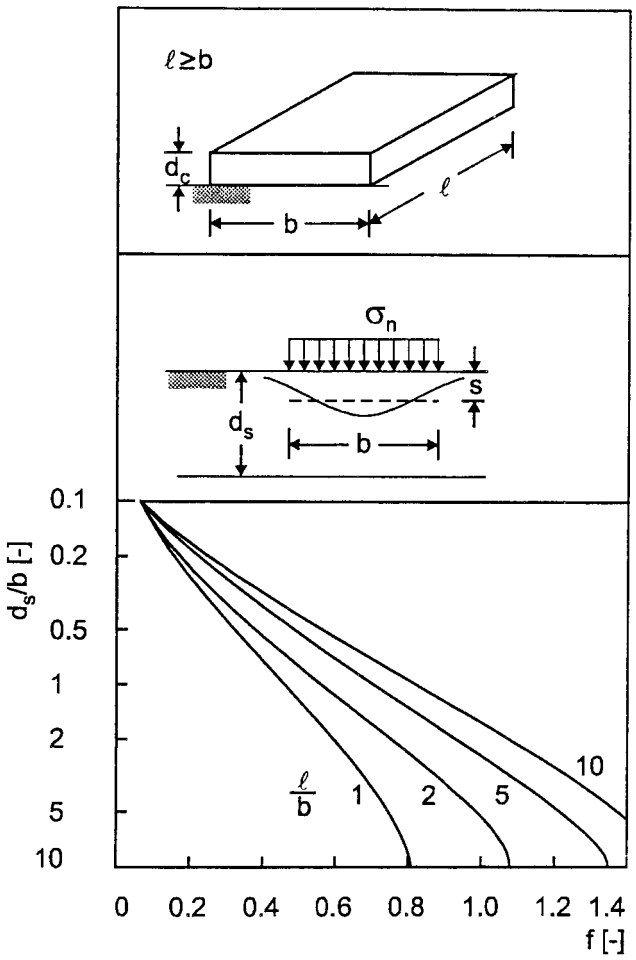

Fig. 3.5: Dependence of the Parameter f of the Modulus of Subgrade Reaction on the Ratios d_s/b and ℓ/b

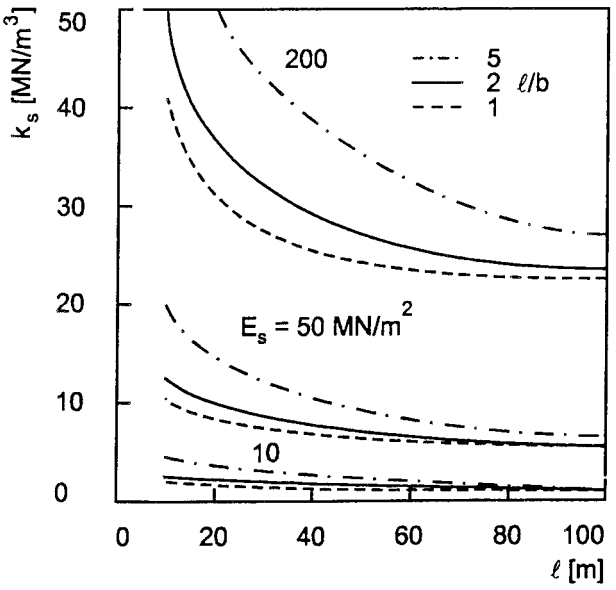

Fig. 3.6: Dependence of Modulus of Subgrade Reaction on Length of Slab, Stiffness Modulus of Soil and on Ratio ℓ/b for Depth d_s = 10 m

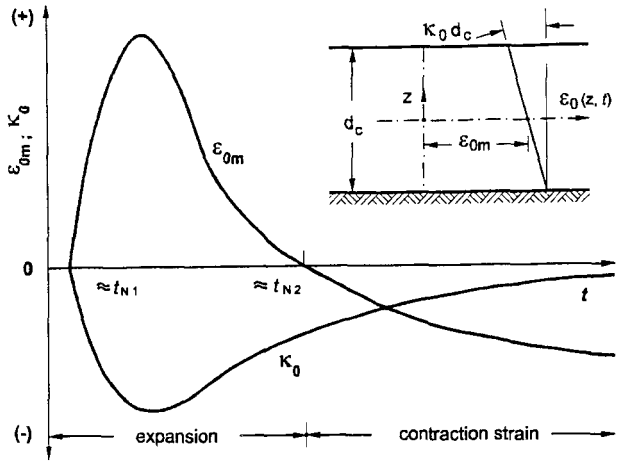

Fig. 3.7: Free Deformations of Slab on Ground During Hardening of Concrete

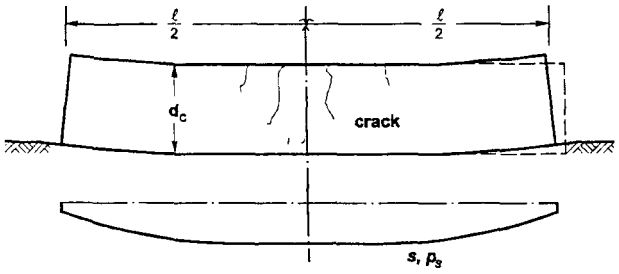

Fig. 3.8: Deformations and Support Conditions of Slab on Ground Without Up-Lift at Ends

4 ENGINEERING MODELS FOR AXIAL RESTRAINT

4.1 Intentions and Models

In this section several engineering models for the assessment of the axial restraint force are presented, discussed and improved [5, 7, 9]. These models are approximate solutions of the complex interaction with ground because of the following reasons. They only render the axial force and mean stress, resp. The non-linear, age-dependent restraint stress $\sigma(z,t)$ can not be derived by this method. The restraint force is pre-supposedly caused by the hindrance of the mean free strain $\varepsilon_{0m}(t)$ alone. The influence of curvature is suppressed (e.g. up-lift at ends). Concrete is assumed to be a quasi-elastic material. Its stiffness can be described by the mean effective elastic modulus E_e over the slab's depth d_c in order to take into account the aging and visco-elasticity of concrete. With the effective modulus E_e the relaxation of concrete can be approximately taken into account. Its determination will be shown in sec. 5.

The horizontal interaction with the ground will be described by the elasto-plastic shear stress-displacement model of Fig. 3.3 b. Because this model does not take the ground's elastic compliance over an interacting depth into account, the overall interaction is improved by the TLM. The cut-out from slab with the width b_c = 1 m is treated.

4.2 Distribution of Shear Stress, Displacement and Normal Force

In Fig. 4.1 the general dependence of the shear stress and restraint force N along the slab's half-length. Three zones of horizontal interaction with the ground can be distinguished.

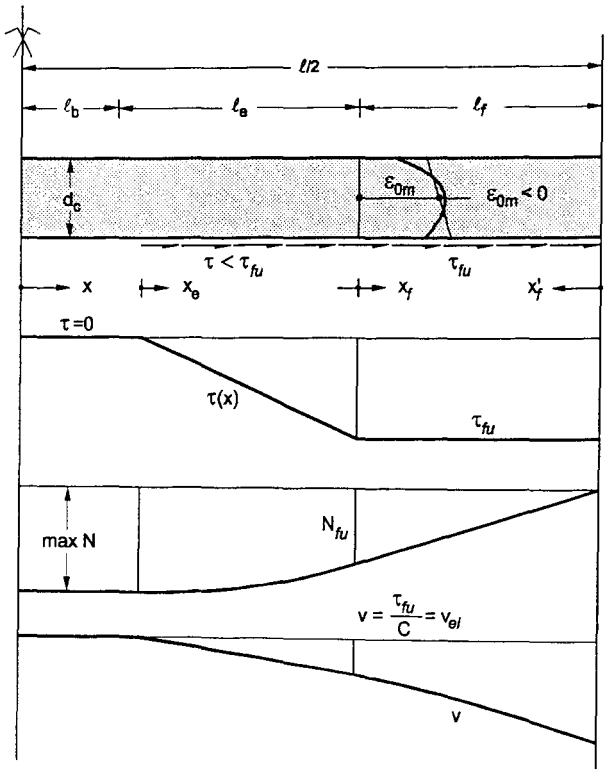

Fig. 4.1: Distribution of Shear Stress, Displacement and Axial Restraint Force of Slab on Ground

- **zone ℓ_b at axis of symmetry**

It is pre-supposed that slab and ground are in this zone - on both sides of the axis of symmetry - totally elastically coupled. Slab, blinding and ground act as a three-layer system (TLM) under the condition of plane strains. The axial restraint force is within ℓ_b constant. Shear stresses do not exist. This inner region of $\pm\ell_b$ is especially prone to cracking. Provided the maximum restraint force has been determined by the TLM, section 4.4, then the maximum degree of axial restraint R_{ae} is known:

$$R_{ae} = \frac{\max N}{N_0},\ 0 \le R_{ae} \le 0 \tag{4.1}$$

with N_0, force of total restraint:

$$N_0 = -\varepsilon_{0m}\, E_e\, d_c. \tag{4.2}$$

With that, we obtain the maximum restraint force at x = 0:

$$\max N = -\varepsilon_{0m}\, E_e\, d_c\, R_{ae}. \tag{4.3}$$

It should not be concealed that the length ℓ_b can not be trivially determined. It will however be shown that this fact does not represent a stumbling block for further deliberation.

- **zone ℓ_f of frictional sliding at slab's ends**

As the axial strain ε_{0m} increases, the sliding shear strength τ_{fu}, viz. Fig. 3.3 b, will be reached at the ends of slab. The frictional restraint force can be expressed by:

$$N_f(x') = x' \, \delta \, \tau_{fu} \tag{4.4}$$

with its maximum at $x' = \ell_f \leq \ell/2$:

$$\max N_f = \ell_f \, \delta \, \tau_{fu} \tag{4.5}$$

with e.g. $\tau_{fu} = \mu_f \, \sigma_n$; $\sigma_n = \rho_c \, d_c$ for dead-weight of slab. In Eq. (4.4) and (4.5) δ represents an integer by which the dependence of the sign of free mean strain on the restraint force can be taken into consideration:

$\delta = +1$ for $\varepsilon_{0m} < 0$ contraction,

$\delta = -1$ for $\varepsilon_{0m} > 0$ expansion.

- **zone ℓ_e, elastically blocked length**

At the point $x' = \ell_f$, the relative displacement between slab and ground corresponds with Fig. 3.3 b to the maximum elastic deformation v_{el}, Eq. (3.10). The zone ℓ_e represents a region of transition between total coupling to sliding of slab. The assessment of length ℓ_e will be treated in section 4.5.

4.3 Magnitude of Mean Free Strain

In Fig. 3.7 the age-dependence of the mean free strain ε_{0m} is schematically depicted. In the early age of concrete member, the mean free strain is positive (expansion), later-on it changes to negative values (contraction). The magnitude of ε_{0m} depends with respect to its thermal component on the same parameters as the mean temperature of slab. Autogenous shrinkage is negative from the onset of solid matter properties (setting time). The absolute values $|\varepsilon_{0m}|$ of expansion phase exceed those of the contraction phase by a factor of about 1.25 to 1.50.

The mean free strains of slabs on ground were numerically investigated for the concrete compositions CO1 and CO23 (viz. Appendix). These compositions differ with respect to their heat liberation potential:

CO1: $Q_{pot} = 38.4$ kWh/m^3,

CO23: $Q_{pot} = 28.5$ kWh/m^3.

Fig. 4.2 shows the results for several values of thickness d_c and different seasons of casting. The values ε_{0m} pertain to the contraction phase ($\varepsilon_{0m} < 0$) at the age of 6 weeks. The contraction strain $|\varepsilon_{0m}|$ decreases with the increase of d_c. The influence of casting season is small. The heat potential is of great influence. Taking also higher cement contents into account, approximate limit values can be formulated for e.g. a 1 m thick slab:

contraction phase: $\lim \varepsilon_{0m} \approx -0.100$ to $-0.150\ 10^{-3}$,

expansion phase: $\lim \varepsilon_{0m} \approx +0.125$ to $+0.250\ 10^{-3}$.

The mean values of tensile Young's modulus and axial tensile strength follow in the early phase of hardening the rise of mean temperature of slab. At the maximum of the expansion strain $+\varepsilon_{0m}(t)$ about 70 to 85 % of the final values of these properties are already reached. From then on, they will grow only with slow rate.

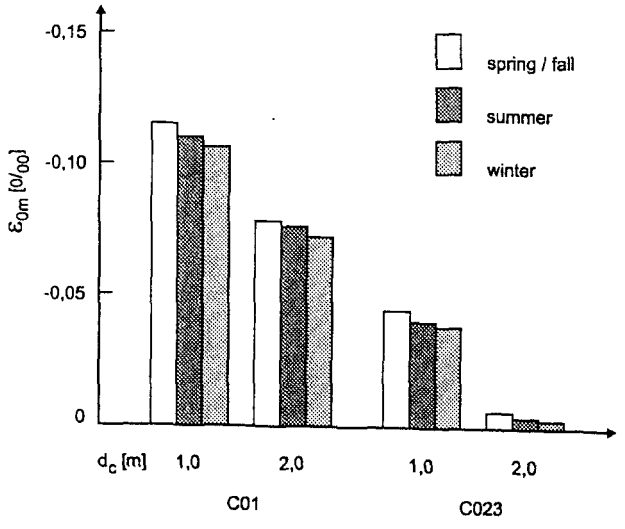

Fig. 4.2: Calculated Mean Free Strain ε_{0m} (Contraction) at the Age of 6 Weeks Dependent on Heat Potential, Slab Thickness and Climate of Casting

4.4 Axial Restraint of Slab due to Elastic Interaction with Soil in Half Space

4.4.1 Three layer model - TLM

It is a weakness of shear interaction approaches, that they do not take into account the soil's horizontal compliance over a greater depth below the slab. The horizontal compliance of soil can be modelled by the so-called elastic three-layer approach TLM (e.g. in [9]). Fig. 4.3 shows the three-layer system and definitions. The TLM pertains to the inner region of $\pm \ell_b$ on both sides of axis of symmetry, viz. Fig. 4.1. In this region, equilibrium of inner forces and compatibility of resultant strains must be fulfilled. The stiffness values of layers are:

slab: $E_e\ d_c$

blinding: $E_b\ d_b \approx 30.000 \cdot 0.1$ MN/m

soil: $E_s\ d_s$; E_s, stiffness modulus, viz. Table 3.1 and Table 3.2.

FE-studies have shown that the interacting depth d_s of soil can be assumed to be $d_s \approx \ell/3$ [8]. All three materials are assumed to be elastic. With the mean effective tensile modulus E_e the visco-elasticity of concrete can be taken into account. It is pre-supposed that the resultant and common strain plane is vertical. The influence of an eventual free curvature in either layer is neglected.

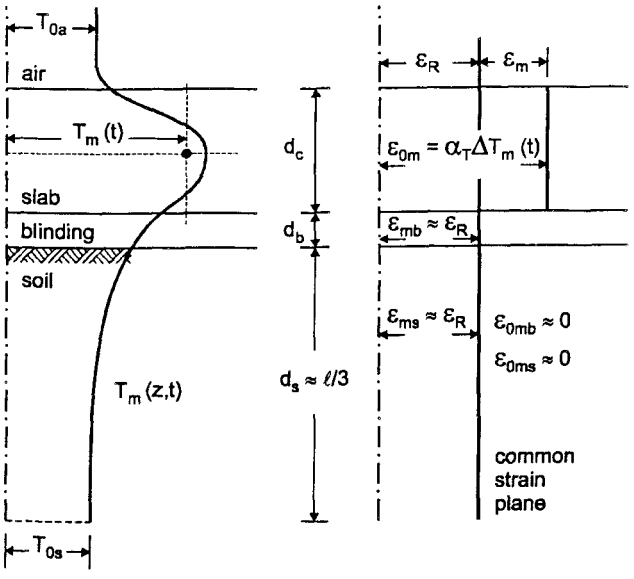

Fig. 4.3: Three-Layer System-Temperatures, Free Strains and Strain Plane

Extensive FE-studies by the authors regarding the temperature distribution during hardening of slab have shown that the soil participates in the heat transfer over a depth of 4 to 6 times of the slab's thickness. During hydration not only the concrete of slab but also the older

blinding and the soil are heated up beyond their initial temperatures T_{b0} and T_{s0}. The relevant free mean strains of blinding and soil ε_{0bm} and ε_{0sm} are here not taken into consideration for the sake of simplicity. This omission leads to a slightly higher axial restraint of slab and is hence conservative.

4.4.2 Restraint forces and restraint factor

The restraint forces are associated with the mean axial strains as follows:

$$\begin{aligned} N &= \varepsilon_m E_e d_s \\ N_b &= \varepsilon_{mb} E_b d_b \\ N_s &= \varepsilon_{ms} E_s d_s \end{aligned} \qquad (4.6)$$

Equilibrium requires:

$$N + N_b + N_s = 0 \qquad (4.7)$$

with ε_m, ε_{mb} and ε_{ms}, strains caused by the restraint forces N, N_b and N_s. The restraint actions force all layers into one and vertical strain plane. Compatibility requires that:

$$\begin{aligned} \varepsilon_m &\approx \varepsilon_R - \varepsilon_{0m} \\ \varepsilon_{mb} &\approx \varepsilon_R \\ \varepsilon_{ms} &\approx \varepsilon_R, \end{aligned} \qquad (4.8)$$

with ε_R, resultant mean strain. By introduction of Eq. (4.8) into Eq. (4.6) we arrive at the axial restraint force of slab (viz. also Eq. (4.3)):

$$N = -\varepsilon_{0m} E_e d_c \frac{1}{\frac{E_e d_c}{E_b d_b + E_s d_s}} = -\varepsilon_{0m} E_e d_c R_{ae} = \max N \qquad (4.9)$$

With the restraint factor

$$R_{ae} = \frac{1}{1 + \frac{E_e d_c}{E_b d_b + E_s d_s}}; \quad 0 \le R_{ae} \le 1 \qquad (4.10)$$

Fig. 4.4 shows the evaluation of Eq. (4.10). The investigated values of the stiffness modulus E_s cover the practical range of cohesive and non-cohesive soils. The restraint factor for the value $E_s = 0$ represents the theoretical restraint by the blinding layer alone (two-layer system). Restraint increases with the length ℓ and the stiffness modulus; it reduces with the

slab's thickness. Axial restraint is rather small. The dependence of restraint factor on length is caused by the increase of interacting depth d_s with the length of slab.

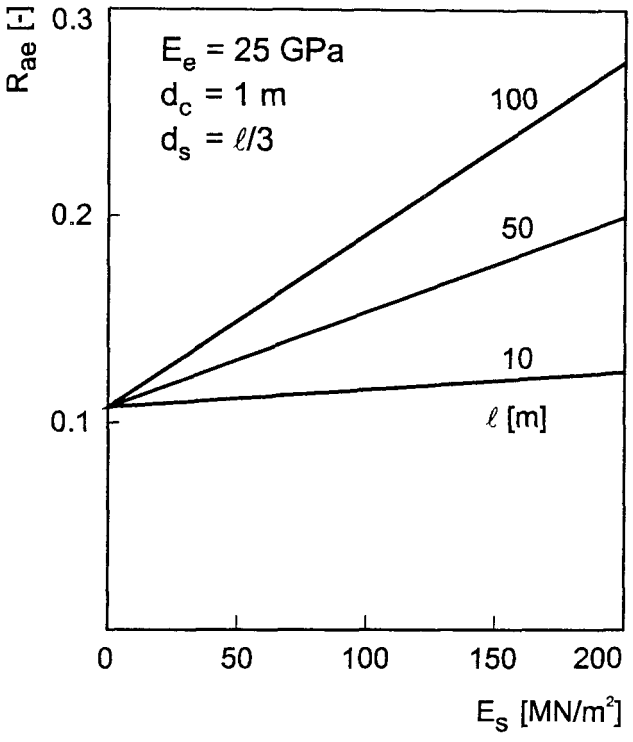

Fig. 4.4: Axial Restraint Factor R_{ae} of Three-Layer System Dependent on Length and Stiffness Modulus of Soil

The evaluation of Eq. (4.10) in Fig. 4.4 was performed with a constant value of effective tensile modulus of $E_e = 25$ GPa. Such value is representative for the contraction phase with the concrete being already well matured. In the early expansion phase (viz. Fig. 3.7, $\varepsilon_{0m} < \max \varepsilon_{0m}$) the modulus will be in the range $0 \leq E_e(t) \leq 25$ GPa. This effect leads to an increase of R_{ae}. In fact, at the end of setting time we obtain $R_{ae}(t_0) = 1$ (first zero stress age) because of $E_e\, d_c = 0$. From $t > t_0$ on, R_{ae} will rapidly decrease. More to this will be dealt with latter.

Comparison with rigid-plastic interaction

For the rigid-plastic shear friction interaction Fig. 3.3 c, the maximum restraint factor R_{af} can be derived with Eq.(4.5) assuming sliding on entire length $\ell/2$:

$$R_{af} = \frac{\tau_{fu}\, \ell}{2|\varepsilon_{0m}|\, E_e\, d_c} \tag{4.11}$$

Eq. (4.11) was evaluated in Fig. 4.5 for three values of $|\varepsilon_{0m}|\, E_e$ [MPa]. The physical unsoundness of the shear-friction theory to describe axial restraint is evident. For

comparison, the restraint factor of elastic interaction, Eq. (4.10) was evaluated for E_s = 200 MPa. Elastic restraint remains rather low.

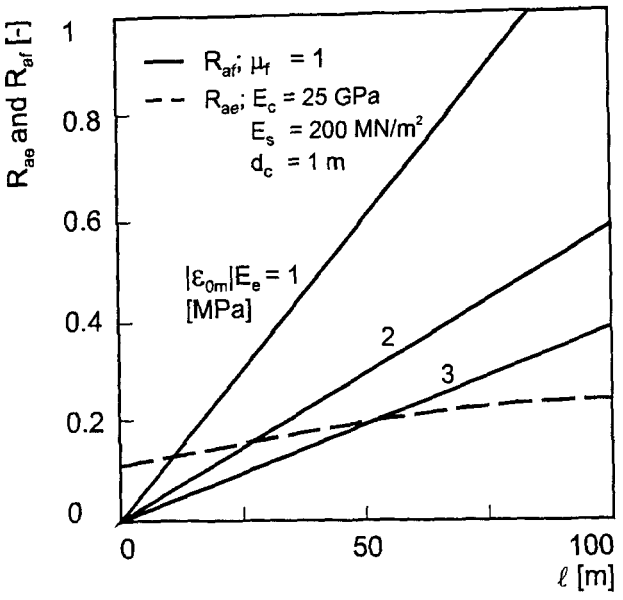

Fig. 4.5: Comparison of Maximum Axial Restraint Factor of Sliding Friction with that of Three-Layer Elastic Interaction R_{ae} at Axis of Symmetry

4.5 Determination of Length ℓ_e and ℓ_f

Once the degree of axial restraint R_{ae} has been determined with Eq. (4.10), the interacting partial lengths ℓ_b, ℓ_e and ℓ_f can be derived. For this procedure the elasto-plastic shear-stress-displacement model of Fig. 3.3 b and the relationships of [7] are used.

For low values of ε_{0m} - irrespective of sign of ε_{0m} - the maximum restraint force can be transferred to the ground by elastic displacements $0 \le v \le v_{el}$ (Eq. (3.10)). Sliding at the ends of slab does not occur, Fig. 4.6.

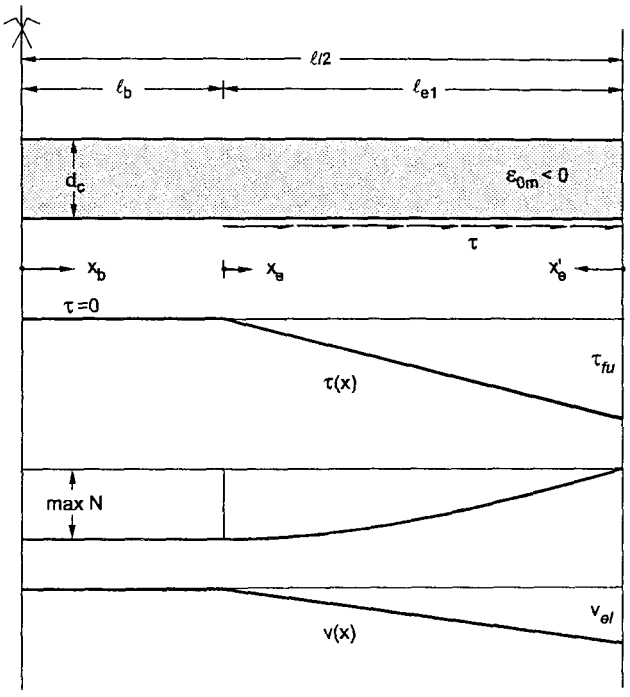

Fig. 4.6: Elastic Shear Interaction for Slab on Ground

The displacement at ends and shear stress must meet the conditions

$$v(x' = 0) \leq v_{el} = \frac{d_v}{\sqrt{D}} \tag{4.12}$$

$$\tau\,(x' = 0) \leq \tau_{fu} = \mu_f\,\sigma_n \tag{4.13}$$

for non-cohesive soil. For $v(x' = 0) = v_{el}$ and $\tau(x' = 0) \leq \tau_{fu}$, we arrive at the necessary length ℓ_{e1} to elastically transfer the force max N to the ground:

$$\ell_{e1} = \frac{-2\,\varepsilon_{0m}\,E_e\,d_c\,R_{ae}}{\delta\,\tau_{fu}} \leq \frac{\ell}{2} \tag{4.14}$$

or in normalized form, resp.:

$$\frac{2\,\ell_{e1}}{\ell} = \frac{-4\,\varepsilon_{0m}\,E_e\,d_C\,R_{ae}}{\delta\,\tau_{fu}\,\ell} \leq 1\,. \tag{4.15}$$

Because of

$$\frac{\ell}{2} = \ell_{e1} + \ell_b\,,$$

we may deduce the length ℓ_b for $\ell_{e1} \leq \ell/2$. The evaluation of Eq. (4.15) is shown in Fig. 4.7 for a specific set of parameters and for self-weight of slab alone:

$$\sigma_n = \rho_c \, d_c ,$$

$$\tau_{fu} = \mu_f \, \rho_c \, d_c .$$

The intersection of the straight line of Eq. (4.15) with the horizontal line $2\,\ell_{e1}/\ell = 1$ marks the maximum value $|\varepsilon^*_{0m}|\,E_e$ associated with elastic interaction on length $\ell/2$. For $|\varepsilon_{0m}| > |\varepsilon^*_{0m}|$ sliding will begin and Eq. (4.15) does not hold any further. Fig. 4.7 shows the dependence of length ℓ_e on $|\varepsilon_{0m}|\,E_e$ and length $\ell/2$.

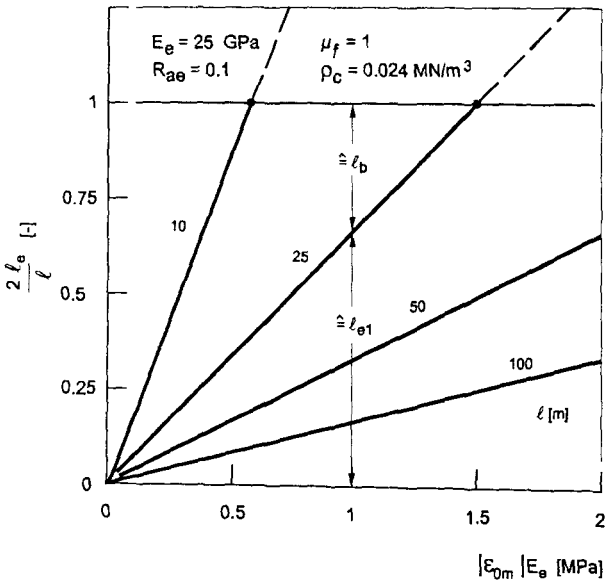

Fig. 4.7: Dependence of Length ℓ_e on Value $|\varepsilon_{0m}|\,E_e$ and Length of Slab (Examples)

As sliding sets on, we obtain with $\ell_b = 0$ and because of

$$\frac{\ell}{2} = \ell_{e2} + \ell_f ,$$

the length ℓ_e for $|\varepsilon_{0m}| \geq |\varepsilon^*_{0m}|$:

$$\ell_{e2} = \ell + \frac{2\,\varepsilon_{0m}\,E_e\,d_c\,R_{ae}}{\delta\,\tau_{fu}} \leq \frac{\ell}{2} \qquad (4.16)$$

or in normalized form, resp.:

$$\frac{2\,\ell_{e2}}{\ell} = 2 + \frac{4\,\varepsilon_{0m}\,E_e\,d_c\,R_{ae}}{\delta\,\tau_{fu}\,\ell} \leq 1 \qquad (4.17)$$

Fig. 4.8 shows the evaluation of Eq. (4.17) for the parameters of Fig. 4.7. Eq. (4.17) is only valid between $|\varepsilon^*_{0m}|\,E_e \leq |\varepsilon_{0m}|\,E_e \leq 2\,|\varepsilon^*_{0m}|\,E_e$. The total coupled length can be denoted by

$$x_{be} = \ell_{e1} + \ell_b. \tag{4.18}$$

It is shown as horizontal line at the ordinate $2\,\ell_{e1}/\ell = 1$ in the region $0 \le |\varepsilon_{0m}|\,E_e \le |\varepsilon^*_{0m}|\,E_e$. Fig. 4.9 shows the influence of length of slab.

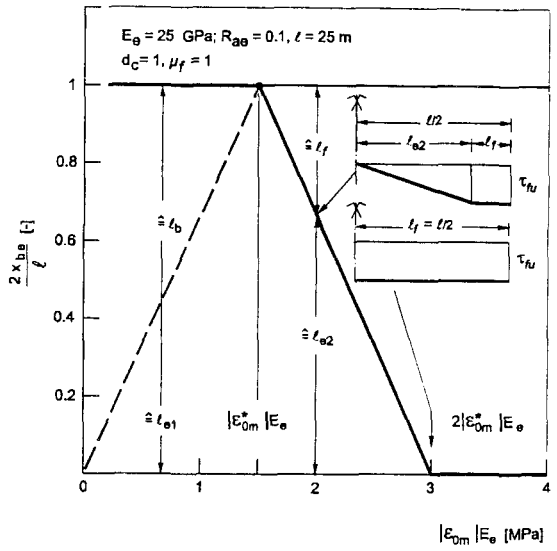

Fig. 4.8: Dependence of Total Coupled Length x_{be} on $|\varepsilon_{0m}|\,E_e$ (Example)

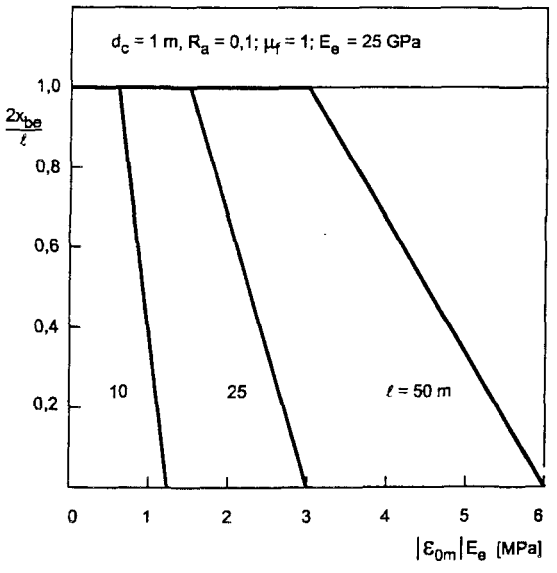

Fig. 4.9: Dependence of Elastically Coupled Length x_{be} on $|\varepsilon_{0m}|\,E_e$ and Length ℓ (Example)

With Fig. 4.10 one can decide which type of interaction will prevail in the specific case. Below the lower straight line, pairs of values (ℓ, ε_{0m}) are associated with sliding on $\ell/2$. Pairs of values (ℓ, ε_{0m}) above the upper line refer to full elastic coupling on $\ell/2$. Pairs of values falling into the wedge between straight lines are associated with elastic coupling and sliding as well. The vertical dashed lines refer to Fig. 4.2. Example: a slab with $d_c = 2$ m and

ℓ = 25 m, cast with concrete CO1, will be partly coupled and partly sliding on ends. The same slab, though with ℓ = 40 m, will be elastically coupled to ground without sliding.

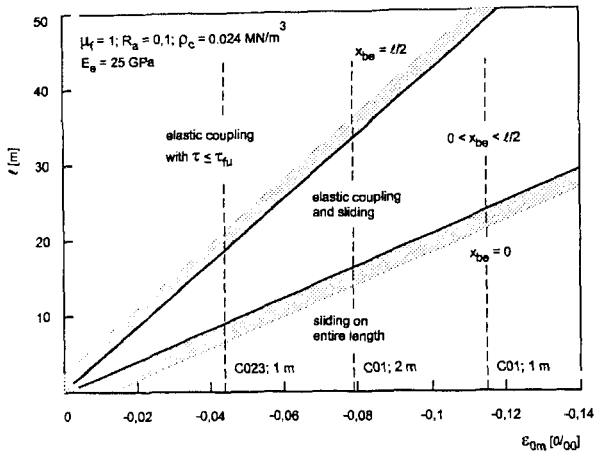

Fig. 4.10: Types of Axial Restraint Dependent on Strain and Length (Examples)

4.6 Dependence of Restraint Force on Free Strain and Location

In Fig. 4.11 the dependence of maximum restraint force is depicted for the shown set of parameters. The force max N depends within the rigidly blocked length ℓ_b and elastically coupled length ℓ_e linearly on the imposed strain $-\varepsilon_{0m}$. Once the strain $|\varepsilon_{0m}| \geq 2\,|\varepsilon^*_{0m}|$ is reached, sliding occurs on the entire length. The distribution of restraint force along the length is schematically shown in Fig. 4.1 and Fig. 4.6. For the case that the slab is coupled along $\ell/2$, we obtain for $\ell_{e1} \leq \ell/2$ and $\ell_b \geq 0$:

$$N(x_b) = \max N = \text{const.} = -\varepsilon_{0m}\, E_e\, A_c\, R_a \tag{4.19}$$

$$N(x_e) = \max N - \delta\tau_{fu}\,\frac{x_e^2}{2\ell_{e1}} \tag{4.20}$$

For the case that sliding sets on and the length ℓ_b has vanished we obtain for $\ell_{e2} \leq \ell/2$; $\ell_b = 0$; $\ell_f = \ell/2 - \ell_{e1}$:

$$N(x_e) = \max N - \delta\tau_{fu}\,\frac{x_e^2}{2\ell_{e2}} \tag{4.21}$$

$$N(x_f) = \delta\tau_{fu}\,(\ell_f - x_f) \tag{4.22}$$

The inner region - on both sides of axis of symmetry - is especially prone to cracking. As the mean stress due to max N remains rather low, through-cracking of slabs is rather unlikely. This is however not true for slabs cast on stiff rock.

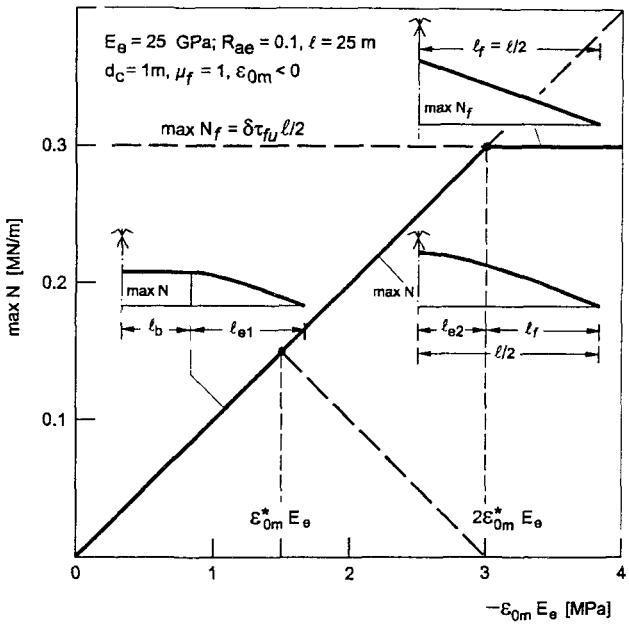

Fig. 4.11: Dependence of Maximum Restraint Force on Mean Free Strain (Example)

4.7 Mitigation of Restraint by Sliding Layers

Especially for large and rather thin slabs (d_c < 50 cm) sliding layers to mitigate friction and thus restraint are applied, e.g. for sewage treatment containers etc. In [9] an overview on the efficiency of such layer is given. In the following the main types of sliding layers and their efficiency are presented. Thereby only such solution in connection with a blinding concrete layer are discussed. Sliding motion has to occur between slab and blinding.

Sliding layers are usually thin and hence vulnerable during work on site, especially the placement of reinforcement of slab. In order to minimize the potential injury of layers, the following pre-requisites have to be fulfilled. The blinding has to be clean and smooth. Local roughness, indentation (foot print) provoke the ineffectiveness of layers. A surface finish by manual screeding and trowelling is usually too rough. A smoother surface is attained with a power trowel.

- Double-layer PE-foils with 2 x 0.3 mm

This is the most common and least expensive type. It requires great care with respect to surface smoothness of blinding. It is also the most vulnerable solution. The friction

coefficient μf was measured in the range of 0.60 to 0.75. It is stated in [7] that such solution becomes ineffective for higher normal pressures σn > 25 kN/m^2 (= dc = 1.0 m).

- Lubricated and coated sliding layers

Such commercial products may consist of 2 PE-foils, 0.3 to 0.5 mm/layer, with a lubricant (e.g. silicon grease) or a PTFE-foil in-between. Protection of top PE-layer is facilitated by a laminated styrofoam layer. The friction coefficient μf was measured in the range of 0.3 to 0.55.

- Welded asphalt sheets

As stated in [9], welded asphalt sheets are very suitable to mitigate the restraint of hardening slabs. They consist of one to two layers of asphalt sheet (d ≈ 4 mm/sheet) on a glass fiber mat to be patch-glued on blinding. Of great influence on the shear modulus of the asphalt sheet is the temperature and the rate of sliding motion. The equivalent coefficient of friction decreases with the normal stress σn. It is for normal temperature and a low slide rate about 0.45 for σn < 10 kN/m^2 and about 0.20 for σn > 45 kN/m^2 [9].

- Bituminous mastic concrete layer

This material exhibits a visco-elastic behaviour. If a soft bitumen is used, the equivalent friction coefficient for the temperature range of 10 to 15 °C and a low slide rate is about 0.3. More to this can be found in [9] and [7].

4.8 Summary

In the foregoing sections, the most frequently used engineering models for the assessment of axial restraint were outlined, discussed and compared. This was done under several pre-suppositions and simplifications.

Commonly, the shear-friction approach is applied in practice. It was found that the restraint force of the simple rigid-plastic shear friction approach only insignificantly differs from that of the more complicated elasto-plastic shear friction approach. Both, violate compatibility with the deformation of soil. The most realistic approach is a combination of the three-layer model of elastic compliance of soil with the rigid plastic shear friction model of sec. 4.2.

In a massive, hardening slab there exists not only axial restraint but also bending restraint. Hence, the isolated treatment of axial restraint and neglect of bending restraint is questionable. Because of that fact, the combined effect of mean free strain and mean

curvature on restraint stresses should be dealt with jointly as shown in chapter 5. Suggestions as to the mitigation of restraint by sliding layer are presented.

5 ENGINEERING MODELS FOR BENDING AND COMBINED RESTRAINT

5.1 Problem and Intentions

In chapter 4 of this report the axial restraint of slab caused by the hindrance of the free strain ε_{0m} has been treated. It was, however, already pointed out, that in a massive slab there will always exist a cross-fall of temperature over the slab's depth during hardening of concrete. This cross-fall is associated with the free curvature κ_0 (viz. Fig. 1.1). Computations prove that the curvature κ_0 is negative. This means that the unrestrained slab has the tendency to curl up on both sides of the axis of symmetry. This free bending deformation is however impeded by the slab's dead weight and the vertical compliance of soil. The hindrance of curvature consequently leads to negative restraint moments (tension on top edge of slab).

From these remarks, we conclude that the realistic assessment of restraint of a slab on ground must take both the vertical and horizontal deformability of soil into account. In sec. 3 the relevant material parameters of soil and the material models of interaction between slab and soil have been outlined.

For the assessment of bending restraint (M) and combined restraint (N, M) the following approaches will be applied:

- Three-layer method TLM, sec. 5.2
- Subgrade reaction modulus method SRMM, sec. 5.4

The TLM was already applied in sec. 4 to assess the degree of R_a of restraint and the axial restraint force. There, the effect of curvature was neglected. In this section, in addition the effect of curvature will be taken into account. The SRMM was already outlined in sec. 3.5. By this method only the bending restraint can be determined. The axial restraint must hence be separately assessed according to section 4 and added to bending restraint.

The TLM and SRMM differ with respect to their mechanical basis. The TLM describes restraint in the inner region of a slab (around axis of symmetry). The influence of slab's length can only be taken implicitly into account via the assumption of interacting depth of soil $d_s \approx \ell/3$. In contrast to that, by the SRMM the dependence of restraint moment on slab's length can be explicitly described.

The TLM and SRMM describe the stiffness of concrete by the mean effective modulus E_e. In consequence, the non-linearity of local stress, cannot be described. Stresses can only be determined with the beam theory. In order to assess the non-linear stresses the

- Finite Strip Method FSM, sec. 5.3

of iBMB is additionally applied. It is an amplification of the TLM by taking the local age- and time-dependence of properties into account.

5.2 Three-Layer Model of Axial and Bending Restraint TLM

5.2.1 Assumptions

In sec. 4.4 the axial restraint of a slab on blinding and soil was dealt with by the TLM. In this approach, a unique and vertical plane of the resultant strain ε_R - common for all three materials - was pre-supposed. However, the bending restraint of the slab which inevitably occurs if a free curvature κ_0 exists was neglected. This neglection is only acceptable for thin slabs. With increasing depth d_c of slab this presupposition is not tolerable. In this section, therefore, an engineering model will be presented which treats the interaction of slab, blinding and soil over the interacting depth of $d_s = \ell / 3$ for both axial and bending restraint.

This approach consists of two steps. In the first step, the two layers, blinding and soil, are depicted by a compound one-layer model which is with respect to restraint of slab mechanically equivalent, called equivalent soil model. Then, in the second step the equivalent soil layer is adjoined to the slab, thereby forming a two-layer model consisting of the slab and equivalent soil layer.

It is assumed that the soil and blinding are ideally elastic materials. The concrete of slab is for short-term stress also considered to be linear-elastic, though the age-dependence of the mean Young's modulus E_{ct} over the depth d_c can be taken into account. Besides that, the visco-elastic behaviour of concrete must be considered in this quasi-elastic TLM approach. This can be realized by replacing E_{ct} by the effective modulus E_e. The procedure to determine the latter will be described. Only the linear components of free deformations, ε_{0m} and κ_0, are considered. It is assumed that the free deformations of the blinding and soil are negligible. This is a conservative assumption with respect to restraint of the slab. The TLM requires the computation of the fields of temperature and free strains $\varepsilon_0(z, t)$ as well as of the mean free deformations $\varepsilon_{0m}(t)$ and $\kappa_0(t)$.

The model describes the mechanical behaviour of slab and soil within the inner region of long slabs, i.e. in the blocked zone $\pm x_{be}$ around the axis of symmetry. Because the ends of slab are free from stress, the gradual transition of the restraint in zone x_{be} to that at ends requires additional deliberations.

The TLM is not new. In Japan the so-called compensation line (CL) and compensation plane (CP) methods have been developed [13, 14, 15]. They predominantly relate to the restraint of young concrete members by rock ($E_e / E_{rock} \leq 40$) and old concrete layers. The CP method was also applied in Scandinavia [16] and Germany [17], especially to model the restraint of young walls on old foundations. The application of this method to model the restraint of hardening concrete slabs by ground and, or piles has only rarely been treated [9].

5.2.2 Stiffness of Equivalent Soil Layer

The thin but stiff blinding layer may significantly contribute to the restraint of slab. The blinding and soil are joined to the equivalent soil layer, Fig. 5.1. Its center of gravity C_{se} has the distance from the top of blinding

$$f_{se} = \frac{d_s}{2} \frac{1}{1+K_D} \quad , \tag{5.1}$$

with the stiffness parameter K_D

$$K_D = \frac{E_b\, d_b}{E_s\, d_s} \quad . \tag{5.2}$$

With Eq. (5.1) the neutral axis is described, into which the actions of soil N_{se} and M_{se} are shifted. With the modulus E_{se} and the thickness d_{se} of the equivalent soil layer

$$E_{se} = E_s (1+K_D)$$

$$d_{se} = d_s + d_b \approx d_s \approx \frac{l}{3} \tag{5.3}$$

the axial and bending stiffness can be expressed by

$$E_{se}\, d_s = E_s\, d_s\, (1+K_D) \tag{5.4}$$

$$E_{se}\, I_{se} = E_s \frac{d_s^3}{12} \frac{(1+2K_D)^2}{1+K_D} \tag{5.5}$$

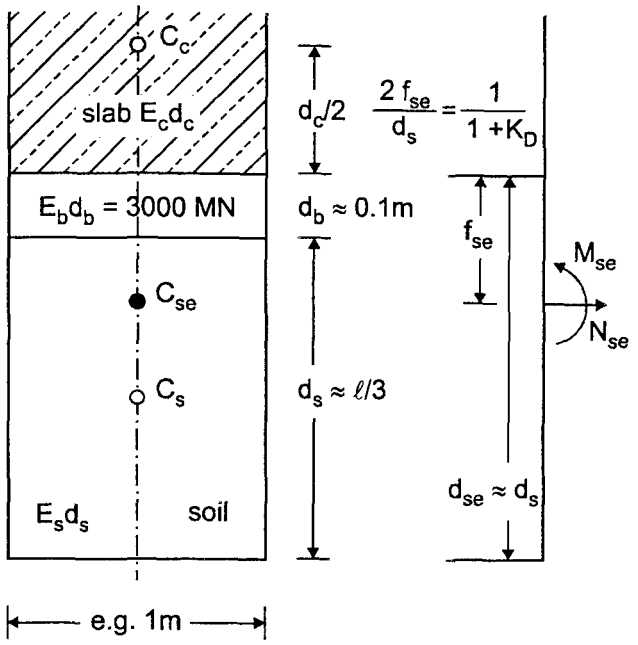

Fig. 5.1: Equivalent Soil Layer and Three-Layer Model

5.2.3 Assessment of Restraint Actions

Fig. 5.2 shows the geometrical and mechanical relationships. The restraint actions enforce the common resultant strain plane. The equations of equilibrium and compatibility are:

$$N_{se} + N = 0 \ , \tag{5.6}$$

$$N_{se} \frac{d_c + 2 f_{se}}{2} + M_{se} + M = 0 .., \tag{5.7}$$

$$\varepsilon_{sR} = \varepsilon_R - \kappa_R \frac{d_c + 2 f_{se}}{2} \ . \tag{5.8}$$

In Eq. (5.8), ε_R and κ_R are the resultant deformations of slab. The terms ε_{sR} and $\kappa_{sR} = \kappa_R$ are the resultant deformations of equivalent soil layer. The value p is a geometrical parameter: $p = (d_c + 2 f_{se}) / d_c$. The expressions for the resultant strains ε_R, ε_{sR} and the resultant curvatures κ_R, κ_{sR} are presented in Fig. 5.2. With the latter, the deformations ε_m, κ caused by the restraint actions can be expressed by:

$$\varepsilon_m = - \frac{\varepsilon_{0m}(1 + S_B) - \kappa_0 \frac{p d_c}{2} S_B}{3 p^2 S_B + (1 + S_B)(1 + S_D)} \tag{5.9}$$

and

$$\kappa = -\frac{\kappa_0\left(3p^2 S_B + 1 + S_D\right) - \varepsilon_{0m}\dfrac{6 S_B\, p}{d_c}}{3p^2 S_B + (1+S_B)(1+S_D)} \tag{5.10}$$

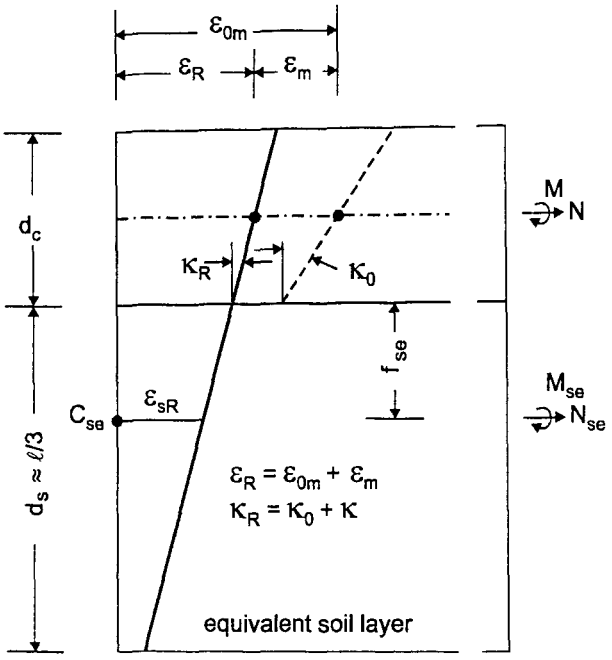

Fig. 5.2: Strains and Curvatures of the Elastic Two-Layer Model-Slab with Equivalent Soil Layer

In Eq. (5.9) and (5.10) S_D and S_B are the normalized stiffness ratios:

$$S_D = \frac{E_e\, d_c}{E_{se}\, d_{se}}; \quad 0 \le S_D \le \infty \ , \tag{5.11}$$

$$S_B = \frac{E_e\, I_c}{E_{se}\, I_{se}}; \quad 0 \le S_B \le \infty \ . \tag{5.12}$$

which can determined with Eq. (5.3) to (5.5). By introducing Eq. (5.11) and (5.12) into Eq. (5.6) to (5.8), we arrive at the restraint actions

$$N = \varepsilon_m\ E_e\, d_c \quad \text{and} \tag{5.13}$$

$$M = -\kappa E_e I_c \, . \tag{5.14}$$

5.2.4 Degrees of Restraint

The degrees of restraint can be expressed by

$$R_a = \frac{N}{N_0} = -\frac{\varepsilon_m}{\varepsilon_{0m}}; \qquad 0 \le R_a \le 1 \tag{5.15}$$

and

$$R_b = \frac{M}{M_0} = -\frac{\kappa}{\kappa_0}; \qquad 0 \le R_b \le 1 \tag{5.16}$$

with N_0 and M_0 the reactions for total restraint:

$$N_0 = -\varepsilon_{0m} E_e d_c \tag{5.17}$$

and

$$M_0 = \kappa_0 E_e I_c \tag{5.18}$$

With Eq. (5.15) to (5.18) the restraint actions can be alternatively expressed by

$$N = -R_a \varepsilon_{0m} E_e d_c \tag{5.19}$$

and

$$M = R_b \kappa_0 E_e I_c \tag{5.20}$$

The assessment of the degrees of restraint, Eq. (5.15) and (5.16) requires the evaluation of Eq. (5.9) and (5.10). These equations show that both R_a and R_b depend on the free deformations ε_{0m} and κ_0. Numerical studies have shown that the degree of axial restraint R_a is rather low for slabs on ordinary ground: $R_a \approx 0.05 \div 0.20$. This conclusion was already drawn in sec. 4.4. This conclusion can also be up-held if the assessment of R_a is performed with Eq. (5.9). In contrast to this, the degree of bending restraint R_b is rather high: $R_b \approx 0.8 \div 1.0$. This behaviour can be explained by the real values of stiffness parameters which for the contraction phase are in the following practical range:

$S_{De} \approx 5 \div 15$ low axial restraint

$S_{Be} \approx 0 \div 0.25$ high bending restraint

These values permit the suppression of the terms associated with S_B versus those terms associated with S_D. By doing so, we arrive at the following satisfactory estimators for the degrees of restraint:

$$\tilde{R}_a \approx \frac{1}{1+S_D} \tag{5.21}$$

and

$$\tilde{R}_b \approx \frac{1}{1+S_B} \tag{5.22}$$

It is mentioned that Eq. (5.21) and (4.10) are identical. To judge the suitability of these expressions, a comparative numerical study was performed for a 1 m thick slab with concrete CO1 for two values of stiffness modulus E_s and for variable length. The results are plotted in Fig. 5.3. The stiffness parameters and degrees of restraint depend on age as shown in Fig. 5.4. In Fig. 5.3, the end values R_{ae} and R_{be} are computed with Eq. (5.15) and (5.16) and are compared with the approximate values $\tilde{R}_a$ and $\tilde{R}_b$ according Eq. (5.21) and (5.22). The differences between R_{ae} and $\tilde{R}_{ae}$ are insignificant. The differences between R_{be} and $\tilde{R}_{be}$ are slightly greater. These statements also holds for other values of d_c and E_s.

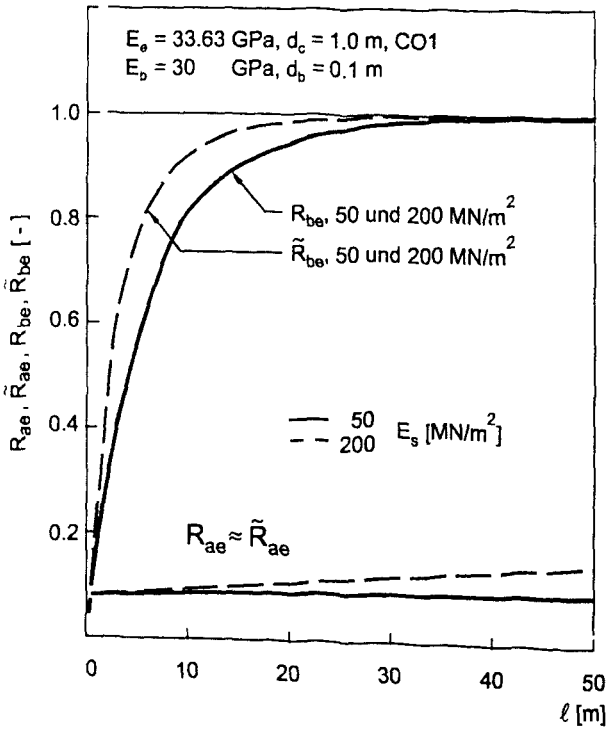

Fig. 5.3: Degrees of Restraint vs. Length of Slab. Exact and Approximative Values for d_c = 1 m, CO1

The restraint varies with age and time-dependent behaviour of concrete. This fact is elucidated in Fig. 5.4. Both stiffness parameters S_D and S_B, Eq. (5.11) and (5.12) are plotted vs. age. The age t_0 denotes the concrete's on-set of being a solid material. The stiffness parameters tend towards their end-values S_{De} and S_{Be}. With Eq. (5.21) and (5.22) the degrees of restraint were determined. They are also plotted in Fig. 5.4. Because of $E_e = 0$ at t_0, they assume the value of 1 at age t_0. From then on, they rapidly drop to their final levels R_{ae} and R_{be}.

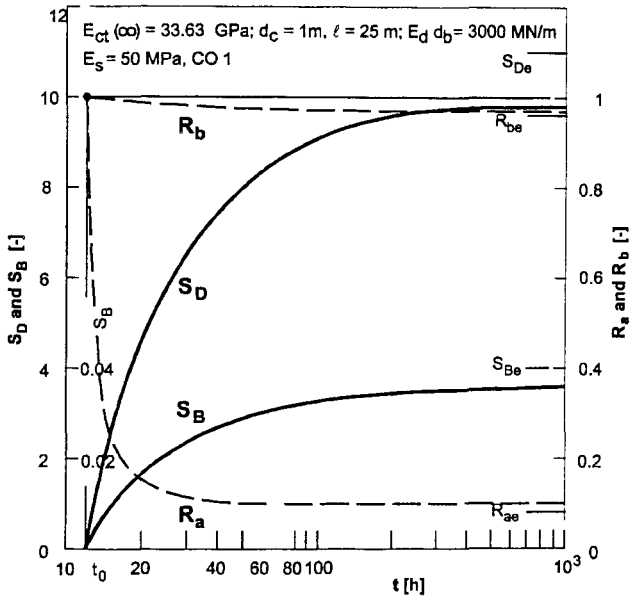

Fig. 5.4: Dependence of Stiffness Parameters and Degrees of Restraint on Age (Example)

5.2.5 Influence of Age of Concrete and Time under Stress on Restraint Actions

5.2.5.1 Age dependence of degrees of restraint

The deformations ε_{0m} and κ_0 depend on age, viz. Fig. 3.7. This is also true for the mean modulus of elasticity E and all other relevant properties of concrete. These facts imply that the restraint actions must be incrementally computed. At the on-set of steps $\Delta\varepsilon_{0mi}$ and $\Delta\kappa_{0i}$ at the age t_i, the mean modulus E_i ($\cong E_{ctm}(t_i)$; $E_{ct} = E_{cc} = E$) must be known. With that the values of S_{Di} and S_{Bi} and the degrees of restraint R_{ai} and R_{bi} can be determined (e.g. viz. Fig. 5.4).

5.2.5.2 Age-adjusted effective modulus and relaxation

If the influence of relaxation is disregarded, the restraint actions and stresses will be significantly overestimated, especially at early age of concrete. The consideration of relaxation necessitates the knowledge of either the creep function $\varphi(t - t_i, t_i)$ or the relaxation function $\psi(t - t_i, t_i)$. The basis of such functions optimally are tests data and adapted models of the concrete of impending cast or suitable models from other sources. It was proved in [33] that the creep models of MC 90 [35] and EC 2, pt. 2 [36] require modifications in order to satisfactorily describe early-age relaxation. Regarding such modifications viz. [34].

A wellknown approach to treat a relaxation problem on basis of creep functions is the age-adjusted effective modulus E_e method (for the sake of brevity it is denoted as effective modulus EM) [30, 31, 32]. To explain the latter, e.g. the axial restraint force, Eq. (5.19), is formulated for the strain history $\Delta\varepsilon_{0mi},\ldots$, starting at t_1 and lasting till t_n:

$$N_{n1} = - d_c \sum_{i=1}^{n} \Delta\varepsilon_{0mi} E_{eni} R_{ai} \tag{5.23}$$

with $E_{eni} = E_{ct}\,\psi(t_n - t_i, t_i)$, EM after the period of time $t_n - t_i$ under stress for the age t_i of on-set of $\Delta\varepsilon_{0mi}$. The restraint force can also alternatively be expressed with the relaxation function ψ:

$$N_{n1} = - d_c \sum_{i=1}^{n} \Delta\varepsilon_{0mi} E_i \psi_{ni} R_{ai} \tag{5.24}$$

with ψ_{ni}, mean relaxation function after the period of time $t_n - t_i$ under stress for the age t_i of on-set of $\Delta\varepsilon_{0mi}$. Hence, the EM is equivalent to

$$E_{eni} = E_i \psi_{ni} . \tag{5.25}$$

It is dependent on time $t_n - t_i$ under stress and on-set t_i of strain increment. If the concrete's visco-elasticity is described by a creep function, then the creep compliance must be inverted into the relaxation function. In [32] this inversion was performed with the creep functions of MC 90 [35]. The EM is expressed by

$$E_{eni} = \frac{E_i}{1 + \chi(t,t_i)\frac{E_i}{E_{28}}\varphi(t,t_i)} \tag{5.26}$$

with E_{28}, modulus of elasticity at the age t = 28 d; $\chi(t, t_i)$, aging coefficient. Regarding the purpose and derivation of $\chi(t, t_i)$, reference is made to [32]. In this source , graphs of $\chi(t, t_i)$ for specific concrete strengths etc. on basis of the creep relationships of MC 90 are presented. Although these graphs do not pertain to young concrete, they may serve as guidance.

In the pre-planning phase of a structure a realistic creep model is usually not available. Therefore, the EM is often expressed as fraction of the mean modulus E_i

$$\tilde{E}_{eni} \approx \tilde{\tilde{E}}_{ei} = E_i \, k_{Ri} \; ; \; 0 < k_{Ri} \leq 1 \tag{5.27}$$

with k_{Ri}, factor which globally reduces the elastic modulus E_i in order to take relaxation into account. Various estimations for the factor k_{Ri} dependent on age t_i at strain step $\Delta\varepsilon_{0mi}$ are presented in literature. Thereby, the end of setting time t_0 ($\cong \alpha_0$) must be known, because of $t_0 \cong t_1$ at the on-set of strain steps $\Delta\varepsilon_{0mi}$. Dependent on cement type, temperature regime etc., t_0 is in the range of 6 to 15 h (without addition of retarding agent) the following factors k_{Ri} seem reasonable for:

Strain increments within	$t_0 \leq t_i \leq t_0 + 24$ h,	$k_{Ri} \approx 0.65 \div 0.70$
Strain increments within	$t_0 + 24$ h $< t_i \leq t_0 + 48$ h,	$k_{Ri} \approx 0.70 \div 0.75$
Strain increments after	$t_i > t_0 + 48$ h	$k_{Ri} \approx 0.80 \div 0.85$

5.2.5.3 Influence of age of concrete and time under stress on axial restraint

With the k_{Ri}-values, the axial restraint force can be expressed by:

$$\tilde{N}_{ni} = -d_c \sum_{i=1}^{n} \Delta\varepsilon_{0mi} \, \tilde{\tilde{E}}_{ei} \, R_{ai} \tag{5.28}$$

In order to judge the forecasting quality of Eq. (5.28), comparative computations were performed for the slab CO1-1-FH-15 (viz. App. B and C). For the sake of simplicity, the degree of axial restraint was set to $R_{ai} = 1$ (this assumption does not afflict the comparisons). Fig. 5.5 shows the free thermal deformations. Fig. 5.6 depicts the age-dependence of the mean value of E ($\cong E_i$), of mean degree of hydration α and relaxation coefficient ρ_i of [33]. In Fig. 5.6 the functions φ and ψ used for the computations are inserted.

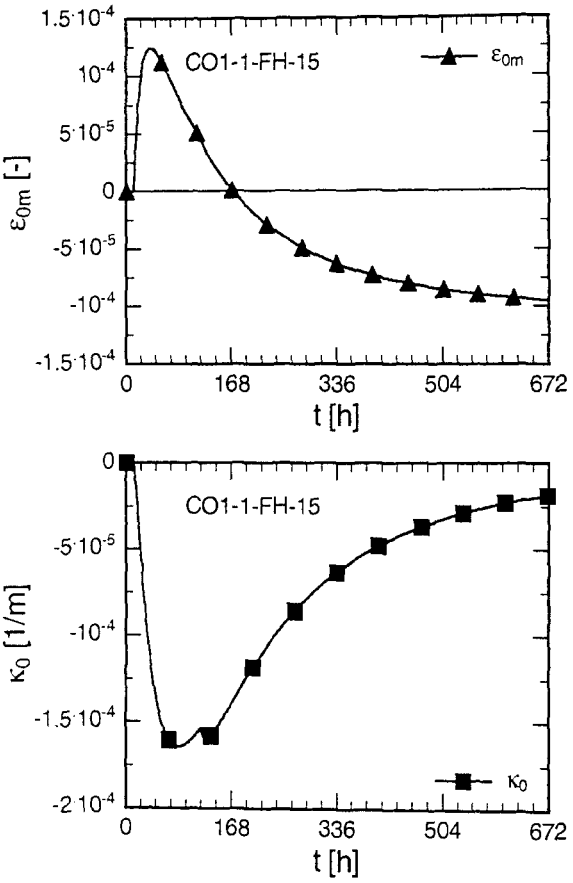

Fig. 5.5: Free Thermal Deformations for Slab CO1-1-FH-15 vs. Age

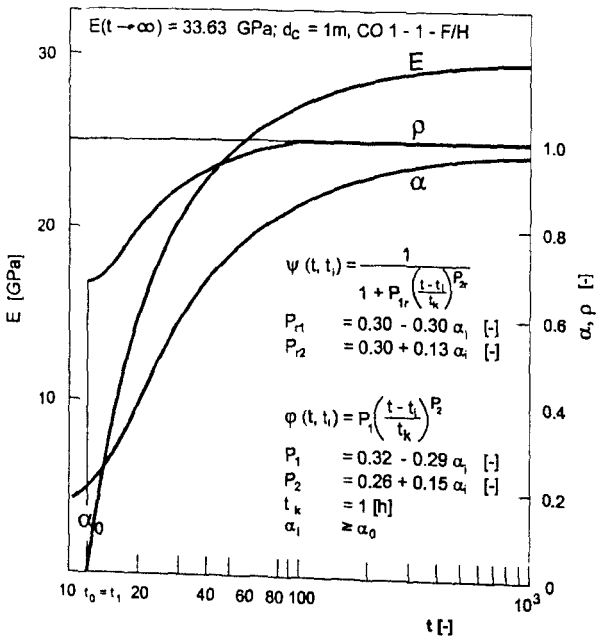

Fig. 5.6: Dependence of Mean Young's Modulus, Degree of Hydration and Relaxation Coefficient on Age (Example)

Three cases were investigated. At first, Eq. (5.24) was evaluated for purely elastic behaviour: $\psi_{ni} = 1$, $N_{ni} \cong N_{elni}$. In the second case, Eq. (5.24) with the relaxation function of Fig. 5.6 was used. Thirdly, Eq. (5.28), using the proposed values for the factor k_{Ri}, was applied (0.70; 0.75; 0.80). The results are presented in Fig. 5.7. The elastic solution grossly overestimates the axial restraint of contraction phase. This is also true if Eq. (5.28) is evaluated. This relationship is rather crude to reliably describe restraint.

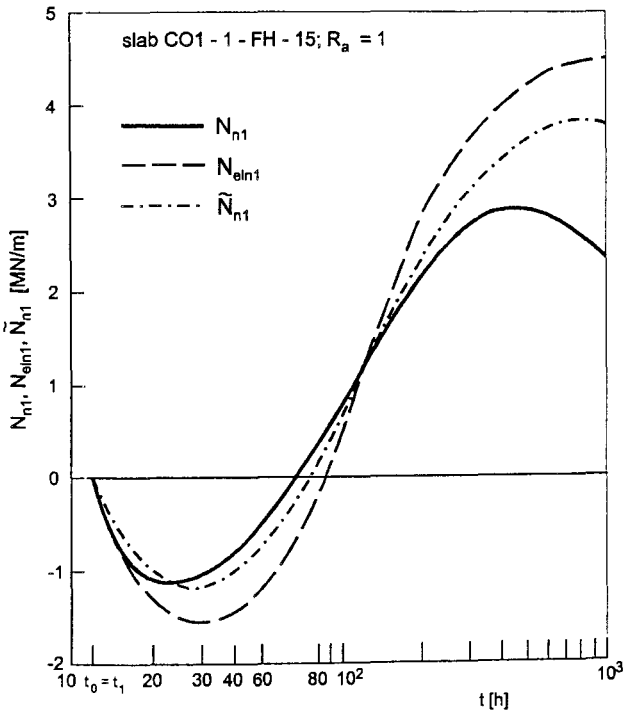

Fig. 5.7: Influence of Different Assumptions for the Material Behaviour of the Assessment of Axial Restraint (Example)

5.2.5.4 Influence of age of concrete and time under stress on bending restraint

In accordance with sec. 5.2.5.3 the influence of age of concrete and time under stress on the restraint moment was examined for the same examples. The degree of bending restraint was set to $R_{bi} = 1$. In Fig. 5.8 the dependence of the restraint moment (Eq. (5.20))

$$M_{ni} = \frac{d_c^3}{12} \sum_{i=1}^{n} \Delta\kappa_{0i} E_i \psi_{ni} R_{bi} \tag{5.29}$$

on age is plotted. It is compared with the purely elastic restraint moment ($\psi_{ni} = 1$):

$$M_{elni} = \frac{d_c^3}{12} \sum_{i=1}^{n} \Delta\kappa_{0i} E_i R_{bi} \tag{5.30}$$

and with the moment using the relationship with the factors k_{Ri} of sec. 5.2.5.2:

$$\tilde{M}_{ni} = \frac{d_c^3}{12} \sum_{i=1}^{n} \Delta\kappa_{0i}\, \tilde{E}_{ei}\, R_{bi} \tag{5.31}$$

Although the thermal curvature is negative in the entire range of age, viz. Fig. 5.5, there is a change of sign of moment which is caused by the age-dependence of modulus of elasticity E_i. Again as for axial restraint, the neglection of relaxation leads in the region of high negative curvature to a poor forecast of restraint moment. Forecast is not improved by the method with the factors k_{Ri}.

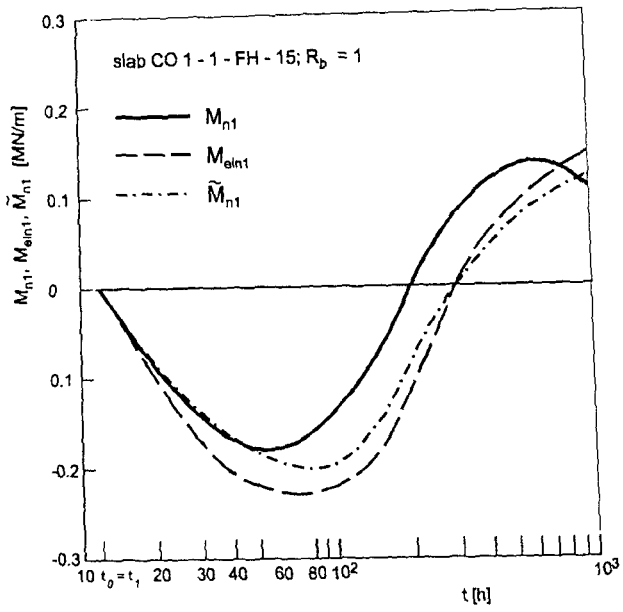

Fig. 5.8: Influence of Different Assumptions for the Material Behaviour of the Assessment of Bending Restraint (Example)

5.3 Finite Strip Method with Aging and Visco-Elastic Concrete

5.3.1 Introductory remarks

The slab is idealized as a linear cut-out with the cross-section 1 m x d_c [m]. One-dimensional heat-flow through the top and bottom face is pre-supposed. The side faces are adiabatic boundaries. The slab is described over its depth d_c by ℓ strips of the height d_c / ℓ, viz. Fig. 5.9. After formulation of the heat source of hydration and thermal boundary conditions, the age-dependent fields of temperature T(z, t), degree of hydration α, mechanical properties f_{ct}, E_{ct} etc. are incrementally computed [3, 12, 29].

Only longitudinal stresses and actions can be computed. The restraint by ground can be modelled by adjustment of the compensation place of free deformations. The soil is assumed to be an elastic material with the stiffness modulus E_s and interacting depth $d_{se} \approx d_s \approx \ell/3$. The slab is regarded as weight-less. The mechanical behaviour of concrete under short-term axial tensile stress is described by the non-linear stress-strain line shown by **Fig. B.3**. The derivation of mechanical properties and their models were described in [29] and in Appendix B. Concrete is treated as an aging and visco-elastic material.

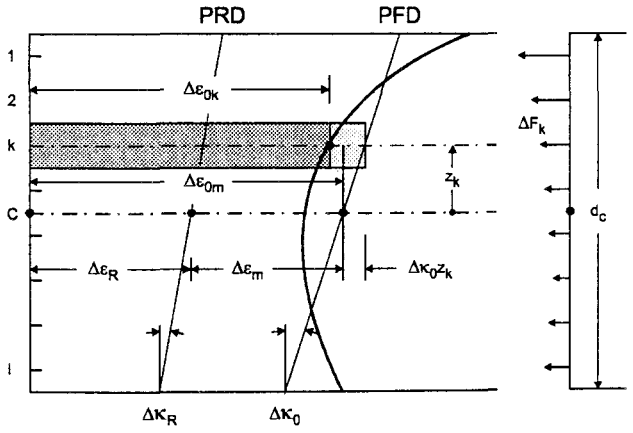

Fig. 5.9: Strip Model-Geometry, Plane of Free and of Resultant Deformation, PFD and PRD

5.3.2 Mean free deformations ε_{0m} and κ_0

Definition and on-set of free strain

Once the field of temperature is known, the free strains ε_0 and free curvature κ_0 can be determined. The free strain ε_0 of the k-th strip at the age t_i comprises the thermal component and autogenous shrinkage component. Incrementally formulated, we obtain:

$$\Delta\varepsilon_{0ki} = \Delta\varepsilon_{Tki} + \Delta\varepsilon_{aski} \,. \tag{5.32}$$

Only such free strains are of interest which cause restraint stresses. Therefore, for each strip its individual on-set of being solid matter must be found. This starting point is the first-zero stress temperature which is marked for the strip k by its initial degree of hydration α_{0k} and the associated temperature T_{0k}. Fig. 5.10 shows the relevant temperature difference $\Delta T_k(t)$ and other properties.

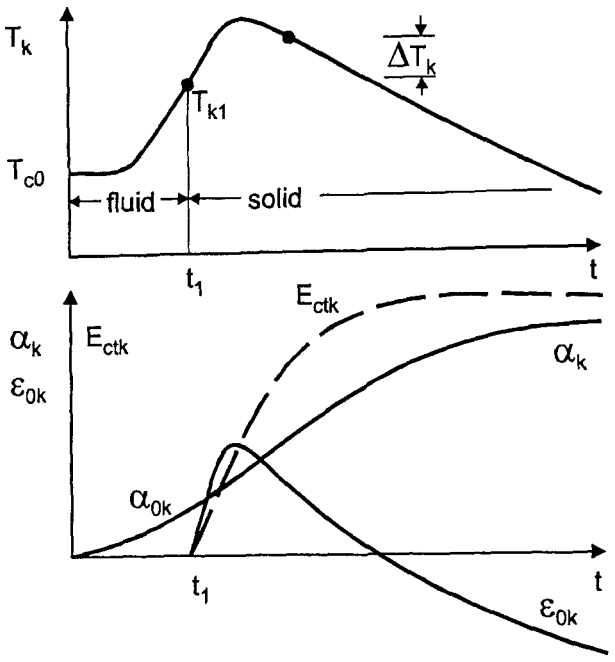

Fig. 5.10: Relevant Starting Temperature T_{k1}, Relevant Free Thermal Strain ε_{0k} and Other Properties of Layer k

Plane of free deformations

The plane of free deformations is defined by the mean free strain ε_{0m} and free curvature κ_0. The strain history of each strip can be depicted by consecutive strain steps $\Delta\varepsilon_{0ki}$ = const. commencing at $\ell = 1,...,j,...,n$. Then, we can incrementally express the mean free deformations at the on-set of strain steps at $t = t_i$ for $d_k = d_c/\ell$ (viz. App. A):

$$\Delta\varepsilon_{0mi} = \frac{\sum_{k=1}^{\ell} \Delta\varepsilon_{0ki} E_{ki}}{\ell E_{mi}} \tag{5.33}$$

$$\Delta\kappa_{0i} = \frac{\sum_{k=1}^{\ell} \Delta\varepsilon_{0ki} E_{ki} z_k}{\sum_{k=1}^{\ell} E_{ki} z_k^2} \tag{5.34}$$

These equations pre-suppose ℓ strips of constant height d_c/ℓ. Furthermore, the mean modulus of elasticity of concrete is:

$$E_i = \frac{1}{\ell}\sum_{k=1}^{\ell} E_{ki} \tag{5.35}$$

$$z_k = \frac{d_c}{2}\left(1 - \frac{2k-1}{\ell}\right) \tag{5.36}$$

$$\sum_{k=1}^{\ell} z_k = 0 \tag{5.37}$$

$$\sum_{k=1}^{\ell} z_k^2 \approx d_c^2 \frac{\ell}{12} \quad \text{for } \ell > 10 \tag{5.38}$$

With the concrete compositions of Appendix C a numerical study was performed. Fig. 5.11 and Fig. 5.12 represent examples from this study. They relate to a 1 m thick slab concrete CO1, cast in spring/fall. Two cases are compared: 1. $E_{ki} = E_i$, variation of E_{ki} over d_c is neglected, arithmetic mean strain (mod 1); 2. Non-linearity of E_{ki}, Eq. (5.33) and (5.34), is taken into account (mod 2). The computation of mean free thermal deformation must be performed with Eq. (5.33) and (5.34). The model 1 is grossly erroneous.

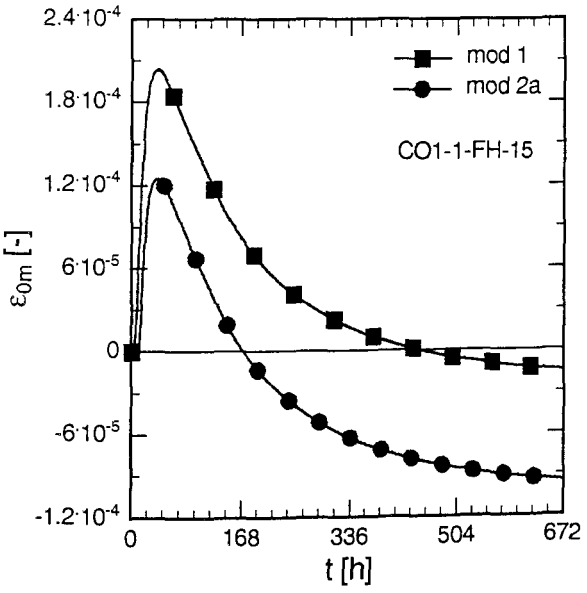

Fig. 5.11: Dependence of Mean Free Strain on Age, (Example CO1). Comparison of Different Models with Respect to Age-Dependence

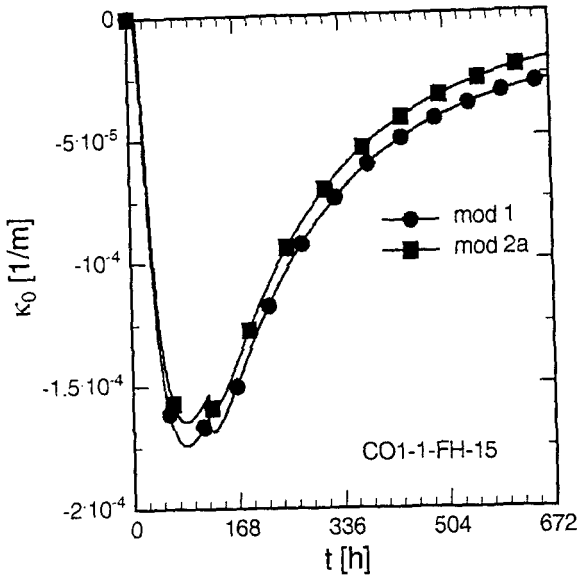

Fig. 5.12 Dependence of Free Curvature on Age, (Example CO1). Comparison of Different Models with Respect to Age Dependence

5.3.3 Compatibility and equilibrium within slab

General relations

The compatibility conditions can be expressed as follows (viz. Fig. 5.9):

$$\varepsilon_R = \varepsilon_{0m} + \varepsilon_m \tag{5.39}$$

$$\kappa_R = \kappa_0 + \kappa \tag{5.40}$$

with ε_m, axial strain caused by restraint force; ε_R, resultant strain; κ, curvature caused by restraint moment; κ_R, resultant curvature. Due to the non-linearity of stress-strain line micro-cracking strains arise above a certain stress level. In consequence, the deformations ε_m and κ consist of elastic and micro-cracking components:

$$\varepsilon_m = \varepsilon_{elm} + \varepsilon_{rm} \tag{5.41}$$

$$\kappa = \kappa_{el} + \kappa_r \tag{5.42}$$

These mean stress-dependent deformations can be determined in analogy to the mean free strain ε_{0m} and free curvature κ_0.

By the terms ε_R and κ_R the interaction of slab with soil can be taken into account. The compatibility conditions of Eq. (5.39) and (5.40) now have to be expressed for the strip k. For the on-set of free strain step $\Delta\varepsilon_{0ki}$ of layer k at t_i we obtain:

$$\Delta\varepsilon_{elki}+\Delta\varepsilon_{rki}+\Delta\varepsilon_{0ki}-\Delta\varepsilon_{Ri}-\Delta\kappa_{Ri}z_k=0 \tag{5.43}$$

From that we find the force ΔF_{ki}, with d_k height of strip k and b = 1 m:

$$\Delta F_{ki}=-d_k(\Delta\varepsilon_{0ki}+\Delta\varepsilon_{rki}-\Delta\varepsilon_{Ri}-\Delta\kappa_{Ri}z_k)E_{ki}\,b \tag{5.44}$$

with $\Delta\varepsilon_{rki}$, instantaneous, plastic cracking strain viz. from the σ-ε-relationship (Appendix B). The force ΔF_{ki} diminishes in course of the time t_n - t_i due to relaxation:

$$\Delta F_{kni}=-d_k(\Delta\varepsilon_{0ki}+\Delta\varepsilon_{rki}-\Delta\varepsilon_{Ri}-\Delta\kappa_{Ri}z_k)\,E_{ki}\Psi_{kni}\,b \tag{5.45}$$

The stress of strip k at t_i is:

$$\Delta\sigma_{kni}=\frac{\Delta F_{kni}}{d_k\,b} \tag{5.46}$$

which is the sum of uniform, linear and non-linear stress components. The restraint reactions at t_n with the on-set of restraint at t_1 are:

$$N_{n1}=\sum_{i=1}^{n}\sum_{k=1}^{\ell}\Delta F_{kni}\,, \tag{5.47}$$

$$M_{n1}=-\sum_{i=1}^{n}\sum_{k=1}^{\ell}\Delta F_{kni}\,z_k\,. \tag{5.48}$$

The total stress of strip k is found by summation of Eq. (5.44) over t_n - t_1:

$$\sigma_{kn1}=\sum_{i=1}^{n}\frac{\Delta F_{kni}}{d_k\,b}=-\sum_{i=1}^{n}(\Delta\varepsilon_{0ki}+\Delta\varepsilon_{rki}-\Delta\varepsilon_{Ri}-\Delta\kappa_{Ri}z_k)E_{ki}\Psi_{kni}\,. \tag{5.49}$$

This stress has to be compared with the effective tensile strength f_{cte} of strip k at age t_n in order to decide on the impending tensile failure (loss) of strip k. The non-linear stress component (eigenstress) is found by:

$$\sigma_{kn1,E}=\sigma_{kn1}-\sigma_{kn1,N}-\sigma_{kn1,M} \tag{5.50}$$

with

$$\sigma_{kn1,N} = \frac{N_{n1}}{d_c\, b} \quad \text{and} \tag{5.51}$$

$$\sigma_{kn1,M} = -\frac{12\, M_{n1}}{d_c^3\, b}\, z_k \tag{5.52}$$

5.3.4 Interaction with soil

Geometry and stiffness parameters

The pre-suppositions, relationships of geometry and stiffness parameters of the equivalent soil layer correspond to Fig. 5.1 and Fig. 5.2. The combined stiffness parameters at t_i are expressed by

$$S_{Di} = \frac{E_i\, d_e}{E_{se}\, d_s} \tag{5.53}$$

and

$$S_{Bi} = \frac{E_i\, I_c}{E_{se}\, I_{se}} \tag{5.54}$$

with E_{mi} acc. to Eq. (5.35); E_{se} acc. to Eq. (5.4) and I_{se} acc. to Eq. (5.5).

Compatibility, equilibrium and resultant deformations

All relationships of sec. 5.2 can be adopted. The resultant deformations however have to incrementally formulated:

$$\Delta\varepsilon_{Ri} = \frac{\Delta\varepsilon_{0mi}\left[3p^2 S_{Bi} + S_{Di}(1+S_{Bi})\right] + \Delta\kappa_{0i}\dfrac{S_{Bi}\, p\, d_c}{2}}{3p^2 S_{Bi} + (1+S_{Bi})(1+S_{Di})} \tag{5.55}$$

and

$$\Delta\kappa_{Ri} = \frac{\Delta\kappa_{0i} S_{Bi}(1+S_{Di}) + \Delta\varepsilon_{0mi} 6\, S_{Bi}\dfrac{p}{d_c}}{3p^2 S_{Bi} + (1+S_{Bi})(1+S_{Di})} \tag{5.56}$$

The deformations $\Delta\varepsilon_{mi}$ and $\Delta\kappa_i$ which are associated with restraint actions can be expressed with Eq. (5.39) and (5.40). Numerical examples will be presented in sec. 6.

5.4 Assessment of Thermal Restraint with the Subgrade Reaction Modulus Method

5.4.1 Introductory remarks

A frequently used method to assess the thermal bending restraint is the subgrade reaction modulus method SRMM (viz. sec. 3.5). Thereby, the distribution of restraint moment and degree of bending restraint along half of span $\ell/2$ can be determined dependent on the length ℓ, elastic length ℓ_e etc. The bottom face of slab is free from shear stresses, the axial degree of restraint can not be derived with the SRMM.

The TLM and SRMM are entirely independent methods. In the following section the main features of the SRMM regarding bending restraint will be presented. Reference is made to the sources [23, 24, 28, 37], in which the bending restraint of slabs on ground is dealt with in detail. It is pre-supposed that the initial settlement of slab due to its dead-weight is large enough that a lift-off from ground due to thermal restraint does not occur (more to this viz. [28]).

5.4.2 Elastic length

The bending restraint in the slab on ground, caused by the free thermal curvature κ_0, can be treated with the SRMM. For that, commercial software and tabulated values exist e.g. [11]. The slab is regarded to be supported by the k_s - springs on $\ell/2$ (Fig. 3.4). The dead-weight of slab causes the settlement, viz. sec. 3.5:

$$s = \frac{\sigma_n}{k_s} = const \tag{3.12}$$

with $\sigma_n = \rho_c d_c$. The interaction of slab and ground is described by the elastic length:

$$\ell_e = \sqrt[4]{\frac{4 E I_c}{k_s b_c}} \tag{5.57}$$

with b_c = 1 m; $I_c = b_c d_c^3/12$; E, mean elastic modulus of concrete.

5.4.3 Degree of bending restraint

In [23, 28] an explicit expression and a graph for the degree of bending restraint at x = 0 were developed. Fig. 5.13 shows the dependence of the degree of bending restraint R_{bS} on the ratio ℓ / ℓ_e. Total bending restraint at the axis of symmetry with $R_{bS} = 1$ occurs for a ratio of $\ell / \ell_e \geq 4.7$. For $\ell / \ell_e < 4.7$ restraint decreases. The restraint moments are:

$$M_0 = \kappa_0 E_e I_c \quad \text{for } R_{bS} = 1 \tag{5.58}$$

$$M = \kappa_0 R_{bS} E_e I_c \text{ for } 0 < R_{bS} < 1 \tag{5.59}$$

With Fig. 5.13 distinction can be made between long slabs with $\lambda > 4.7$ and short slabs with $\lambda < 4.7$.

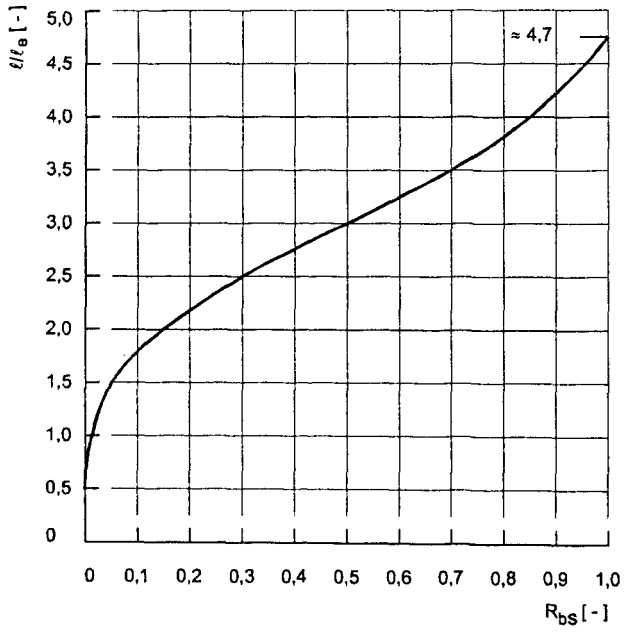

Fig. 5.13: Degree of Bending Restraint vs. Ratio ℓ / ℓ_e in the Axis of Symmetry of Slab [23, 28]

The distribution of R_{bS} over the half of span is shown in Fig. 5.14. For the stiffness modulus $E_s = 50$ MN/m^2, the degree of bending restraint is plotted over the length of 10, 25 and 50 m of slab with $d_c = 1$ m along the distance x'. For $\ell = 50$ m , total bending restraint is attained. For $\ell = 25$ m, a degree of bending restraint of $R_{bS} = 0.96$ is reached. For the 10 m slab, the restraint corresponds to only 0.15.

In Fig. 5.15 the dependence of the parameter λ on the support reaction modulus k_s for different lengths of a 1 m thick slab is plotted. The SRM was calculated as described in

sec. 3.5 for a thickness of compressible soil layer of d_s = 10 m. The horizontal line for λ = 4.7 separates the long from the short slabs. Slabs with $\ell \leq 20$ m, generally are short slabs with respect to thermal bending restraint. As the lengths of slabs increase, $\ell > 20$ m, they gradually become long slabs, also for lower values of stiffness modulus of soil. The thickness of slab exerts a great influence on the elastic length because of the $d_c^{3/4}$-power in Eq. (5.57). Because of this effect, many of the curves will for $d_c > 1$ m fall below the line λ = 4.7 and are denoted short slabs.

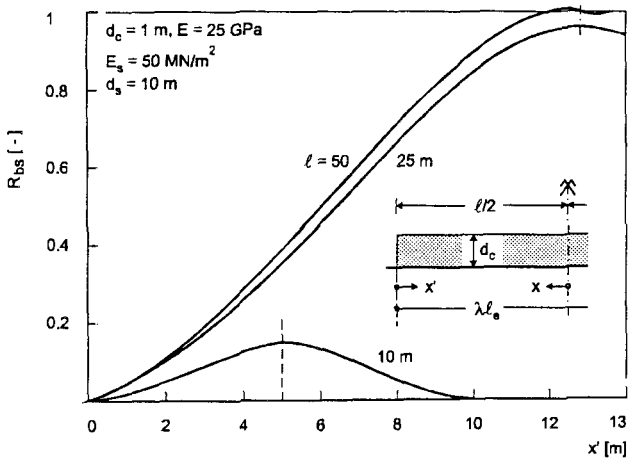

Fig. 5.14: Build-up of Thermal Bending Restraint from End of Slab Dependent on Length ℓ (Example) - SRMM

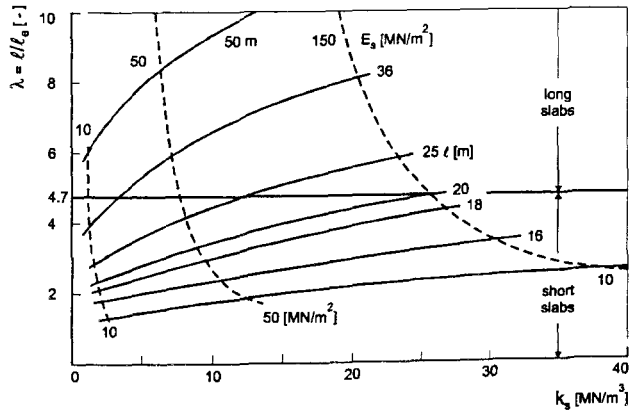

Fig. 5.15: Parameter λ Dependent on Support Reaction Modulus, Length ℓ and Stiffness Modulus for 1 m Thick Slab - SRMM

The dependence of R_{bS} at the axis of symmetry and several parameters is shown in Fig. 5.16. The curves smoothly turn into the horizontal line of total bending restraint, R_{bS} = 1 at the relevant lengths ℓ^*. Any length $\ell < \ell^*$ is associated with a lower degree of thermal bending restraint. The figure also shows that for a chosen length ℓ, the restraint increases with the stiffness modulus E_s and decreases with the thickness d_c of slab.

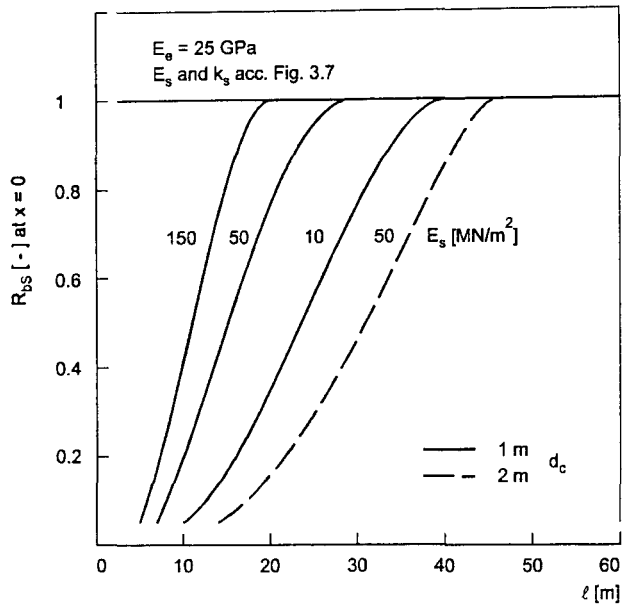

Fig. 5.16: Degree of Thermal Bending Restraint Dependent on Length of Slab and Stiffness Modulus of Soil - SRMM

5.4.4 Restraint caused by friction moment

According to the mechanical model of axial restraint (sec. 4), the friction shear stresses cause the axial restraint force on the decoupled length ($\ell/2$ - x_{be}) of

$$N_f = \tau_{fu}\left(\frac{\ell}{2} - x\right), \tag{5.60}$$

with

$$x \geq x_{be} = \frac{\ell}{2}\left(2 - \frac{4\,R_a|\varepsilon_{0m}|E_e}{\tau_{fu}\,\ell}\right); \tag{5.61}$$

and with $R_a = R_a\,(x = 0)$ from TLM and ε_{0m}, absolute value of mean free strain. Along the elastically coupled length the restraint force is:

$$N_f = \tau_{fu}\left(\frac{\ell}{2} - x - \frac{(x_{be} - x)^2}{2x_{be}}\right) \leq -R_a\varepsilon_{0m}E_e\,d_c\,. \tag{5.62}$$

The friction force is associated with the moment

$$M_f = N_f\frac{d_c}{2}\,. \tag{5.63}$$

Usually, this moment is disregarded for thin slabs. In a numerical investigation the sign, magnitude and distribution of the restraint moment were studied for the elastically bedded slab d_c / ℓ = 1.0 m / 50 m. Fig. 5.17 shows the results. Three values of the coupled length $2\,x_{be} / \ell$ were investigated: 0, 0.2 and 0.5. Contraction is presupposed. The restraint moments M_{fr} are shown on the bottom. At the axis of symmetry, they increase as the coupled length decreases. At the end region of slab, they are not influenced by the magnitude of x_{be}.

The restraint moment M_{fr} is compared with the thermal restraint moment M_{Tr} for this example: With the free curvature of $\kappa_0 = 0.15\ 10^{-3}\ m^{-1}$ the thermal restraint moment amounts to M = – 0.31 MNm. In comparison with this value, the moments due to the eccentricity of friction force are negligible.

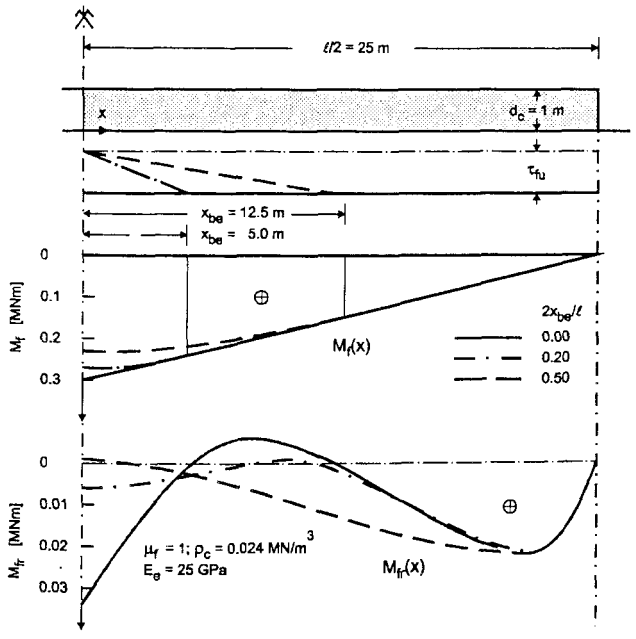

Fig. 5.17: Restraint Moment Caused by Friction Force (Example)

5.4.5 Consideration of age and relaxation of concrete in the SRMM

The SRMM as presented here is based on the theory of elasticity. The development of the mean modulus E of concrete dependent on age can be modelled and taken into account in an increment computation of restraint moment [28]. In the elastic length ℓ_e, Eq. (5.56) the modulus E_i can be inserted. Then the age-dependence of restraint moment, Eq. (5.57) and (5.58) can be evaluated with the help of Fig. 5.13. However, such procedure will lead to the overestimation of restraint moment because young concrete's visco-elasticity is not taken into account (viz. sec. 5.2.5).

The influence of relaxation can be taken into consideration as described in sec. 5.2.5.2. This may be realized with the age-adjusted effective modulus method or with the relaxation

function, dependent on the available model of visco-elastic behaviour. In addition to these ways, sec. 5.2.5.2 contains an approximative method using the factor k_{Ri}.

5.5 Comparison Between TLM and SRMM

Both, the TLM and SRMM are tarnished by several uncertainties, irrespective of the assumed age- and time-dependent behaviour of concrete. One uncertainty relates to the soil mechanical parameters E_s and k_s, which is though common for both methods. More important, however, is the uncertainty of the assumed interaction between slab and ground of both methods.

With the TLM the maximum values of degrees of restraint in the axis of symmetry of slab $x = 0$ are determined. The method pre-supposes that the slab is long enough so that the restraint actions can be built-up by shear stress. The TLM requires for that a slenderness of $\ell / d_c \geq 5$. In section 4 an approximative way was presented by which the elastically blocked length x_{be} – necessary for the build-up of restraint actions – can be assessed. Nonetheless, the dependence of degree of restraint on length of slab is presently not yet satisfactorily described. It is at the moment expressed via the effective thickness of soil layer $d_s \approx \ell / 3$.

In contrast to the TLM, the dependence of bending restraint on length of slab can be explicitly described by the SRMM. As this method depicts the slab as a "flexible mattress on bedsprings", it disregards the horizontal interaction with the ground.

Fig. 5.18 compares the maximum degrees of bending restraint according to both methods for the same set of input parameters and for two values of elastic modulus of concrete. For long slabs with $\ell \geq 4.7\ \ell_e$ the difference between the two methods is small. The difference though increases with the decrease of length ℓ ($\ell < 4.7\ \ell_e$). For short slabs the values R_{bT} of TLM are much higher than those of SRMM. It is believed that in this range of length the TLM overestimates the bending restraint, because for the build-up of plane strains a certain unknown transfer length (St. Venant) is necessary. On the other hand, The SRMM may in this range of length underestimate the bending restraint as it disregards the soil's horizontal stiffness. Because of this discrepancy, the degrees of bending restraint by both methods will be compared with the degree R_M of JSCE.

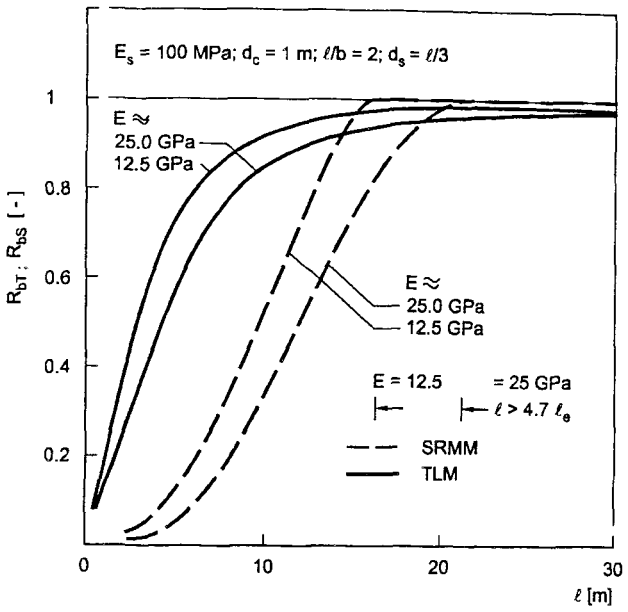

Fig. 5.18: Dependence of Degree of Bending Restraint at Axis of Symmetry on Length. Comparison of TLM and SRMM (Example)

5.6 Degrees of Restraint of JSCE and Comparison with TLM

Fig. 5.19 and Fig. 5.20 show the degrees of axial restraint R_N and bending restraint R_M acc. to the JSCE standard [13, 14]. The relationships pertain to a young concrete layer on a restraining body (soil, concrete, rock). They were obtained by elastic FEM computations for the system young concrete layer/semi-infinite restraining body pre-supposing symmetry of cross-section with respect to vertical axis of double-layer system. Furthermore, the free curvature must be κ_0 (t) ≤ 0. The axes of graphs carry both the Japanese notations and those of TLM, sec. 5. The degrees of restraint represent maximum values. With E_c, the mean elastic modulus of concrete at 28 d is defined.

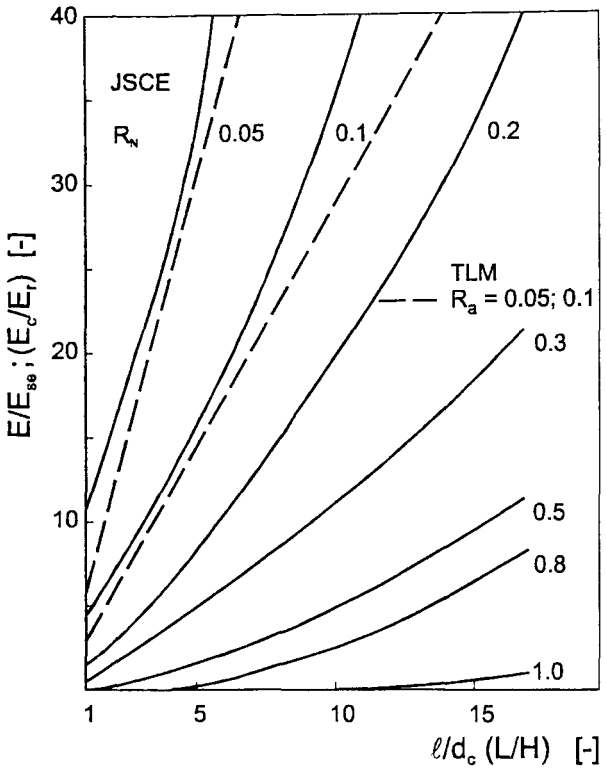

Fig. 5.19: Degree of Axial Restraint Dependent on Ratio E/E_{se} and ℓ/d_c Acc. to JSCE Standard

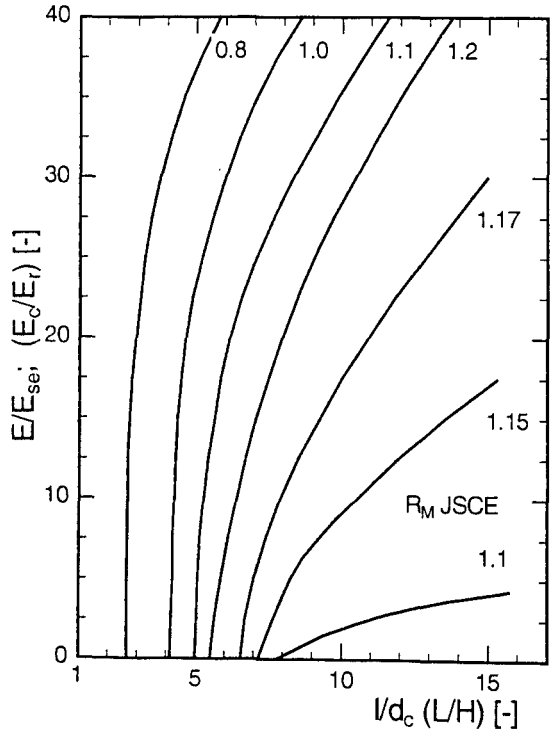

Fig. 5.20: Degree of Bending Restraint Dependent on Ratio E/E_{se} and ℓ/d_c Acc. to JSCE Standard

For the sake of comparison the following relationships from sec. 5.2.3 are presented:

$$\frac{E}{E_{se}} = \frac{E}{E_s(1+K_D)} \cong \frac{E_c}{E_r}, \tag{5.3}$$

$$K_D = \frac{E_b}{E_s}\frac{3\alpha_b d_c}{\ell}, \tag{5.64}$$

with $d_b = \alpha_b d_c$ and with R_a, Eq. (5.21)

$$R_a \approx \frac{1}{1+\frac{E}{E_{se}}\frac{3d_c}{\ell}} \cong R_N \quad . \tag{5.65}$$

In Fig. 5.21 Eq. (5.3) and (5.65) were evaluated for $25 \le E_s \le 200$ M/m^2 and $1 \le \ell/d_c \le 17$. The value E/E_s increases with ℓ/d_c and E_s. Acc. to [49] the graphs relate to E_c at the age of 28 d. Its influence on R_a is low. In Fig. 5.22 the values R_N and R_a are plotted vs. ℓ/d_s for several values of E/E_s. The lines R_a are somewhat below those of R_N. The comparison proves that the assumption of $d_{se} \approx \ell/3$ is reasonable. If one would increase the thickness of equivalent soil layer to $\ell/2$, the lines of R_a would correspond to those of R_N.

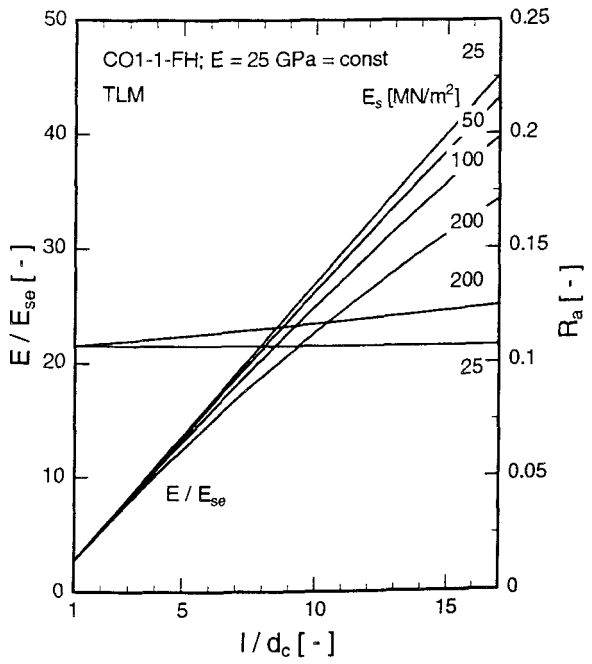

Fig. 5.21: Dependence of Ratio E/E_{se} and R_b on Ratio ℓ/d_c (Example)

In Fig. 5.23 the degrees R_M and R_b are compared. For that Eq. (5.22) is rewritten:

$$R_b \approx \frac{1}{1+\frac{E}{E_{se}}\left(\frac{3d_c}{\ell}\right)^3\left(\frac{1+K_D}{1+2K_D}\right)^2} \qquad (5.66)$$

The lines R_b exhibits the same dependence on ℓ/d_c and E/E_{se} as those of R_M though on a distinctly lower level. The degree of bending restraint of JSCE exceeds $R_M \geq 0.8$ even for ratios $1 < \ell/d_c \leq 4$. The values R_M increase with ℓ/d_c to 1.2 and from then on, they apparently level off to 1. Further explanations are not presented in [13, 14]. The transgression of the level $R_M = 1$ by 0.1 to 0.2 is in our opinion a theoretical artifact, especially for low values ℓ/d_c on common soils. One would rather expect the separation of slab's ends from ground associated with a significant decrease of R_M at $x = \ell/2$ if $\ell/d_c < 5$. Again, the curves R_b would be significantly shifted upward if the thickness of equivalent soil layer would be increased to $\ell/2$, though they would not exceed the level $R_b = 1$.

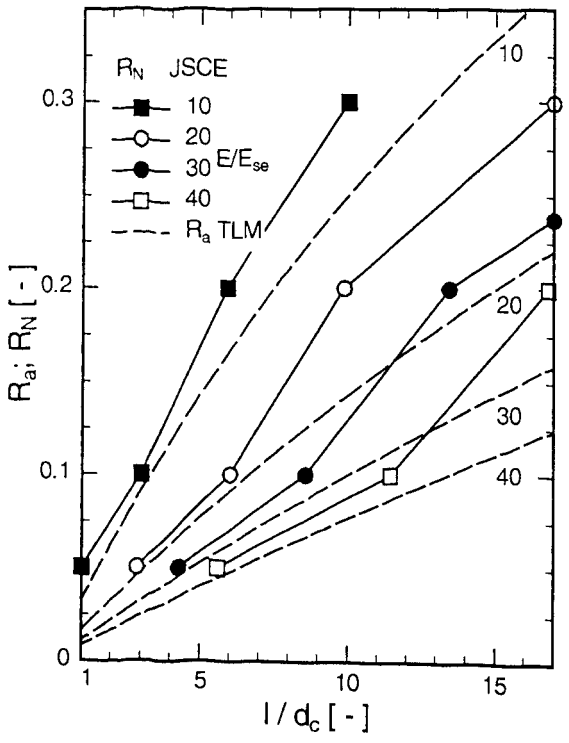

Fig. 5.22: Comparison Between Degrees of Axial Restraint Acc. JSCE Standard and TLM

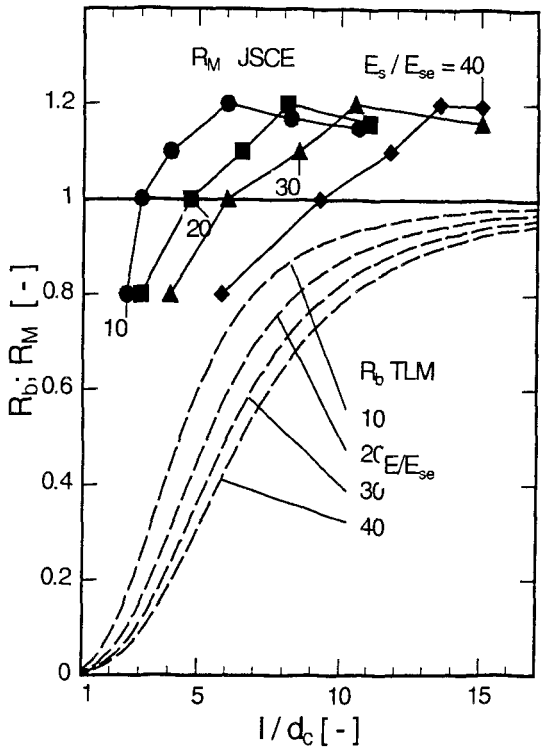

Fig. 5.23: Comparison Between Degrees of Bending Restraint Acc. JSCE Standard and TLM

5.7 Summary

In this section several engineering approaches for the assessment of restraint of slabs on ground are presented. It was shown that the disregard of concrete's visco-elastic behaviour leads to a poor forecast of restraint. An approximative method to improve the forecast was presented although this hardly satisfies. Several examples elucidate the quality of forecast by the different models. A more concise study on this will be presented in sec. 6 which contains a numerical study and examples. The authors believe that the assessment of degrees of restraint with the TLM is mechanically superior to that with the SRMM which - with significant consequence for short slabs – disregards the soil's horizontal stiffness. Furthermore, the authors think that the overshooting of R_M (JSCE) over the line 1 is not relevant for slabs on common natural soils.

6 NUMERICAL STUDY

6.1 Scope

For the concrete compositions CO1 and CO23 a numerical study of the restraint of slabs was performed. The material data for these concrete compositions, the models and parameters of material behaviour are presented in App. A and C. The OPC-concrete CO1 and GBFS-PC-concrete CO23 were comprehensively tested [33]. They distinctly differ with respect to their heat liberation Q_{pot}: CO1, 38.4 kWh/m^3, max $\Delta T_{ad} \approx 51$ K; CO23, 28.5 kWh/m^3, max $\Delta T_{ad} \approx 38$ K. The concrete CO1 is suited for cool weather periods, CO23 more for warm weather.

App. C contains the results of study. The following variables were chosen: d_c = 1 to 3 m, type of concrete, season of casting with associated values T_{c0}, T_{a0} etc. Stresses and reactions were computed with the Finite Strip Method of iBMB in conjunction with the TLM for the following age-dependent degrees of restraint with the final values of $R_{ae} = 0.15$ and $R_{be} = 0.95$. All three models 2 a, 2 b and 4 were applied to study the effect of σ-ε-line etc. The specific case is denoted by: concrete composition – d_c – season – fresh concrete temperature, e.g. CO1-1-FH-15 with FH, spring/fall.

Model 4 with the non-linear σ-ε-line in tension has the best prognostic quality. Model 2 b with the straight σ-ε-line unto f_{cte} is inferior to model 4, though often implemented in commercial software. The model 2 a is identical with model 2 b, though without creep and relaxation. Comparison of model 2 a with model 2 b renders information regarding the effective modulus. Furthermore, the FSM is compared with the SRMM. Examples will elucidate the application of models.

6.2 Temperature in Slabs

6.2.1 Distributions and maximum values

From App. C only few results are selected. Fig. 6.1 and Fig. 6.2 show for a 1 m thick slab, cast in spring/fall, the distribution of temperature dependent on age and elevation z' (z' = 0, bottom of slab). The concrete compositions CO1 and CO23 are compared. The effect of heat potential Q_{pot} is significant.

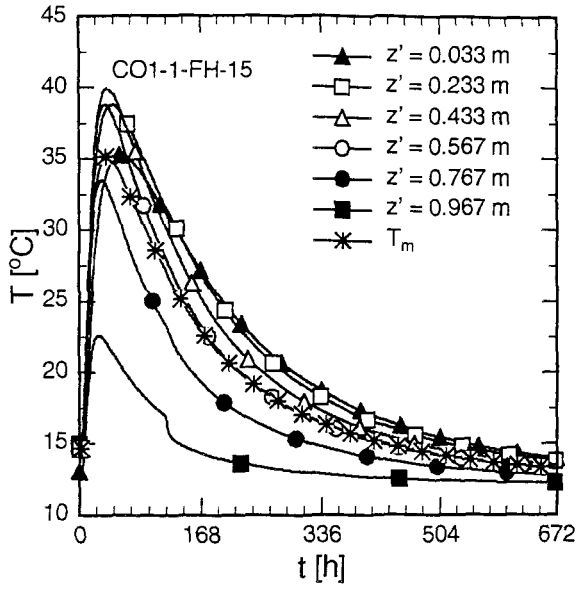

Fig. 6.1: Dependence of Temperature on Age for several Elevations. Slab CO1-1-FH-15

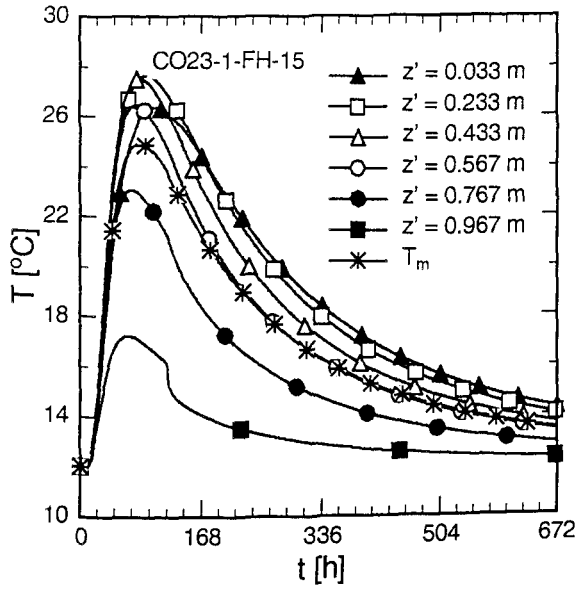

Fig. 6.2: Dependence of Temperature on Age for several Elevations. Slab CO23-1-FH-15

In Fig. 6.3 the two concrete compositions are again compared, where-by the thickness of slab is varied, casting in FH. Plotted are the maximum temperature and the maximum of mean temperature which approximately coincide with respect to time. The influence of thickness d_c and heat liberation is evident. The values max T and max T_m of the two concrete compositions are – for a specific d_c – about proportional to Q_{pot}.

The influence of ambient temperature is for CO1 depicted in Fig. 6.4, with the slab cast in spring/fall (T_{c0} = 15°C, T_{a0} = 12°C) and in summer (T_{c0} = 5°C, T_{a0} = °C). The size of temperature in summer is higher than the increase of fresh concrete and air temperature. We may conclude that the concrete temperatures can only then be realistically forecast if the heat release is known and if the temperature field for the boundary conditions of impending concrete work has been computed.

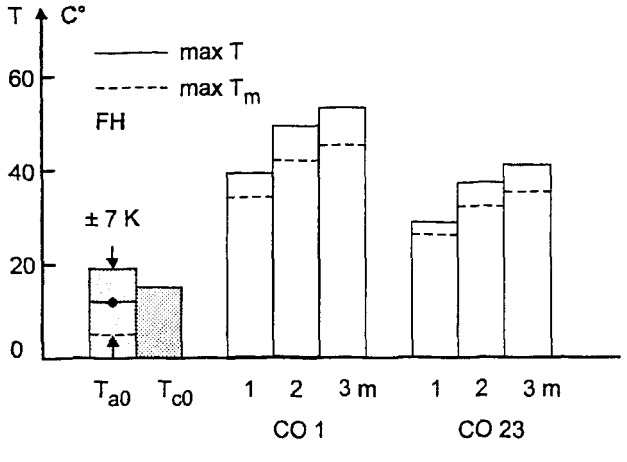

Fig. 6.3: Dependence on Maximum and Maximum Mean Temperature on Thickness of Slab for CO1 and CO23, Cast in Spring/Fall

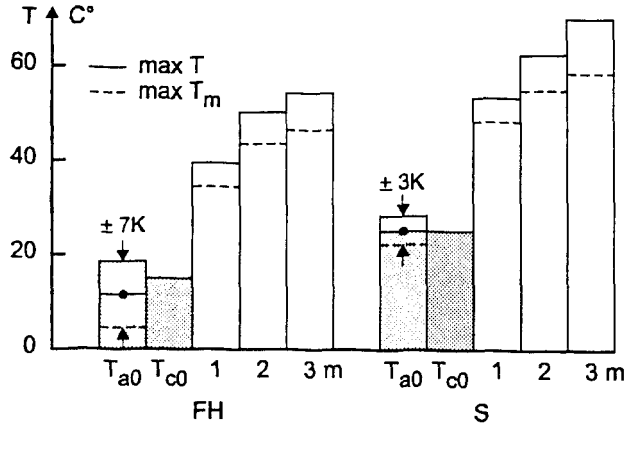

Fig. 6.4: Dependence on Maximum and Maximum Mean Temperature on Thickness of Slab, Fresh Concrete Temperature and Season of Cast (CO1-d_c)

6.2.2 Temperature differences

The occurrence of cracking is often judged by a temperature criterion [29, 37]. The computations have shown that long slabs are primarily subjected to bending restraint. The axial restraint is rather low. The possible occurrence of cracks due to eigenstresses can be assessed by the difference for the upper edge of slabs z' = d_c:

$$\max \Delta T_E (t) = \max [T_m (t) - T (d_c, t)]. \qquad (6.1)$$

Fig. 6.5 shows this difference for CO1 dependent on d_c and season of cast. According to [37], cracks due to eigenstresses can be avoided if $\max \Delta T_E \leq 15$ K. According to this rule, one would have to expect such cracks for all slab thicknesses, with the cracking probability increasing with d_c. The possible occurrence of bending cracks can be assessed with the curvature κ_0 if the degree of bending restraint is known ($M_{er} = M(\kappa_0)$):

$$\text{crit}\,\kappa_0 \approx \frac{2 f_{cte}}{E_e R_b d_c} \qquad (6.2)$$

If the value cal κ_0 exceeds crit κ_0, bending cracks will arise. In Appendix C the value of f_{ct}, E_{ct} and κ_0 are presented in graphs. The equivalent modulus is approximated by $E_e \approx 0.80\, E_{ctm}$; $R_b \approx 1$. The likelihood for cracks is greatest between the 4th and 8th day. In this range of age crit κ_0 can be expressed by

$$\text{crit}\,\kappa_0 \approx -\frac{0.15\,10^{-3}}{d_c} \quad [m^{-1}] \qquad (6.3)$$

As Appendix C shows, this value is transgressed in all cases.

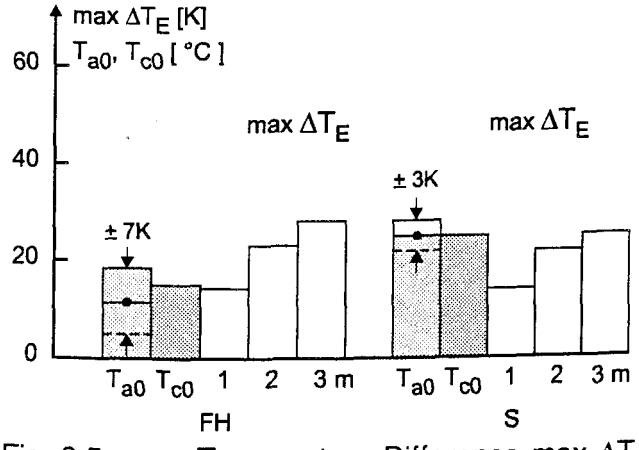

Fig. 6.5: Temperature Difference max ΔT_E Dependent on Thickness of Slab for CO1, Cast in Spring/Fall and Summer

6.3 Degrees of Restraint, Mechanical Properties and Free Thermal Deformations

6.3.1 Degrees of restraint acc. TLM

In Fig. 6.6 the degrees of restraint versus age are depicted for slab $d_c = 1$ m and the conditions noted. In this example the concrete commenced to be solid matter at $t_1 \approx 13$ h.

Hence, at that age, restraint is highest. The influence of stiffness modulus E_s of soil on R_a is small. The bending restraint increases with slab length, not so the axial restraint. After about 50 h, the age dependence of restraint has almost ended. The bending restraint exceeds the axial restraint by far. It increases with the stiffness modulus of soil. For the slab with d_c = 2 m similar results are obtained. It takes however longer until the values R_a and R_b become independent on age.

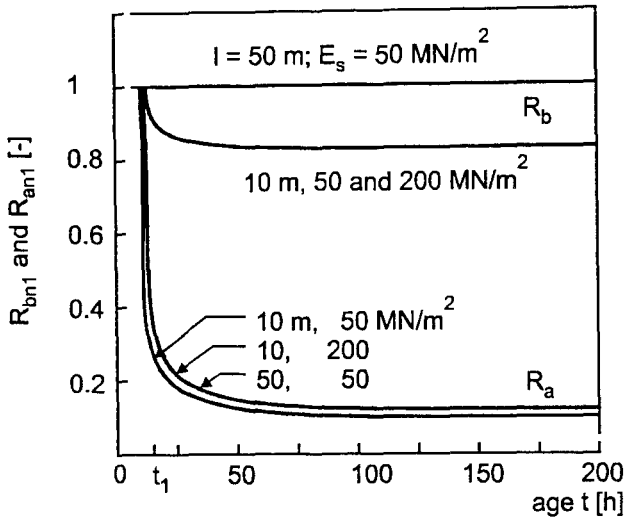

Fig. 6.6: Dependence of Degrees of Restraint of Soil on Ground on Stiffness Modulus and Age (CO1-1-FH-15)

6.3.2 Comparison of degrees of restraint for different approaches

Presently three approaches are available to assess the degree of bending restraint: TLM, SRMM and JSCE. For a specific example a comparison is performed. Thereby the maximum values R_a and R_b in the axis of symmetry of slab ($x = \ell/2$ from end) are determined. The mean modulus of concrete was assumed to be 25 GPa, as such value is relevant for the contraction phase of slab in which bending cracks may occur.

TLM

Slab:

E = 25000 MPa; ℓ = 18 m; b = 9 m; d_c = 2 m; ℓ/d_c = 9

Blinding:

E_b = 25000 MPa; d_c = 0.1 m

Soil:

E_s = 25000 MPa; d_s = 18/3 = 6 m; K_D = 2.083; E_{se} = 616 MPa; E/E_{se} = 40.5; I_{se} = 50.5 m^4/m

S_D = 13.53; $R_a \approx 0.07$

S_B = 0.535; $R_b \approx 0.65$

SRMM

$\ell/b = 2$; $d_s/b = 0.67$; $k_s \approx 45$ MN/m^3

ℓ_e = 6.2 m; $\ell/\ell_e = 2.9 < 4.7$, short slab

$R_a \approx 0.07$ e.g. from TLM

$R_b \approx 0.48$

JSCE [13, 14]

$\ell/d_c = 9$; $E/E_{se} \approx 40.5$

$R_a \approx 0.08$

$R_b \approx 1.00$

The degrees of axial restraint acc. To TLM and JSCE are similar. The bending restraint is highest for the method of JSCE and lowest for the SRMM. With the TLM an intermediate value of R_b is computed.

6.3.3 Some mechanical properties

In App. C for each case the dependencies on elevation z' and age of the Young's modulus E_{ctk} and axial tensile strength f_{ctk} are depicted. The degree of hydration varies in time and over depth of slab. Consequently, the values E_{ctk} and f_{ctk} of edge strips (especially the ones on top) lag behind those of the core of slab. The distributions of E_{ctk} and f_{ctk} are – because of this effect – slightly asymmetric: lower values on top of slab. After short time E_{ctk} and f_{ctk} are uniform.

6.3.4 Free Thermal Deformations

For the slab CO1-1-FH-15 Fig. 5.5 and Fig. 5.6 have already shown the dependence of ε_{0m} and κ_0 on age. Appendix C contains graphs of these values for all cases.

6.4 Stresses

6.4.1 Dependence of stress on age and elevation

Fig. 6.7 and Fig. 6.8 show the distribution of stresses for the slab CO1-1-FH-15. Computation was performed with model 4. It is interesting to note that the initial tensile stress in the top layer changes its sign after about 1 week. After 4 weeks the top layers are under compression and the core of slab is under rather low tension. These statements also hold true for other values of d_c and for different casting seasons.

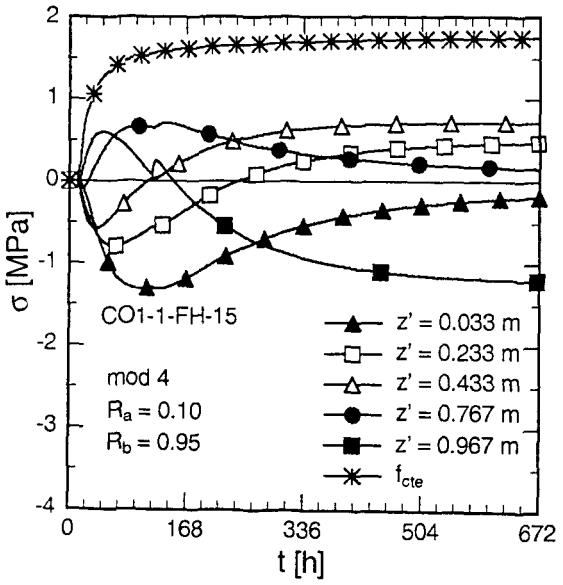

Fig. 6.7: Dependence of Stress on Age and Elevation. Slab CO1-1-FH-15, mod 4

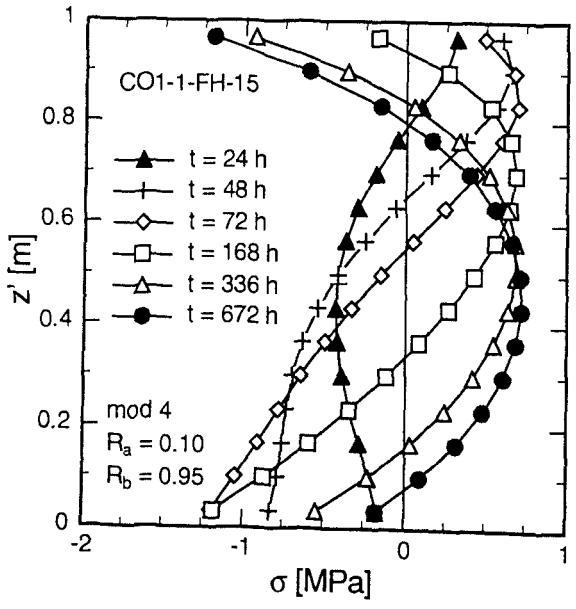

Fig. 6.8: Dependence of Stress on Elevation and Age. Slab CO1-1-FH-15, mod 4

6.4.2 Magnitude of stresses dependent on material model

The results of computation performed with the models 2 a and 2 b are depicted in Fig. 6.9 and Fig. 6.10. The elastic model 2 a renders the highest tensile stresses. The tensile stresses computed with the linear-viscoelastic model 2 b are slightly higher than those of model 4. The model 4 is associated with the lowest stresses. In all, the stresses are low and far below the effective tensile strength f_{cte}.

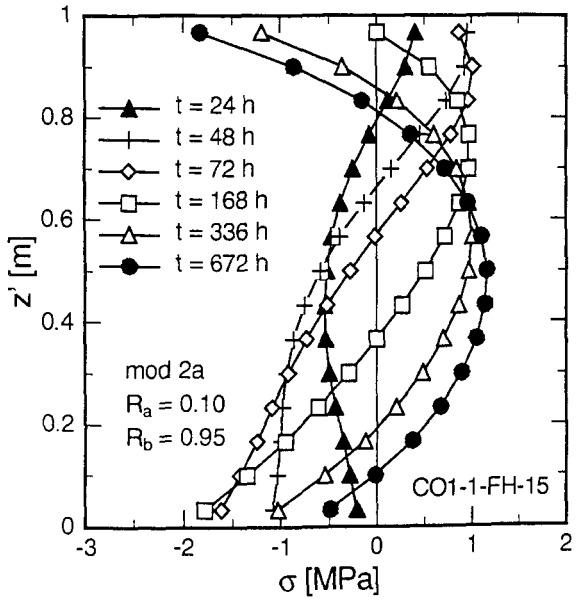

Fig. 6.9: Dependence of Stress on Elevation and Age. Slab CO1-1-FH-15, mod 2 a

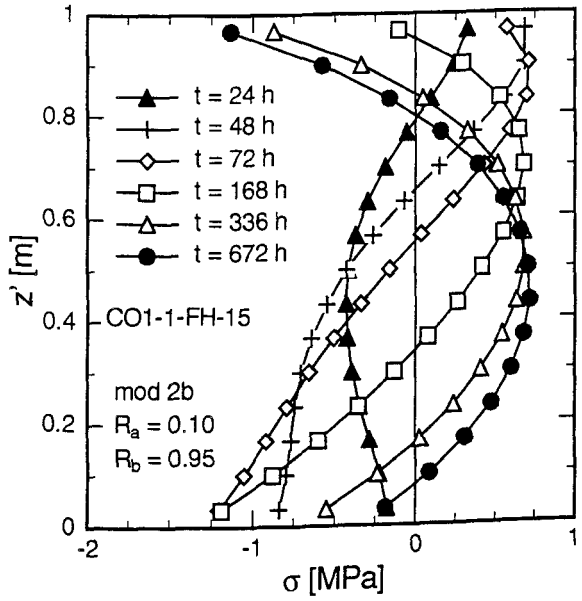

Fig. 6.10: Dependence of Stress on Elevation and Age. Slab CO1-1-FH-15, mod 2 b

The tensile stresses increase with the thickness of slab. For a thickness of 2 and 3 m, the tensile stresses computed with the models 2 a and 2 b warrant bending cracks starting at the top level of slab (Fig. C.48 and Fig. C.60). In contrast to that, stresses computed with the non-linear, visco-elastic model 4 do not entail cracks (Fig. C.62).

6.4.3 Influence of season of cast and slab thickness

The highest stresses occur if the slab is cast in summer, compare Fig. C.11 with Fig. C.25 etc., the lowest in winter. The tensile edge stresses increase with the slab's thickness. For the slabs with d_c = 2 m and 3 m the edge strips fail in tension if the models 2 a and 2 b are applied (Fig. C.48 and Fig. C.60).

6.5 Restraint Actions

6.5.1 Influence of material model

In Fig. 6.11 the dependence of restraint force and moment are plotted versus age for models 2 b and 4 for the slab CO1-2-FH-15. With model 2 a, the restraint force is overestimated in comparison with the linear-viscoelastic model 2 b. The nonlinear-viscoelastic model 4 renders the lowest force when compared with model 2 a and 2 b. It is also possible to study the effects of micro-cracking plasticity and relaxation. In addition to these models, the restraint forces were computed with the method of effective modulus. The relaxation factors used for this are shown in Fig. C.82: 0.70, 0.75 and 0.80.

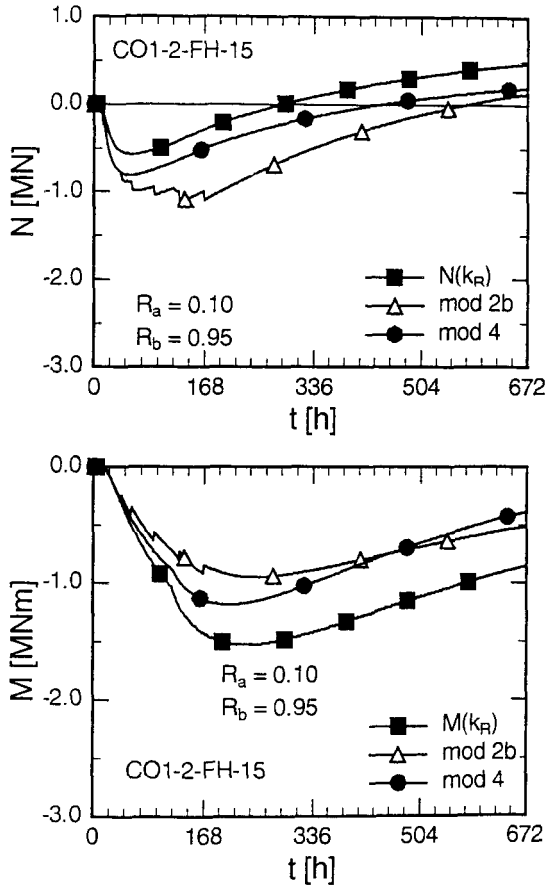

Fig. 6.11: Restraint Actions for Several Models. Slab CO1-2-FH-15

The statements made for the restraint force are also valid for the restraint moment.

6.5.2 Influence of thickness of slab

The great influence of the thickness of slab is depicted in Fig. 6.12 for model 4.

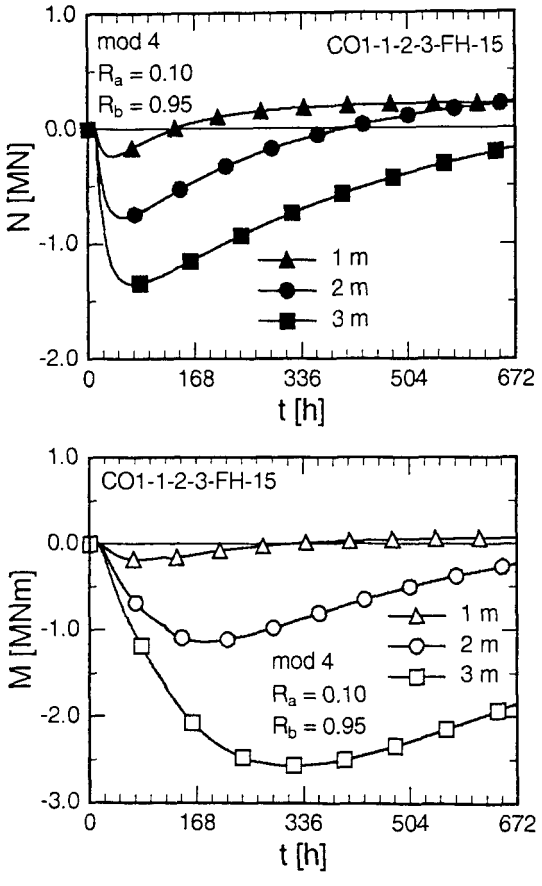

Fig. 6.12: Influence of Slab's Thickness on Restraint Actions. CO1-FH, mod 4

6.5.3 Influence of heat liberation

The influence of heat liberation potential of concrete is very significant, viz. Fig. C.65 to Fig. C.77. Fig. 6.13 presents an example for the 1 m slab cast in spring.

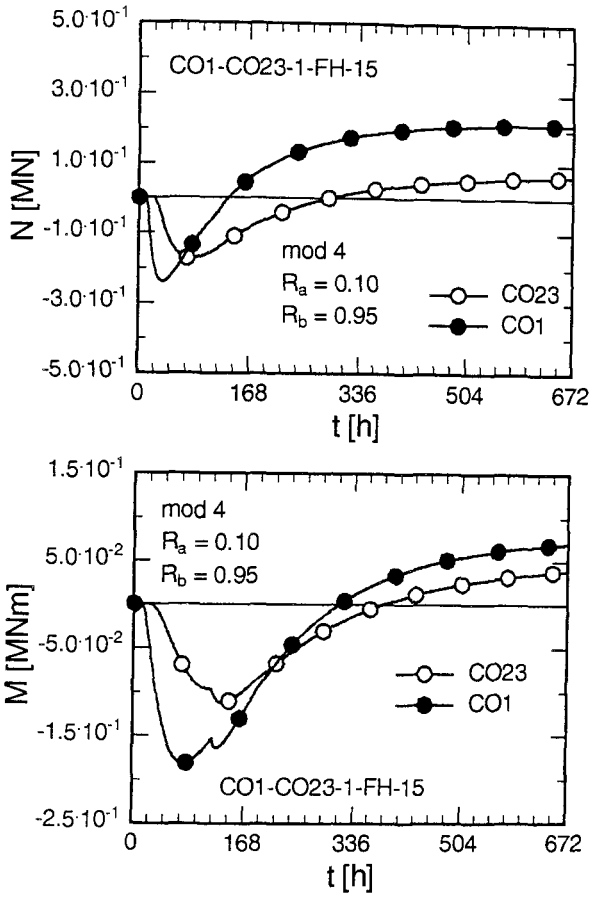

Fig. 6.13: Influence of Heat Potential of Concrete on Restraint Actions. Slabs with CO1-FH and CO23-FH, model 4

6.6 Non-Linear Stresses vs. Stresses Acc. to Beam Theory and Crack Risk

6.6.1 Comparison of stresses

With the restraint actions assessed with any of the presented models, the stress acc. to the beam theory can be computed with:

$$\sigma(z) = \frac{N}{A_c} - \frac{M}{I_c} z \qquad (6.4)$$

In Fig. 6.14 the beam stresses are compared for the slab CO1-2-FH-15 computed with the non-linear stresses of Fig. C.50 (mod 4). This comparison is performed for the ages 168 h and 336 h. The difference between the linear stress and non-linear stress, both at edges, is not significant. However, it is in essence not possible to determine realistically the edge stresses with the beam theory even if the restraint actions have been reasonably estimated (e.g. with the effective modulus method $E_{ei} = k_{Ri} E_i$).

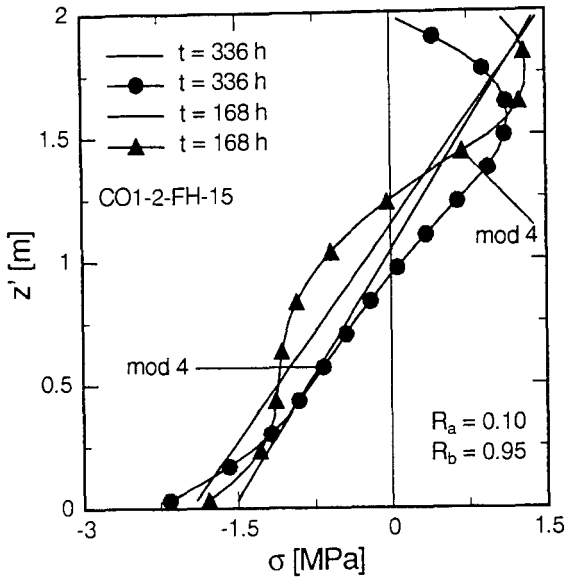

Fig. 6.14: Comparison of Non-Linear and Linear Beam Stresses. Slab CO1-2-FH-15, mod 4

6.6.2 Crack Ratio

In Fig. 6.15 the crack ratio

$$\mathrm{cal}\,C_{cr} = \frac{f_{cte}}{\mathrm{cal}\,\sigma}$$

is computed with model 4 for the elevations z' = 1.663 m and z' = 1.967 m. In these elevations the maximum non-linear stresses occur especially at early age (viz. Fig. C.49). The crack ratio is in excess of 1.5. Hence, the probability for bending cracks is very low. In contrast to that the crack ratio has dropped to 1 if model 2 b is applied (viz. Fig. C.80).

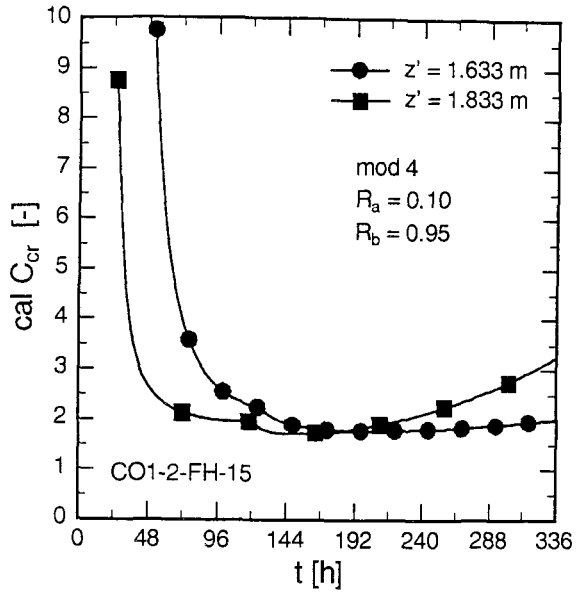

Fig. 6.15: Crack Ratio for 2 Elevations vs. Age. Slab CO1-2-FH-15, mod 4

6.7 Summary

Slabs are restrained if cast on natural soil. The degree of axial restraint is usually rather low, that of bending is much higher. Hence, if the stresses lead to cracks then the latter will be bending cracks not endangering tightness of slab. For the assessment of stresses several engineering approaches, the TLM and SRMM, and a more complex one, the FSM, are presented.

The distribution of stresses over the thickness of slab is non-linear for each of the models and at any age. The main reason for this, is the early non-linearity of the modulus of elasticity and thermal strain. As could be expected the model 2 a leads to the highest stress at the top of slab. The lowest is computed with model 4.

The restraint actions follow the same order. The elastic solution with model 2 a renders the highest actions, the non-linear model 4 the lowest ones. For approximate purpose, the method with the effective modulus renders reasonable estimations. This method is a simplification of model 2 b.

An important factor is especially the degree of bending restraint and the way of its assessment. The authors believe that with the SRMM a too low degree of bending restraint is forecast for short slabs. This is caused by the method's disregard of horizontal stiffness of subsoil. The degree of bending restraint acc. to the JSCE is based on extensive numerical

studies. It leads to the highest values R_b. The values R_b acc. to the TLM are lower. They describe the restraint for low ratios ℓ / d_c more realistically than the JSCE method.

7 RESTRAINT OF SLABS BY PILES

7.1 Problem and Scope

Massive slabs are often additionally supported by piles. The reasons for such measure are manifold. Two examples are presented: the soil layers beneath slab tend to significant subsidence which may lead to damage in the up-rising structure. Such weak layers can be "bridged" by piles reaching into lower layers of stiff ground. Piles are often used to permanently or temporarily back-anchor the foundation slab against buoyancy (e.g. deep underwater concrete slabs in Berlin, tension piles).

Dependent on many parameters, the free deformations of the hardening slab may be impeded by the piles, in conjunction with shear friction between slab and ground and also due to the elastic interaction of slab with ground. There exists commercial software to assess this problem. Thereby, usually linear elastic behaviour of concrete and soil is pre-supposed. Mostly the subgrade reaction modulus method is applied. It is the aim of this chapter to present engineering models especially for the pre-design phase to decide whether this type of restraint will and to which extent contribute to crack risk.

7.2 Deformations at Pile's Head

7.2.1 Horizontal subgrade reaction modulus

The interaction of a pile - actively loaded by a horizontal force H and/or by a bending moment M at its upper end - is usually described with the subgrade reaction modulus method [18, 19, 21]. Fig. 7.1 shows the static system of a single pile, the deformations and two possible distributions of the subgrade reaction modulus (SRM). The SRM is defined by (d_p, equivalent circular pile diameter)

$$k_s = \frac{E_s}{d_p} \cdot d_p \leq 1.0 m \,. \tag{7.1}$$

The variation of k_s along the pile's length ℓ_p can be expressed by

$$k_s(z) = k_{sR} f(z) \tag{7.2}$$

with k_{sR}, SRM at pile's foot and f(z), distribution function. According to [20] the distribution function depends on the type of soil: for non-cohesive soil a linear distribution (line 1) and for cohesive soil a constant distribution of SRM (line 2) are recommended.

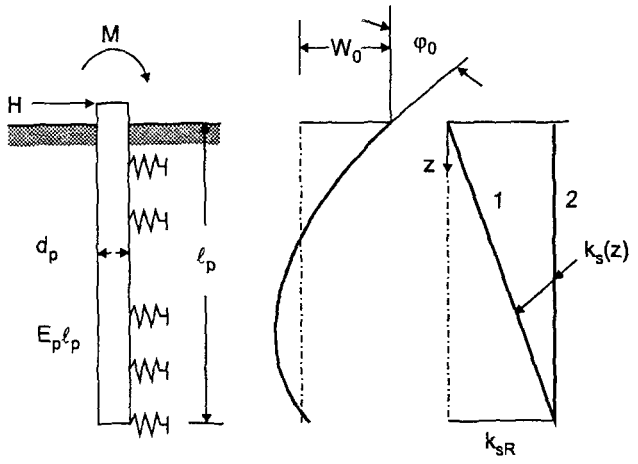

Fig. 7.1: Actively Loaded Pile, Deformations and Distribution of SRM

Table 7.1: Approximate Values of Horizontal Subgrade Reaction Modulus Dependent on Soil (from [6])

type of soil	k_{sR} [MN/m3]
washed-up sand, gravel and humus	10 - 20
peat and bog, light	5 - 10
peat and bog, heavy	10 - 15
wet loam	20 - 30
moist loam	40 - 50
dry loam	60 - 80
dry and hard loam	100
loose sand	10 - 15
fine gravel + fine sand	80 - 100
med. gravel + sand	120 - 150
coarse gravel + sand	200 - 250

As mentioned in sec. 3.5, the values found in literature for the subgrade reaction modulus SRM are widely differing and uncertain. This is even more the case for the so-called

horizontal SRM. Eq. (7.1) implies that the SRM can be derived with the stiffness modulus E_s. This was however only proved for large diameter piles with $d_p \geq 0.8$ m on basis of pile tests. The Table 7.1 presents approximate values from literature.

It should be mentioned that the first 2 to 3 m of the pile in ground decide on its deformation at the head. The SRM is reduced below level of ground water. Without in-situ geotechnical measurements, the value of SRM will be rather uncertain.

7.2.2 Relationships of Displacement and Rotation

With respect to the restraint of slab by piles, especially the horizontal displacement w_0 and angle of rotation φ_0 at the top end of pile under unit actions are of interest. In [19] the displacement and angle of end rotation were derived and tabulated for the distributions of SRM shown in Fig. 7.1. Elastic materials are pre-supposed. The main variable is the elastic length

$$\ell_0 = \sqrt[4]{\frac{4E_p I_p}{k_{sR} d_p}} \quad [\text{m}] \tag{7.3}$$

and its reciprocal value

$$\lambda_0 = \ell_0^{-1} \quad [\text{m}^{-1}]. \tag{7.4}$$

The deflection and rotation angle caused by the horizontal force H are:

$$w_{0H} = \kappa_{wH} \frac{H \ell_0^3}{E_p I_p} \quad [\text{m}], \tag{7.5}$$

$$\varphi_{0H} = \kappa_{\varphi H} \frac{H \ell_0^2}{E_p I_p} \quad [-]. \tag{7.6}$$

and for the end moment M:

$$w_{0M} = \kappa_{wM} \frac{M \ell_0^2}{E_p I_p} \quad [\text{m}], \tag{7.7}$$

$$\varphi_{0M} = \kappa\varphi M \frac{M \ell_0}{E_p I_p} \quad [-]. \tag{7.8}$$

The coefficients κ are plotted in Fig. 7.2 and Fig. 7.3 dependent on the ratio ℓ_p / ℓ_0, with ℓ_p, pile length.

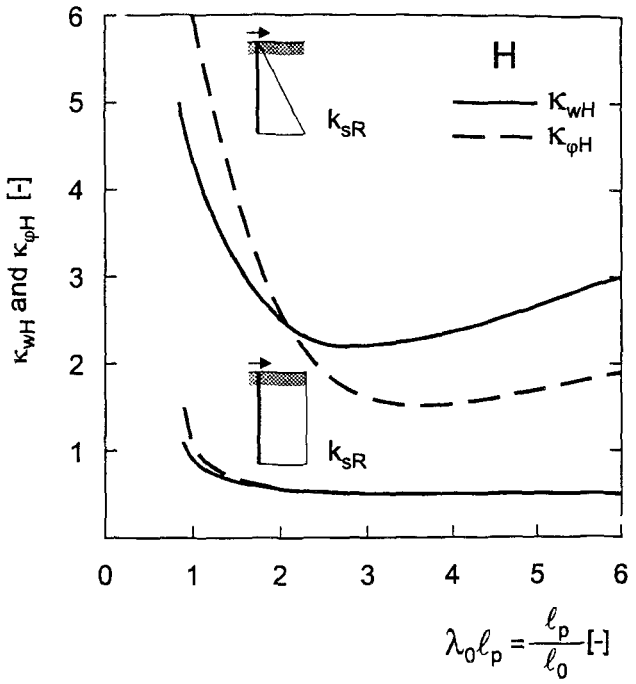

Fig. 7.2: Normalized Deflection and End Rotation of Pile Dependent on Normalized Pile Length - Load Case Horizontal Force

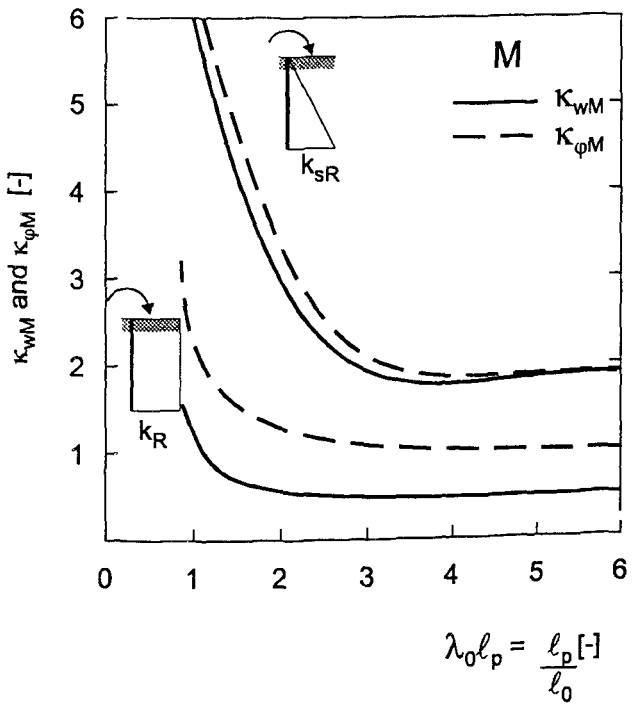

Fig. 7.3: Normalized Deflection and End Rotation of Pile Dependent on Normalized Pile Length - Load Case End Moment

The Eq. (7.5) to (7.8) can also be expressed in terms of the actions. We obtain e.g. for the horizontal force H which is for the assessment of restraint of major importance with I_p, moment of inertia of pile:

$$H = w_{0H} \frac{E_p I_p}{\kappa_{wH} \ell_0^3} \tag{7.9}$$

We may also write for Eq. (7.9):

$$H = w_{0H} \cdot c_H \,, \tag{7.10}$$

with c_H representing a spring constant:

$$c_H = \frac{E_p I_p}{\kappa_{wH} \ell_0^3} \quad \text{[MN/m]}. \tag{7.11}$$

The elastic length ℓ_0 of Eq. (7.3) can be re-written:

$$\ell_0 = \left(\frac{4 E_p I_p}{d_p} \right)^{1/4} \cdot k_{sR}^{-1/4} \tag{7.12}$$

The first term of Eq. (7.12) essentially represents the bending stiffness of the pile. It is clearly defined for a reinforced concrete or steel pile. An injection pile is a composite member with a steel profile etc. embedded in cementitious grout. It is possible to express its bending stiffness in terms of that of a circular concrete pile. In Fig. 7.4 the dependence of elastic length of the equivalent circular concrete pile (E_p = 30 GPa) on SRM for the relationship of $k_{sR}(z)$ = const. is depicted.

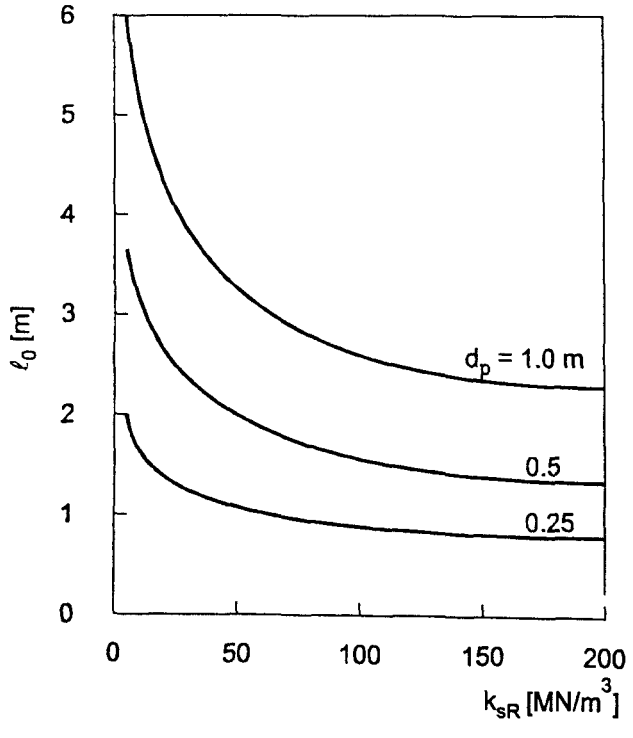

Fig. 7.4: Dependence of Elastic Length on SRM for the Equivalent Circular Concrete Pile

Although the pile length ℓ_p may differ widely in practice, we may for most cases assume that $\ell_p \geq 3$ to 4 ℓ_0. In such case, we speak of a long pile in relation to its elastic length. On basis of this, it is acceptable - as shown e.g. in Fig. 7.2 - to assume for the estimation of the restraint force a mean and constant value for the coefficient κ_{wH}: ≈ 2.5 for the linear and ≈ 0.5 for the constant distribution of SRM over depth. These values are then inserted into Eq. (7.9) and (7.11).

7.3 Restraint Caused by a Group of Piles

7.3.1 Axial restraint force (example)

Fig. 7.5 shows as an example the ground plan of a slab for a particular quadratic or rectangular arrangement of piles. The axis of symmetry at $\ell/2$ is in this example the point of zero horizontal movement in direction y. Both directions x and y are equivalent. It is at first assumed that the piles are connected to slab by hinges and that there is no friction between slab and ground. The restraint force of specific pile can be derived with Eq. (7.5) by setting for the head displacement:

$$w_{0H} = \varepsilon_{0m}\, m\, a_p \tag{7.13}$$

with a_p, distance between piles and m = 1, 2, ... ,n, number of equidistant piles within $\ell/2$. Eq. (7.13) pre-supposes a very stiff slab which does not deform under the horizontal force H. With that we obtain the horizontal restraint with Eq. (7.5) for the single pile with the distance $m\, a_p$ from the axis of symmetry:

$$H_m = \frac{\varepsilon_{0m} E_p I_p m a_p}{\kappa_{wH} \ell_0^3} \quad \text{[MN]} \tag{7.14}$$

The total force at the axis of symmetry is obtained by summation of H_m over n piles:

$$N_{pr} = \sum_{m=1}^{n} H_m = -\frac{\varepsilon_{0m} E_p I_p a_p}{\kappa_{wH} \ell_0^3} \sum_{m=1}^{n} m \tag{7.15}$$

(Remark: $\sum_{m=1}^{n} m = n(n+1)/2$).

Fig. 7.5 shows the step-wise increase of the restraint force towards the axis of symmetry. Its sign depends on that of mean free strain: $\varepsilon_{0m} < 0$; $N_{pr} > 0$ and vice versa.

7.3.2 End moment of fixed pile

If the upper end of pile is embedded in a slab of great bending stiffness, then its head can be regarded as fully fixed. The moment at pile m can be expressed by:

$$M_m = -H_m \ell_0 \frac{\kappa_{\varphi H}}{\kappa_{\varphi M}} \tag{7.16}$$

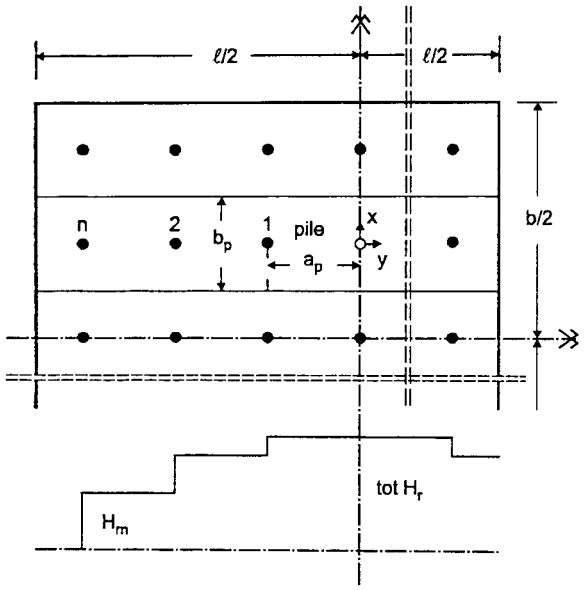

Fig. 7.5: Arrangement of Piles in Ground Plan; Development of Normal Force (Example)

As can be deduced from Fig. 7.2 and Fig. 7.3, that for $\ell_p / \ell_0 > 3$ the coefficients $\kappa_{\varphi H}$ and $\kappa_{\varphi M}$ are not differing significantly from another. Hence, the moment can approximately be expressed by

$$M_m \approx H_m \ell_0 \tag{7.17}$$

Irrespective of the sign of the strain ε_{0m}, this moment spreads linearly on both sides of the pile m. It thereby changes its sign and decreases. The neighbouring piles m+1 and m-1 will diminish the moment at pile m. Hence, we may express the resultant moment at pile m by:

$$\tilde{M}_m \approx M_m - \frac{M_{m-1} + M_{m+1}}{2}, \tag{7.18}$$

thereby neglecting the self-eliminating contributions of piles further away from the direct neighbours. By introduction of Eq. (7.14) and (7.17) into Eq. (7.18), we find that

$$\tilde{M}_m \approx \frac{\varepsilon_{0m} E_p I_p a_p}{\kappa_{wH} \ell_0^2} \left(m - \frac{m-1+m+1}{2} \right) \approx 0 \tag{7.19}$$

The slab hence can be assumed to be free of moment due to the force H_m. This is also valid for the off-set moment $H_m\, d_c/2$.

7.3.3 Influences on restraint by piles

The models of sec. 7.2 and 7.3 pre-suppose the linear-elastic behaviour of soil and uncracked concrete of piles. Besides that they describe the mean behaviour of system. They do not take several effects into consideration such as:

- Tests show that if a constant deflection w_{0H} is imposed for some time, the force H decreases significantly (viz. sec. 7.4). This "relaxation" is caused by creep of soil under lateral pressure. This effect can be taken into account by reducing the pile restraint force N_{pr}, Eq. (7.15), with a factor $\psi_{pr} = 0.6 - 0.8$ (sec. 7.4).

- The mean thermal strain ε_{0m} varies in sign and over age. Fig. 5.11 presents an example from the numerical study of Appendix C. It sets on as expansion and then turns into contraction. At early age the concrete of slab exhibits a visco-elastic behaviour, the development of ε_{0m} and κ_0 is gradual. Drying shrinkage can for slabs with $d_c \geq 50$ cm be neglected.

- If the pile cracks due to bending, its bending stiffness $E_p I_p$ will decrease. Eventual cracking can be determined with Eq. (7.16). However, this effect must not be taken into account.

- The models, sec. 7.2 and 7.3, describe the mean behaviour. Their model uncertainty is not known, unless in-situ pile tests have been performed. If such tests are not available, at least a superior value of pile force should be estimated. Thereby, the variability of SRM and model uncertainty etc. can be taken into account.

7.3.4 Parameters of restraint and degree of restraint

In order to study the different influences on the restraint of a slab due to piles alone, the piles can be depicted by an elastic spring as shown in Fig. 7.6. The spring constant c_p can be expressed with Eq. (7.11) and (7.15):

$$c_p = \frac{E_p I_p}{2.5 \cdot \ell_0^3} n \frac{(1+n)}{2} \tag{7.20}$$

By formulating the conditions of equilibrium and compatibility at the axis of symmetry, the axial restraint for N_p in the slab can be expressed (viz. Fig. 7.6)

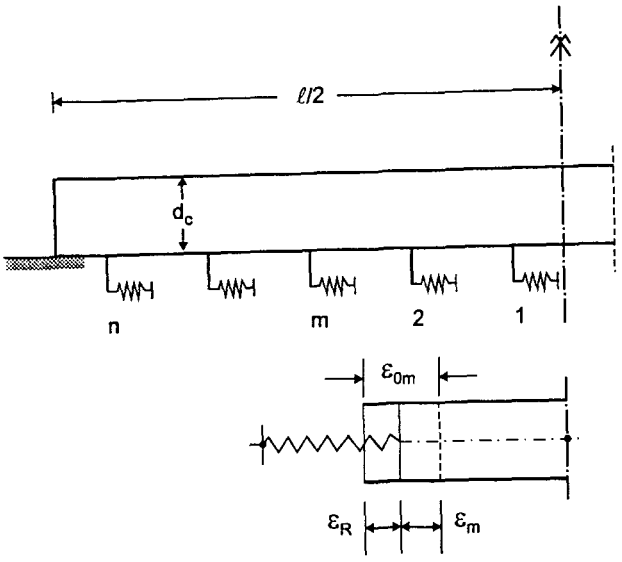

Fig. 7.6: Model for Assessment of Restraint of Slab Caused by Piles

$$N_p = -\varepsilon_{0m} E_e d_c b_p \frac{1}{1+\dfrac{E_e d_c b_p}{c_p \cdot a_p}} \tag{7.21}$$

with $N_0 = -\varepsilon_{0m} E_e d_c b_p$, total restraint force at the axis of symmetry, we obtain the axial restraint factor:

$$R_{ap} = \frac{1}{1+\dfrac{E_e d_c b_p}{c_p \cdot a_p}} \tag{7.22}$$

Eq. (7.22) contains several variables. Hence, only a few representative evaluations are performed. Fig. 7.7 shows the dependence of the degree of restraint for a slab with $d_c = 0.4$ m and a pile with $d_p = 0.4$ m and for two values of SRM dependent on number of piles. Fig. 7.7 relates to the tests described in sec. 7.4. The restraint factor increases with the number of piles and with SRM. The two values of the effective modulus E_e of concrete were included to study young and matured concrete. Only for very stiff ground and long slabs (i.e. increasing number of piles), the restraint caused by piles becomes significant. For back-anchoring injection piles and slabs of 1 to 2 m thickness, restraint is negligible. The full dot represents the measured restraint factor deduced from the tests of sec. 7.4.

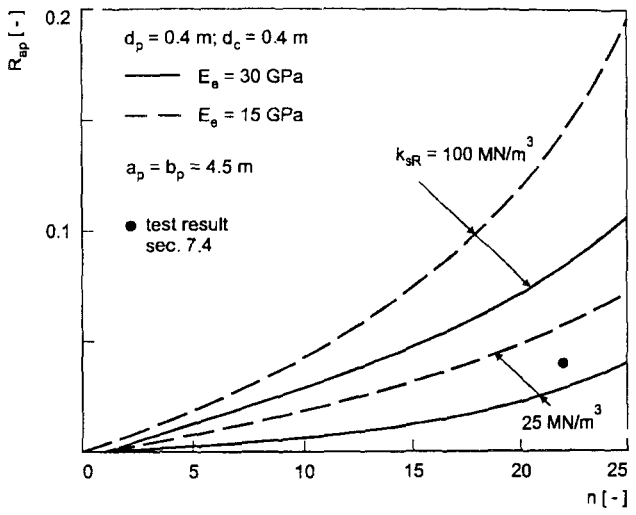

Fig. 7.7: Axial Restraint Factor R_{ap} for a Slab with $d_c = 0.4$ m and for Piles with $d_p = 0.4$ m Dependent on SRM and Number of Piles

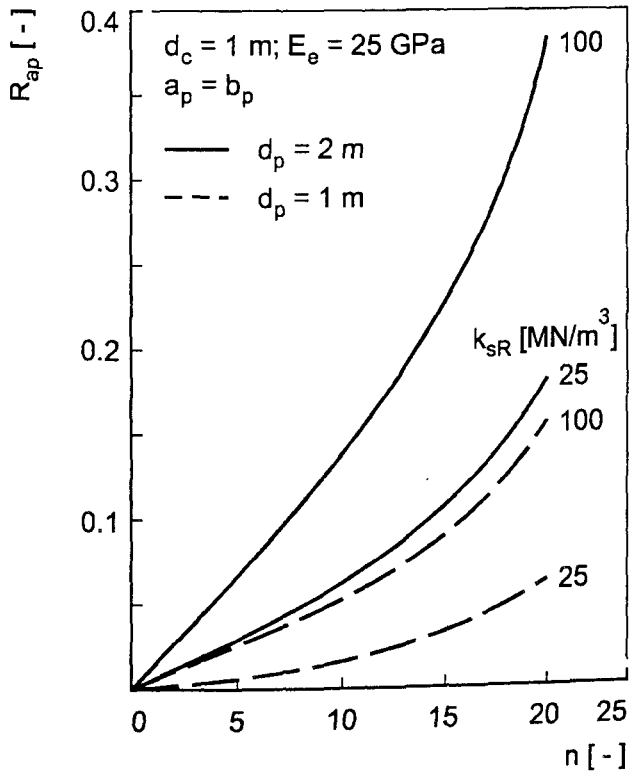

Fig. 7.8: Axial Restraint Factor R_{ap} for a Slab with $d_c = 1$ m and Pile Diameters 1 and 2 m Dependent on SRM and Number of Piles

The axial restraint caused by piles increases with the bending stiffness $E_p I_p$ and the number n of piles within half-length $\ell/2$. It should however be kept in mind that in practice the thickness of slab will increase with the increase of pile diameter. In Fig. 7.8 the restraint caused by large diameter piles of $d_p = 1$ and 2 m in a slab with $d_c = 1$ m is depicted. The magnitude of SRM is of great influence. It should be noted that for large diameter piles the number n of piles per half-length will in practice depend on several aspects such as: length ℓ

of slab (between expansion joints or in total); concrete volume of continuous pour; structural design etc. It is hence believed that the number of thick piles hardly ever exceeds 10 to 15. In such cases the degree of restraint will be rather low.

7.3.5 Combined restraint by piles and shear-friction

The slab's expansion and contraction will not only be impeded by the piles but also by the ground. The restraint by ground can be described in various ways as shown in chapters 4 and 5. In this section, the combined restraint by piles and shear-friction is dealt with (rigid-plastic shear friction). It is thereby pre-supposed that the sliding of slab occurs on the entire length $\ell/2$ and that a blocked zone x_{be} does not exist. This pre-supposition requires that the half-length of slab (in total or between expansion joints) fulfils the requirement of:

$$\frac{\ell}{2} \leq \frac{|\varepsilon_{0m}|\, E_e\, d_c\, R_a}{\tau_{fu}} \tag{4.12}$$

The numerical study of App. C shows that the mean axial strain in the contraction phase of slabs with a thickness of 1 and 2 m and for all casting seasons is in the range of:

$$\varepsilon_{0m} \geq -0.15 \cdot 10^{-3}$$

which corresponds for $t \geq t_{N2}$ to

$$\Delta T_m \leq 15\,K \quad \text{and to}$$

$$|\varepsilon_{0m}|\, E_e \leq 3.75\,MPa \quad \text{with } E_e \approx 25\ GPa.$$

Corresponding to Fig. 7.6, a model for the combined restraint is developed. With the restraint factor R_{ap} of Eq. (7.22) and with the restraint force max N_f due to shear friction of Eq. (4.5)

$$\max N_f = \frac{\tau_{fu}\, \ell\, b_p}{2},$$

the total restraint force at the axis of symmetry is expressed by:

$$N_{pf} = -\varepsilon_{0m} E_e d_c b_p R_{ap} + \max N_f \left(1 - R_{ap}\right) \tag{7.23}$$

with b_p distance between pile rows, viz. Fig. 7.5. In comparison with the restraint by piles alone, the restraint force increases. In soft ground with a SRM between 10 and 50 MN/m^3,

the reaction degree R_{ap} will remain low, especially for slabs with $d_c \leq 1$ m and piles with $d_p \leq 1$ m. If we relate Eq. (7.23) to the maximum restraint force $N_0 = -\varepsilon_{0m} E_e d_c b_p$, we obtain

$$\frac{N_{pf}}{N_0} = R_{ap} + R_{af}\left(1 - R_{ap}\right) = R_{apf} \tag{7.24}$$

with

$$R_{af} = \frac{\max N_f}{N_0} \leq 1, \tag{4.3}$$

maximum degree of restraint for plastic shear-friction at the axis of symmetry, viz. Eq. (4.5). Fig. 7.9 presents an example. The contribution of pile restraint to the total restraint force is very small. Each situation must be studied for itself in spite of the above-mentioned remarks.

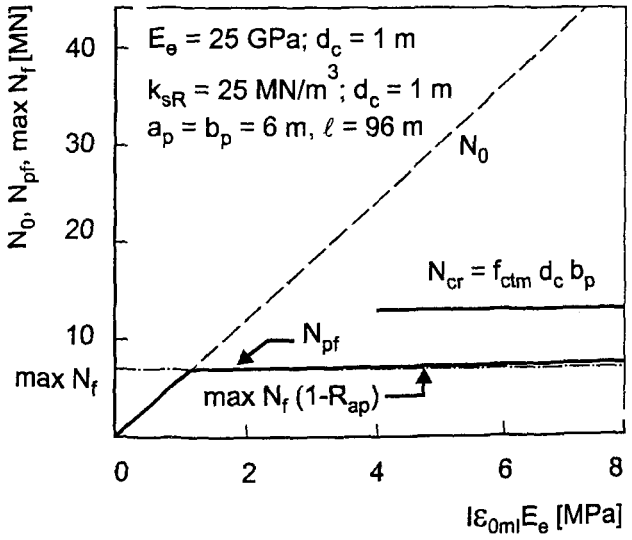

Fig. 7.9: Combined Restraint by Piles and Shear Friction (Example)

For small values of $|\varepsilon_{0m}|E_e$ and long slabs, $\ell > \ell_f$ Eq. (4.18) a blocked length x_{be} on both sides of the axis of symmetry will exist. In this length x_{be}, the piles do not cause restraint because no differential slip between slab and ground will occur. Slip will only occur in the length $(\ell/2 - x_{be})$. In this length piles will produce restraint. We may conclude in such case that the pile restraint must be smaller than for sliding on entire length $\ell/2$.

7.3.6 Additional restraint effects

The region $\pm x_{be}$ on both sides of axis of symmetry may not only be blocked to frictional sliding but will by submitted to in elastic compliance with the ground (sec. 4.5 and 5.2). It was found that the degree of axial restraint R_{ae} was rather low: 0.1 to 0.2. However the degree of

bending restraint R_{be} was high: 0.85 to 1.00. It is recommended to assume such value R_{be} for crack control also for slabs additionally restrained by piles. If the restraint expressed by R_{apf}, Eq. (7.24), exceeds the value R_{ae}, then this value should be applied for crack control.

7.4 Assessment of Force-Displacement Response by In-Situ Pile Tests-Case Study

As stressed in [18], the actual resistance of piles in soil against deformations imposed at the head of pile can only be reliably determined by in-situ testing. There exist several reports on such tests which however mostly deal with the load carrying capacity of large diameter, reinforced concrete piles with d_p = 1.0 to 2.0 m and not with the restraint response.

In [22] results of in-situ horizontal loading tests on reinforced concrete piles are reported. Fig. 7.10 shows the pile and vertical profile through ground. The piles have to support the base slab of a shipbuilding hall with the dimensions 202 x 66 x 0.4 m in ground plan. The slab was designed as joint free construction with the pile heads being fully fixed in the slab. The grid of piles varies between 3.0 x 3.0 m and 6.0 x 4.5 m. A maximum contraction strain due to temperature and drying shrinkage of -0.3 x 10-3 was expected. This value would lead to a maximum head displacement of far-end piles of about 30 mm. It was the aim of tests to derive the spring stiffness of piles for the realistic assessment of restraint stresses in the slab.

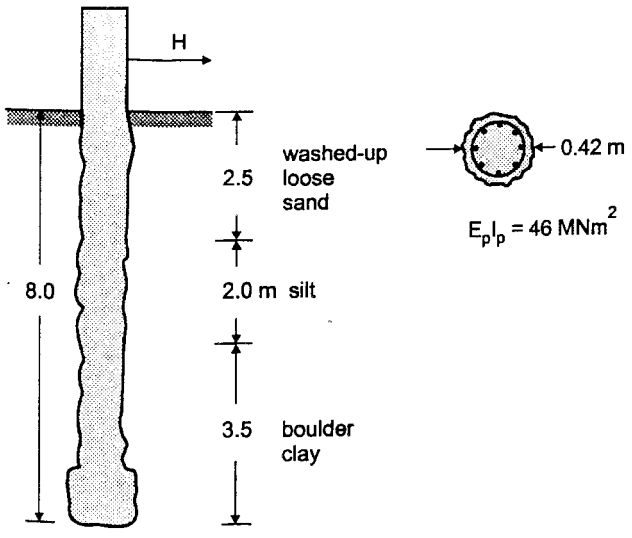

Fig. 7.10: Test Pile for Force-Deflection Measurement and Soil Layers [22]

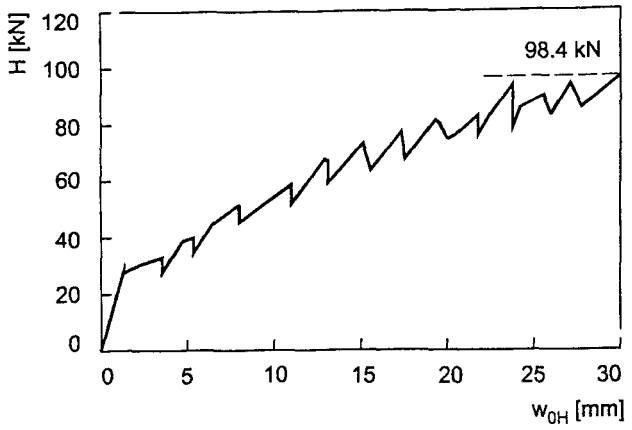

Fig. 7.11: Horizontal Force vs. Displacement in Pile Test [22]

The tests were performed on two pile pairs, i.e. 4 piles. The tests comprised three phases: displacement-controlled loading; relaxation of horizontal force H over 4 weeks under max w_0 = const. and de-loading. Only a few results are presented. Fig. 7.11 shows the loading phase of one specific pile. After a stiff initial branch, a slightly non-linear increase of the H-w_0-line can be observed. Upon reaching the maximum displacement of 30 mm, the relaxation phase began, viz. Fig. 7.12. During this phase, the force decreased to about 60 % of its initial value of 98.4 kN. This observation can be attributed to the time-dependent deformation of especially the upper-most sand layer.

The measured response line of Fig. 7.11 can be approximated by the bilinear function:

$$H = H_0 + \Delta H(w_{0H}) \tag{7.25}$$

with H_0 = 35 kN at w_{0H} = 0 and ΔH = 63.4 kN at w_{0H} = 30 mm.

Fig. 7.2 shows that for a so-called long pile with $\ell_p/\ell_0 > 3$, the value of κ_{wH} remains fairly constant: $\kappa_{wH} \approx 2.5$. With that value the elastic length ℓ_0 can be computed ($\ell_p/\ell_0 \approx 3.9$; long pile). The SRM can then be estimated with Eq. (7.1) to k_{sR} = 25 MN/m^3. Pre-supposing a pile spacing of 4.5 m and 22 piles on both sides of the axis of symmetry of the slab's side length of 201 m, we arrive at the mean total restraint force of at y = 0:

$$N_{pm} \approx n \cdot H_0 + \frac{E_p I_p}{\kappa_{wH} \ell_0^3} \varepsilon_{0m} a_p \sum_1^{22} m \approx 1.5MN \tag{7.26}$$

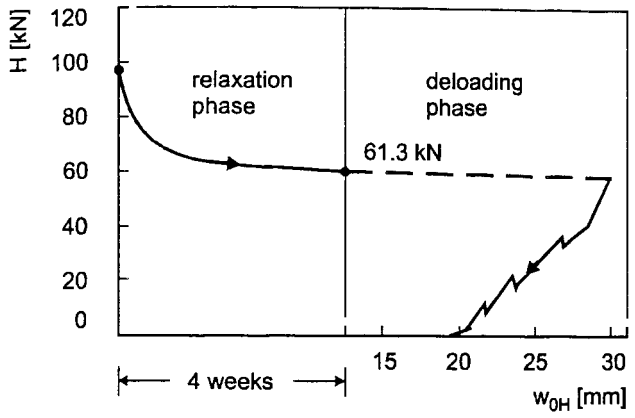

Fig. 7.12: Relaxation of Force; Force vs. Displacement during Loading

As the dilation caused by shrinkage and seasonal change of temperature is slow, relaxation of restraint force acc. to Fig. 7.12 can be taken into account by reducing N_{pm} by a factor of 0.6 to 0.8. Eq. (7.24) represents a mean value. In order to take the model uncertainty, and the scatter of soil properties etc. into consideration, N_{pm} has to be increased to a superior value sup N_p. This superior value must then be compared with an inferior value of cracking force

$$\inf N_{cr} = d_c b_p \inf f_{ct} \tag{7.27}$$

in order to assess the risk of through-cracks. This can be realized by partial safety factors, e.g.: $\gamma_p \approx 1.3$ and $\gamma_{ct} \approx 1.25$. With that we obtain:

sup N_p $\approx 1.3 \cdot 1.5$ = 1.95 MN

inf N_{cr} $\approx 0.4 \cdot 4.5 \cdot 2/1.2$ = 3.00 MN

Through-cracking is unlikely. It should be noted that in this approach, neither the friction between slab and ground nor the bending restraint caused by the free curvature were taken into account.

7.5 Summary

In many cases slabs have to founded on piles in order to transfer the dead and live loads of structure to deeper layers of stiff soil. The piles restrain the free thermal strain of concrete. In this chapter of the report, engineering models for the pre-design and design phase are presented. Thereby, the elastic behaviour of slab, pile and soil is pre-supposed. This is justified for the older pile but also for the slab. Studies have shown that the young concrete exhibits at early age on expansion. The contraction phase sets on-depending on various

parameters - at an age of 100 to 300 h. By that age, the slab's concrete has become a pre-dominantly elastic material.

The greatest uncertainty is caused by the assumption of the subgrade reaction modulus. This uncertainty can eliminated by on-site pile testing. Unless such tests are available, computations within a range of SRM are advised.

Generally, the thickness dc of slab, pile spacing a_p and diameter d_p are chosen within certain practical relation such as $a_p/d_c \approx 10 \div 15$ and $d_p \cong d_c$. Concrete piles usually exceed $d_p = 0.4$ m. Within this range, the restraint by piles is small, especially for soft soil with SRM ≤ 50 MN/m^3.

If shear-friction between slab and soil has to be taken into account, its restraint usually exceeds that by piles markedly. Injection piles (steel profile or large diameter reinforcing bars embedded in cementitious grout) for the back-anchorage of high ground water pressure on slabs are pre-dominantly tension piles. The restraint caused by such piles is usually insignificant.

8 CONCLUSIONS AND RECOMMENDATIONS

In this report several engineering models for the assessment of restraint of slabs on natural soils (not rock) are presented. For stiffness moduli soil $E_s \leq 200$ MPa, the axial restraint remains low, the bending restraint is compared with this significantly higher.

Two approaches were dealt with. The first is the three-layer model TLM, the other is the subgrade reaction modulus method SRMM. With the TLM, the axial and bending restraint can be jointly determined. With the SRMM only the bending restraint can be assessed, axial restraint must be independently determined (e.g. by TLM).

The TLM was presented in two ways: In the first approach, the restraint actions are determined with mean mechanical properties across section, mean free deformations and degrees of restraint of member, all of these parameters are age-dependent. On this basis, the restraint stress is linear over thickness of slab. The non-linearity of thermal strain can be taken into account by stress differentials added to linear stress. In the second approach, the non-linearity of all parameters across section is taken into account by the FSM, Finite Strip Method. The FSM is an amplification of TLM. The non-linear total stress can be computed. The consecutive tensile failure of strips and the redistribution of stress can be modelled. The FSM is an incremental and iterative approach.

The stresses and restraint actions depend on the in-put of mechanical properties. This aspect was studied with linear and non-linear σ-ε-lines with and without inclusion of relaxation of concrete. The results of computation with the model 4 (non-linear σ-ε-line plus relaxation) are the most realistic ones and serve as bench mark. The Appendices of report present numerous examples.

The FSM requires tedious numerics. Therefore, several approximative solutions are presented. Common to these solutions is that they follow the first approach of TLM. With these solutions, the restraint force N and restraint moment M are computed with age- and time-variant mean properties. Again, only the linear stress can be determined, viz. previous paragraphs. For the pre-planning phase, the method of effective E-modulus was investigated and compared with the incremental methods, such as model 4 and model 2 b (linear σ-ε-line with relaxation). It proved to be fairly suitable.

The FSM is compared with the SRMM. The authors believe that the SRMM underestimates the bending restraint of short slabs with $\ell < 4.7\ \ell_e$, because of its disregard of the horizontal stiffness of ground. In order to fortify this opinion, the restraint of slabs – as described by the TLM (FSM)- was compared with the approach of the Japanese Society of Civil Engineers.

The method of JSCE to assess the axial and bending restraint totally differs from that of TLM and SRMM. It can hence be used as an "independent" arbiter. The comparative study showed that the bending restraint acc. to JSCE is much higher for short slabs than that calculated with the SRMM. It also exceeds that of TRM though not significantly. However, the approach of JSCE is like the two other methods also tarnished by certain model uncertainties. It was concluded that in view of all uncertainties the TLM is at the moment the best suited method for the assessment of restraint.

9 LITERATURE

[1] Graßhoff; H.; Kany, M.: Berechnung von Flächengründungen. In: Grundbautaschenbuch, 4. Auflage, 1997, Ernst & Sohn, Berlin.

[2] Springenschmid, R. (Ed.): Prevention of Thermal Cracking in Concrete at Early Ages, State of Art Report, RILEM Report 15, Ed. & FN Spon 1998.

[3] Rostásy, F.S., Laube, M., Onken, P.: Zur Kontrolle früher Temperaturrisse in Betonbauteilen, Bauingenieur 68, S. 5-14, 1993.

[4] Kolb, H.: Ermittlung der Sohlreibung von Gründungskörpern unter horizontalem kinematischen Zwang, Diss., Universität Stuttgart, Grundbauinstitut, 1988.

[5] Petersson, D.: Stresses in Concrete Structures from Ground Restraint, Doct. Thesis, Lund Institute of Technology, 1998.

[6] Rodatz, W. (Ed.): Lecture Notes on Geotechnique and Underground Construction, 8th Edition, 1999, TU Braunschweig.

[7] Schütte, J.: Einfluß der Lagerungsbedingungen auf Zwang in Betonbodenplatten, Diss., TU Braunschweig, iBMB, 1997.

[8] Smoltzyk, U.; Netzel, D.: Flachgründungen (Fundamente, Plattengründungen). In: Grundbautaschenbuch, 4. Auflage, 1997, Ernst & Sohn, Berlin.

[9] Sommer, R.: Wasserundurchlässige Becken und Behälter in Stahlbeton, Diss., Universität-Gesamthochschule-Essen, 1993.

[10] Stief, H.: Wirkungen horizontaler Baugrundverformungen auf Bauwerke unter Annahme elasto-plastischer Stoffgesetze, Diss., TU Braunschweig, 1983.

[11] Wölfer, K.-H.: Elastically Supported Beams and Plates, Cylindrical Shells, 4th Edition, Bauverlag GmbH, 1978.

[12] Rostásy, F. S., Gutsch, A., Krauß, M.: Zwangsspannungen in massigen Betonbauteilen: Problem und Beherrschung, Braunschweiger Bauseminar 1998, TU Braunschweig.

[13] JSCE (Japan Society of Civil Engineers): Standard Specification for Design and Construction of Concrete Structures, Part 1: Design and Part 2: Construction (in English), 1986.

[14] Ibid [13], 2nd edition (in Japanese), 1995.

[15] JCI (Japan Concrete Society): A Proposal of a Method of Calculating Crack Widths Due to Thermal Stress. Committee Report September 1992 (in English).

[16] Emborg, M.; Bernander, St.: Assessment of Risk of Thermal Cracking in Hardening Concrete. ASCE, Journal of Structural Engineering, Vol. 120, No. 10, October 1994, pp. 2893-2912.

[17] Rostásy, F.S.; Henning, W.: Zwang und Oberflächenbewehrung dicker Wände, Beton- und Stahlbetonbau 4/1985, S. 108-136.

[18] Franke, E.: Pfähle. In: Grundbautaschenbuch, 5. Auflage, Teil 3, 1997, Ernst & Sohn, Berlin.

[19] Werner, H.: Biegemomente elastisch eingespannter Pfähle. Beton- und Stahlbetonbau 1970, S. 39-43.

[20] Baldauf, H.; Timm, H.: Betonkonstruktionen im Tiefbau. In: Handbuch für Beton-, Stahlbeton- und Spannbetonbau (Hrg. H. Kupfer), Ernst & Sohn, Berlin, 1988.

[21] Sherif, G.: Elastically fixed structures, Ernst & Sohn, Berlin 1974.

[22] Falkner, H.; Teutsch, M.; Klinker, H.: Horizontale Probebelastung von Ortbetonpfählen auf dem Gelände der Kvaerner Warnow-Werft (Rostock-Warnemünde), iBMB-Bericht, Mai, 1984.

[23] Nilsson, M.: Influence of Restraint in Casting Joints and in Concrete Structures on Elastic Foundation, M. Sc.-Thesis, Luleå University of Technology, No. 1998: 90 CIV (in Swedish).

[24] Bernander, St.: Beam on Resilient Ground Loaded by Bending Moments M_1 at its Ends. ConGeoAB Notes etc. Göteborg, Sweden, 1993.

[25] Bouma, A.L.: Mechanik schlanker Tragwerke, Springer Verlag, 1993.

[26] Gutsch, A.-W.; Sprenger, K.-H.: Versuche zum Werkstoffverhalten jungen Betons, iBMB, TU Braunschweig. In: iBMB-Heft 128, 1997.

[27] Onken, P.; Rostásy, F.S.: Wirksame Betonzugfestigkeit im Bauwerk bei früh einsetzendem Temperaturzwang, DAfStb-Heft 449, 1995.

[28] Nilsson, M.: Thermal Cracking of Young Concrete. Partial Coefficients, Restraint Effects and Influence of Casting Joints, Lic. Thesis, Luleå University of Technology, No. 2000: 27.

[29] Rostásy, F.S.; Krauß, M.; Gutsch, A.-W.: Computation of Stresses and Cracking Criteria for Early-Age Concrete – Methods of iBMB, Brite-Euram Project BRPR-CT-97-0437, Report, September, 2000, TU Braunschweig.

[30] Bažant, Z.: Prediction of Concrete Creep Effects Using Age-Adjusted Effective Modulus Method, Journal of ACI, April, 1972, pp. 212-217.

[31] Trost, H.: Auswirkungen des Superpositionsprinzips auf Kriech- und Relaxations-probleme bei Beton, Beton- und Stahlbeton, H. 11, S. 261-269, 1967.

[32] Chiorino, M.A.: Guidelines for the Creep Analysis of Concrete Structures: Criteria for a Code Type Formulation. In: Baustofftechnische Einflüsse auf Konstruktionen (Festschrift H. Hilsdorf), Ernst & Sohn, 1980.

[33] Gutsch, A.-W.: Stoffeigenschaften jungen Betons – Versuche und Modelle, Diss., TU Braunschweig, 1998.

[34] Westman, G.: Concrete Creep and Thermal Stresses, Doct. Thesis, Luleå University of Technology, No. 1999:10.

[35] CEB-FIP Model Code 1990, CEB Bulletin No. 203, 1991.

[36] Eurocode 2: Design of Concrete structures, Part 1: General Rules for Buildings, 07.1999 (EN 1992-1: 2000, 1st draft)

[37] Eierle, B.; Schikora, K.: Bodenplatten unter frühen Temperaturzwang – Rechen-modelle und Tragverhalten, Bauingenieur 75, Oktober, 2000, S. 671-676.

[38] HETEK: Control of Early Age Cracking in Concrete-Guidelines, The Danish Road Directorate, Report No. 120, 1997.

APPENDICES

A DERIVATION OF RELATIONSHIPS FOR THE METHOD OF IBMB

A.1 Effective Center of Cross-Section

Fig. A.1 shows the cross-section of slab. It is described by ℓ strips of constant or variable height d_k. Because the modulus of elasticity varies across the slab's depth d_c and with age, the effective center C_e of section will differ from the geometrical center C_c. This difference is expressed by the value e_i:

$$\sum_{k=1}^{\ell} z_k E_{ki} = e_i d_c E_{mi} \tag{A.1}$$

and by

$$e_i = \frac{\sum_{k=1}^{\ell} z_k d_k E_{ki}}{d_c E_{mi}} \tag{A.2}$$

with i, subscript expressing the age t_i at strain step. Furthermore,

$$d_c = \sum_{k=1}^{\ell} d_k \tag{A.3}$$

If the Young's modulus is set to $E_{ki} = E_{mi}$, then $e_i = 0$ because of

$$\sum_{1}^{\ell} z_k = 0 .$$

Studies shows that e_i vanishes with age (after 50 to 100 h). It is however also small at early age, depending on the thermal boundary conditions. It is then in the range $< 0.05\ d_c$. Hence, in the following derivations, the parameter e_i is disregarded ($e_i \approx 0$).

A.2 Free Mean Strain

By expressing the mean strain as arithmetic mean at $t = t_i$ (viz. Fig. A.2 and Fig. A.3)

$$\Delta\varepsilon_{0mi} = \frac{\sum_{k=1}^{\ell} \Delta\varepsilon_{0ki} d_k}{d_c} \tag{A.4}$$

or with the $d_k = d_c / \ell$ = const.

$$\Delta\varepsilon_{0mi} = \frac{1}{\ell} \sum_{k=1}^{\ell} \Delta\varepsilon_{0ki} \tag{A.5}$$

it is pre-supposed that the modulus of elasticity is invariant with respect to age and location. This however is not true for young concrete. Because of the non-uniformity of the modulus of elasticity across the section, the free mean strain must - at the time t_i - be expressed by:

$$\Delta\varepsilon_{0mi} = \frac{\sum_{k=1}^{\ell} \Delta\varepsilon_{0ki} d_k E_{ki}}{d_c E_{mi}} \tag{A.6}$$

with

$$E_{mi} = \frac{\sum_{k=1}^{\ell} E_{ki}}{d_c} \tag{A.7}$$

If we choose $d_k = d_c / \ell$ = const, Eq. (A.6) and (A.7) can be simplified. The total mean strain at time t_n is found by summation of increments over time beginning with $t_1,\ldots,t_i,\ldots,t_n$:

$$\varepsilon_{0mn1} = \sum_{i=1}^{n} \Delta\varepsilon_{0mi} \tag{A.8}$$

A.3 Free Curvature

The free curvature can be derived with the first-order moment around effective center, viz. Fig. A.1 and Fig. A.3. With $d_k = d_c / \ell$ = const, we obtain for the strain step at $t = t_i$, if we at first pre-suppose a constant, age-invariant modulus of elasticity:

$$\Delta\kappa_{0i} = \frac{\sum_{k=1}^{\ell} \Delta\varepsilon_{Dmi} z_k d_k}{\sum_{k=1}^{\ell} z_k^2 d_k} \tag{A.9}$$

or with $d_k = d_c / \ell$ = const:

$$\Delta\kappa_{0i} = \frac{\sum_{k=1}^{\ell} \Delta\varepsilon_{0mi} z_k}{\sum_{k=1}^{\ell} z_k^2} \tag{A.10}$$

If the aging of Young's modulus is taken into account, the first order moment is:

$$\sum_{k=1}^{\ell} [\Delta\varepsilon_{0mi} + \Delta\kappa_{0i}(z_k - e_i)](z_k - e_i)E_{ki} = \sum_{k=1}^{\ell} \Delta\varepsilon_{0ki}(z_k - e_i)E_{ki} \tag{A.11}$$

and

$$\Delta\kappa_{0i} = \frac{\sum_{1}^{\ell} \Delta\varepsilon_{0ki}(z_k - e_i)E_{ki} - \Delta\varepsilon_{0mi}\sum_{1}^{\ell}(z_k - e_i)E_{ki}}{\sum_{1}^{\ell}(z_k - e_i)^2 E_{ki}} \tag{A.12}$$

Numerical studies show that Eq. (A.12) can be simplified. The second term of the nominator of Eq. (A.12) is negligible vs. the first term, especially if the age $t_i > 16$ to 24 h. Hence we obtain with $e_i = 0$:

$$\Delta\kappa_{0i} = \frac{\sum_{1}^{k} \Delta\varepsilon_{0ki} z_k E_{ki}}{\sum_{1}^{\ell} z_k^2 E_{ki}} \tag{A.13}$$

The total curvature is obtained by summation over time:

$$\kappa_{0m1} = \sum_{i=1}^{n} \Delta\kappa_{0i} \tag{A.14}$$

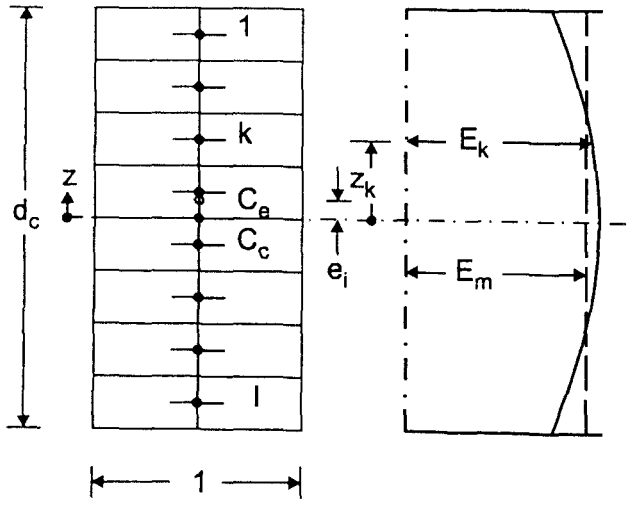

Fig. A.1: Effective Center of Gravity of Section and Distribution of Modulus of Elasticity (Schematic)

By the free deformations ε_{0m} and κ_0 the plane of free deformation PFD can be described, viz. Fig. A.3).

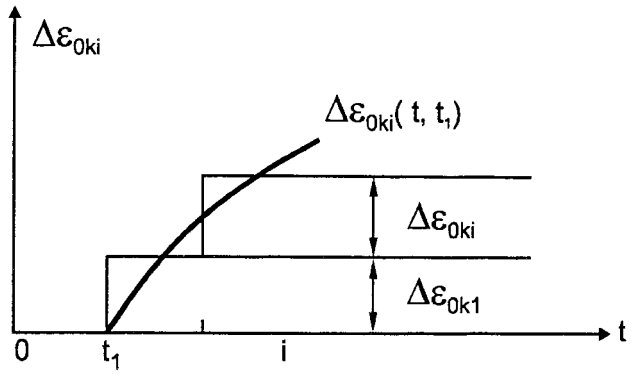

Fig. A.2: History of Mean Free Strain, Depiction by Strain Steps

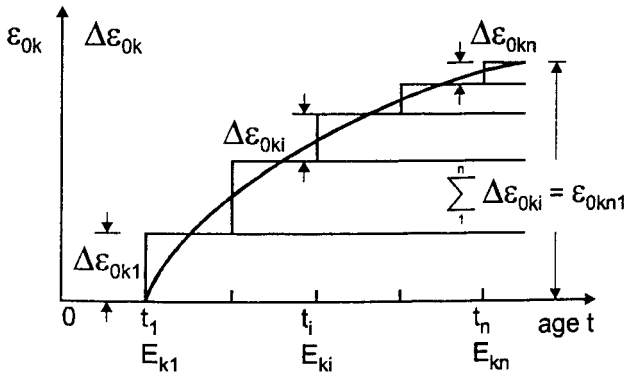

Fig. A.3: Planes of Free and Resultant Deformations

B MATERIAL MODELS

All models presented here are deterministic and pertain to the mean behaviour. Their model uncertainty is very small. Their scatter can be described by the standard Gaussian distribution coefficients of variation COV [29, 33].

B.1 Equivalent Concrete Age

$$t_e = \int_0^t \exp\frac{E}{R}\left[\frac{1}{293}-\frac{1}{273+T(t)}\right]dt \qquad (B.1)$$

with

T(t): temperature of concrete in °C at any point in structure

R: universal gas constant, R = 8.315 J/mol K

E: activation energy, $T > 20$ °C: $E(T) = 33.5$ kJ/mol

$T \leq 20$ °C: $E(T) = 33.5 + 1.47 \cdot (20 - T)$ kJ/mol

B.2 Degree of Hydration

$$\alpha(t_e) = \frac{\Delta T_{ad}(t)}{\max \Delta T_{ad}} = \exp\left(-\left[\ln\left(1+\frac{t_e}{t_k}\right)\right]^{c_1}\right) \qquad (B.2)$$

values of c_1 [-] and t_k [h] are listed in App. C.

B.3 Development of Axial Tensile Strength, Compressive Strength, Modulus of Elasticity

$$\hat{f}_{ct} = \frac{f_{ct}(\alpha)}{f_c(\alpha=1)} = \frac{f_{ct}(\alpha)}{f_{ct1}} = \frac{\alpha-\alpha_0}{1-\alpha_0} \qquad (B.3)$$

$$\hat{f}_c = \frac{f_c(\alpha)}{f_c(\alpha=1)} = \frac{f_c(\alpha)}{f_{c1}} = \left[\frac{\alpha-\alpha_0}{1-\alpha_0}\right]^{3/2} \qquad (B.4)$$

$$\hat{E}_{ct} = \frac{E_{ct}(\alpha)}{E_{ct}(\alpha=1)} = \frac{E_{ct}(\alpha)}{E_{ct1}} = \left[\frac{\alpha-\alpha_0}{1-\alpha_0}\right]^{1/2} \qquad (B.5)$$

with α_0, degree of hydration at the end of dormant phase. Values of α_0 [-], end of dormant phase, and f_{ct1}, ... etc. are listed in App. C. Fig. B.1 shows these relationships.

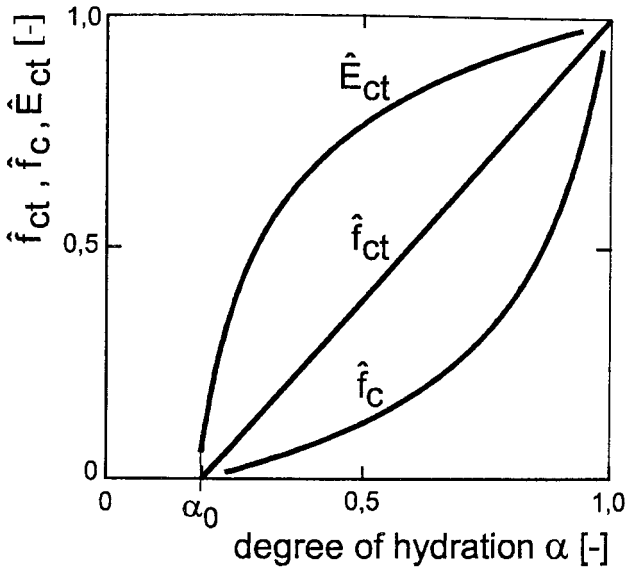

Fig. B.1: Development of Axial Tensile Strength, Compressive Strength, Modulus of Elasticity vs. Degree of Hydration

The coefficients of variation COV are: $V_{ct} \approx 0.15$; $V_c \approx 0.10$; $V_E \approx 0.10$.

B.4 Stress-Strain-Line under Tension

B.4.1 Basic model

The stress-strain line as found by many authors is schematically shown by Fig. B.2. Basis for this are strain-controlled uni-axial tensile tests on prisms or cylinders (viz. e.g. [26]). Its model is hence a research model not taking into account possible adverse effects to the strength in the actual structure. The stress-strain line can be divided into 3 sections, Fig. B.2.

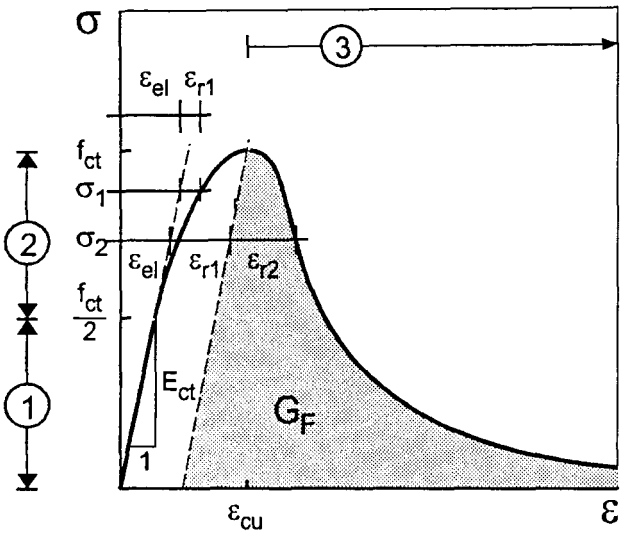

Fig. B.2: Stress-Strain-Line under Axial Tension (Schematic)

1. $0 \le \sigma \le 0.5\, f_{ct}$ $\varepsilon = \varepsilon_{el}$

$$\sigma(\varepsilon) = E_{ct} \cdot \varepsilon \tag{B.6}$$

2. $0.5\, f_{ct} < \sigma \le f_{ct}$ $\varepsilon = \varepsilon_{el} + \varepsilon_{r1}$

$$\sigma(\varepsilon) = \frac{f_{ct}}{2}\left[2 - \left(1 - \frac{\varepsilon - \varepsilon_{0.5}}{\varepsilon_{cu} - \varepsilon_{0.5}}\right)^{B}\right] \tag{B.7}$$

with

ε_{r1}, inelastic micro-cracking strain in ascending branch,

$$\varepsilon_{cu} \approx (0.35 + \alpha)10^{-4} \quad \text{with } \alpha \ge \alpha_0 \ , \tag{B.8}$$

$$\varepsilon_{0.5} = \frac{f_{ct}}{2\, E_{ct}} \ ,$$

$$B = \frac{\varepsilon_{cu} - \varepsilon_{0.5}}{\varepsilon_{0.5}} \ .$$

3. $\varepsilon \ge \varepsilon_{cu}$ $\varepsilon = \varepsilon_{el} + \varepsilon_{r1} + \varepsilon_{r2}$

ε_{r2}, inelastic strain in the descending branch due to micro-cracking; $\varepsilon_{r2} = w / \ell_{r2}$.

$$\sigma(\varepsilon_{r2}) = \frac{2}{3} f_{ct} \cdot \exp\left(-\left[\frac{\varepsilon_{r2}}{\varepsilon_a} \right]^2 \right) + \frac{1}{3} f_{ct} \cdot \exp\left(-\left[\frac{\varepsilon_{r2}}{\varepsilon_b} \right]^{1{,}01} \right) , \qquad \text{(B.9)}$$

with

$$\varepsilon_a = \frac{w_a}{l_{pr}} = \frac{3}{9+\sqrt{\pi}} \cdot \frac{G_F}{f_{ct} \cdot l_{pr}}, \quad \varepsilon_b = \frac{w_b}{l_{pr}} = \frac{27}{9+\sqrt{\pi}} \cdot \frac{G_F}{f_{ct} \cdot l_{pr}} \qquad \text{(B.10)}$$

and with w, crack opening; w_a, w_b, crack opening parameters; G_F, fracture energy; ℓ_{pr}, width of crack process zone. More to this is found e.g. in [33]

B.4.2 Stress-strain line for the concrete in the structure

Extensive investigations by iBMB [27] have shown that the effective tensile strength of concrete in the structure is lower than that of parallel laboratory specimens of the same concrete. The main reasons are: The compaction of the lab specimens is more intensive than that of the on-site concrete cast. The gradual build-up of tensile restraint stress damages the tensile strength in comparison with that of unloaded parallel lab specimens under the same curing conditions and for the same effective age. The reduction can for the mean tensile strength be expressed by:

$$f_{cte} \approx \omega_e \, f_{ct} \qquad \text{(B.11)}$$

with f_{cte}, mean effective tensile strength in structure; f_{ct}, mean tensile strength of lab specimens of the same concrete; $\omega_e \approx 0.75$, reduction factor, independent on degree of hydration.

Fig. B.3 shows that the basic model can be transformed with the reduction factor ω_e. For the sections 1 and 2 of the σ-ε-line we obtain:

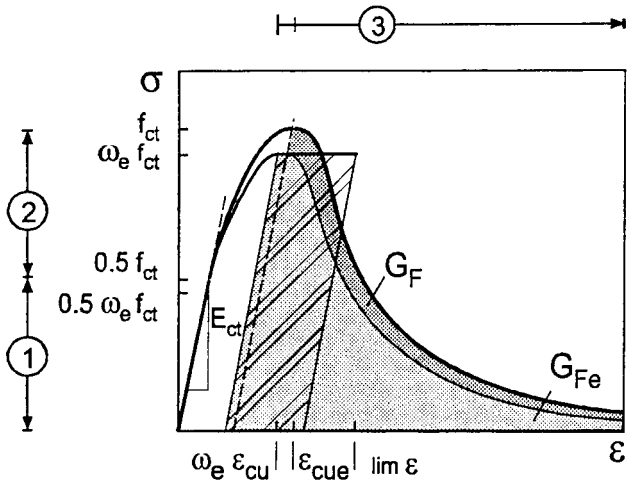

Fig. B.3: Stress-Strain-Line for Concrete in the Structure (Tension)

1. $0 \le \sigma \le 0.5\, f_{cte}$, $\varepsilon = \varepsilon_{ele}$

$$\sigma(\varepsilon) = E_{ct} \cdot \varepsilon \qquad \text{(B.12)}$$

with E_{ct} according to sec. 4.1 and Eq.(B.4).

2. $0.5\, f_{ct} < \sigma \le f_{ct}$ $\varepsilon = \varepsilon_{el} + \varepsilon_{r1}$

$$\sigma(\varepsilon) = \frac{f_{cte}}{2}\left[2 - \left(1 - \frac{\varepsilon - \varepsilon_{0.5e}}{\varepsilon_{cu} - \varepsilon_{0.5e}}\right)^{B_e}\right] , \qquad \text{(B.13)}$$

with

ε_{r1}, inelastic micro-cracking strain in ascending branch,

$$\varepsilon_{cue} \approx \omega_e\, \varepsilon_{cu} = 0.75\,(0.35 + \alpha)10^{-4} \quad \text{with } \alpha \ge \alpha_0 \qquad \text{(B.14)}$$

$$\varepsilon_{0.5e} = \frac{f_{cte}}{2\,E_{ct}} \quad [-]$$

$$B_e = \frac{\varepsilon_{cue} - \varepsilon_{0.5e}}{\varepsilon_{0.5}} \equiv B$$

3. $\varepsilon \ge \varepsilon_{cue}$ $\varepsilon = \varepsilon_{el} + \varepsilon_{r1} + \varepsilon_{r2}$

The descending branch of σ-ε-line can be formulated as shown in sec. B.4.1. The total fracture energy in the structure can be expressed by:

$$G_{Fe} \approx \omega_e f_{ct}\, \omega_e \varepsilon_{r2} l_{pr} = \omega_e{}^2 G_F \,. \tag{B.15}$$

The stress-strain line in the descending branch is then:

$$\sigma(\varepsilon_{r2}) = \frac{2}{3}\,\omega_e\, f_{ct} \cdot \exp\left(-\left[\frac{\varepsilon_{r2}}{\varepsilon'_a}\right]^2\right) + \frac{1}{3}\,\omega_e\, f_{ct} \cdot \exp\left(-\left[\frac{\varepsilon_{r2}}{\varepsilon'_b}\right]^{1{,}01}\right), \tag{B.16}$$

with

$$\varepsilon'_a = \omega_e\, \varepsilon_a = \frac{\omega_e\, w_a}{l_{pr}} = \frac{3}{9+\sqrt{\pi}} \cdot \frac{\alpha^2\, G_F}{\alpha f_{ct} \cdot \ell_{pr}}, \qquad \varepsilon'_b = \omega_e\, \varepsilon_b = \frac{\omega_e\, w_b}{l_{pr}} = \frac{27}{9+\sqrt{\pi}} \cdot \frac{\alpha^2\, G_F}{\alpha\, f_{ct} \cdot \ell_{pr}} \tag{B.17}$$

B.4.3 Tensile failure criterion

Concrete is in axial tension an elasto-plastic material due to micro-cracking strains ε_r. Hence, for the formulation of a failure criterion, the failure strain of concrete would have to be the relevant property. The fracture energy $G_F(\alpha)$ depicts the total plastic deformational work. Acc. to [26, 33] it is for $\alpha = 1$ in the range of $G_{F1} \approx 0.17$ N/m for a maximum grain size of 32 mm.

For the formulation of a tensile failure criterion, it is proposed not to entirely exploit the available fracture energy $G_{fe}(\alpha)$. Inevitable defects in the concrete member (inhomogeneties, fine superficial early shrinkage cracks, surface-near reinforcing bars as crack raises etc.) and the scatter of tensile strength are weakening factors. It is proposed to replace the descending branch of σ-ε-line by a stress-block with the limit fracture energy:

$$\lim G_{Fe} = \eta\, \varepsilon_{cue}\, f_{cte}\, l_{pr},$$

with $l_{pr} \approx 2.5 \max d_k$ and with $\eta \geq 0$, integer. The limit failure strain is then:

$$\lim \varepsilon_{cue} = \varepsilon_{cue}\,(1+\eta)$$

The stress computations of App. C were preformed with $\eta = 0$. Hence only the sections 1 and 2 of the stress-strain are used, which is a rather conservative approach.

In the future deliberations will become necessary in order to determine the factor η. For $\eta = 1$ about 1/6 of the total fracture energy is exploited. The crack opening w would then be in the range of 5 to 10 µm.

B.4.4 Stress-strain-line under compression

As the compressive strength is about five to ten time higher than the tensile strength, the stress-strain line under compression is approximated with the Young's modulus

$$E_{cc}(\alpha) \approx E_{ct}(\alpha) \ . \tag{B.18}$$

The non-linearity under compression may be approximated by using Eq. (B.4) also for compression.

B.4.5 De- and reloading under tension and compression

Detailed models for de- and reloading in the descending branch of the stress-strain-line are presented in literature (viz. in [33]). A phenomenological approximation is shown in Fig. B.4.

If the stresses turn into compression, the cracks will close again and the inelastic cracking strain is set to zero. For loading under compression the Young's modulus acc. sec. B.4.4 can be used. In this report the de- and reloading is assumed to follow on the straight line with the slope $E_{ct}/1$.

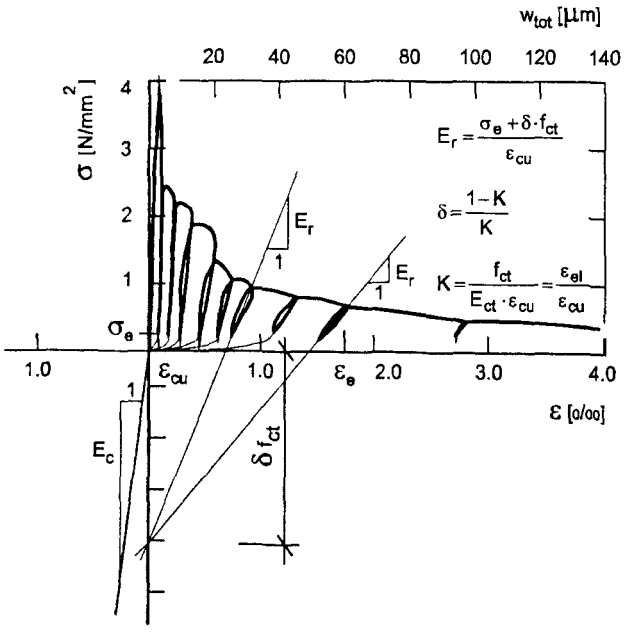

Fig. B.4: Model of Cyclic De- and Reloading in the Descending Branch of the Stress-Strain-Line under Tension

B.4.6 Creep and relaxation

B.4.6.1 Creep function

$$\varphi(t-t_1,t_1)=\frac{\varepsilon_c(t,t_1,\alpha_1,T(t,t_1))}{\varepsilon_{el}(t_1)}=P_{1c}(\alpha_1)\left[\frac{t_{el}-t_{el1}}{t_c}\right]^{P_{2c}(\alpha_1)}, \tag{B.19}$$

with

$$P_{1c}(\alpha_1)=a_{1c}+b_{1c}\,\alpha_1 \tag{B.20}$$

$$P_{2c}(\alpha_1)=a_{2c}+b_{2c}\,\alpha_1 \tag{B.21}$$

B.4.6.2 Relaxation function

$$\psi(t-t_1,t_1)=\frac{\sigma(t,t_1,\alpha_1,T(t,t_1))}{\sigma(t_1)}=\frac{1}{1+P_{1r}(\alpha_1)\left[\frac{t_{el}-t_{el1}}{t_c}\right]^{P_{2r}(\alpha_1)}}, \tag{B.22}$$

with

$$P_{1r}(\alpha_1)=a_{1r}+b_{1r}\,\alpha_1 \tag{B.23}$$

$$P_{2r}(\alpha_1)=a_{2r}+b_{2r}\,\alpha_1 \tag{B.24}$$

Equivalent time under load for taking the temperature effect on the visco-elastic behaviour into account:

$$t_{el}=\int_0^t \exp\frac{E_v}{R}\left[\frac{1}{293}-\frac{1}{273+T(t_i)}\right]dt_i, \tag{B. 25}$$

$$t_{el1}=\int_0^{t_1} \exp\frac{E_v}{R}\left[\frac{1}{293}-\frac{1}{273+T(t_i)}\right]dt_i \tag{B.26}$$

with E_V = 50.000 J/mol.

B.4.6.3 Data and parameters

The data and parameters to evaluate these relationships are listed in Appendix C.

C DATA FOR COMPUTATIONS AND EXAMPLES

C.1 Concretes

Table C.1: Concrete Compositions

	notation	unit	CO1	CO23
cement type	CEM	-	I 32.5 R	III / B 32.5
cement content	C	kg/m^3	270	280
slag content	SL	kg/m^3	-	-
fly ash content	FA	kg/m^3	60	80
water content	W	kg/m^3	175	150
siliceous aggr. content	A 0/16 A-B 0/32	kg/m^3	1849	 1855
super plasticizers	FM	kg/m^3	2.7	2.1
plasticizers	BV	kg/m^3	-	1.0
retarder	VZ	kg/m^3	-	1.0
consistence	spread	-	KR	KF
strength class 20 cm cubes	B	MPa	25	25

C.2 Geometry

Strips of slab of width b_c = 1 m and d_c = 1, 2 and 3 m are investigated.

Table C.2: Geometrical Data

thickness of slab d_c	length of slab ℓ	thickness of soil layer d'_s
[m]	[m]	[m]
1	>10	4
2	>20	8
3	>30	12

With d'_s the thickness of thermally interacting soil layer below slab is defined.

C.3 Fields of Temperature

A cut-out of b_c = 1 m x (air + d_c + d'_s) with one-dimensional heat flow is regarded. Boundary conditions are given in Table C.3, material data in Table C.4. It is assumed that the top of slab is covered the first 120 h with a plastic sheet.

Table C.3: Thermal Boundary Conditions

property	notation	unit	spring/fall	summer	winter
fresh concrete temp.	T_{c0}	°C	15	25	10
soil temperature $d'_{s1} < 4$ dc	T_{s01}	°C	8	12	5
soil temperature $d'_{s2} = 4$ dc	T_{s02}	°C	12	12	12
air temperature (sine wave)	T_{a0}	°C	12 ± 7	25 ± 3	7 ± 3
heat transfer coeff. t = 0 to t = 120 h	α_e	W/m^2K	10	10	10
after t = 120 h	α_e	W/m^2K	20	20	20

Table C.4: Material Data for Temperature Field Computation

property	notation	unit	CO 1	CO 23	soil
coeff. of heat conduction	λ_c λ_s	W/mK	2.1	2.1	- 1
spec. heat capacity	c_c c_s	Wh/kgK	0.32	0.32	- 0.22
density	ρ_c ρ_s	kg/m^3	2350 -	-	- 1700
cement type	CEM	-	I 32.5 R	III / B 32.5	-
cement content	C	kg/m^3	270	280	-
max. heat release of concrete per m^3 concrete	max Q_c	kWh/m^3	38.44	28.52	-
Parameters of heat release function (Jonasson)	c_1 t_k	[-] h	-1.135 12.055	-1.34 23.8	- -

C.4 Fields of Stress and Restraint Actions

C.4.1 Stress fields

Table C.5 shows the data and parameters for the computation of concrete stresses. Table C.6 shows the restraint conditions. Friction and elastic bedding by SRMM are not considered here.

Table C.5: Data and Parameters for the Computation of Stresses

property	notation	unit	CO 1	CO 23
end of dormant phase	α_0	[-]	0.1995	0.09
final value of tensile strength	f_{ct1}	MPa	3.005	3.00
final value of compressive strength	f_{cc1}	MPa	47.87	40.7
final value of Young's modulus	E_{ct1}	GPa	33.630	31.500
final value of fracture energy	G_{f1}	N/m	144.47	130.0
exponent of fracture energy	a_{Gf}	[-]	0.9205	0.80
constant of failure strain ε_{ctu}	a_{eu}	[10^{-3}]	0.35	0.35
model parameter of relaxation function (Eq. (B.23), (B.24))	a_{1r}	[-]	0.299	0.263
	b_{1r}	[-]	-0.298	-0.239
	a_{2r}	[-]	0.296	0.196
	b_{2r}	[-]	0.133	0.355

Table C.6: Modeling of Restraint

type of restraint	R_a	R_b
eigenstresses	0	0
restraint	0.10	0.95

C.4.2 Numerical Examples

Computations were performed for the concrete compositions CO1 and CO23, 3 slab thickness, three seasons of casting, and the restraint conditions according to Table C.6. For each parameter combination a set of diagrams is presented on the following pages. The coordinate z' [m] has its origin at the bottom face of slab. The individual value z'* denotes the center of specific strip measured from bottom.

C.4.2.1 CO1, 1 m, Spring/Fall (T_{c0} = 15°C)

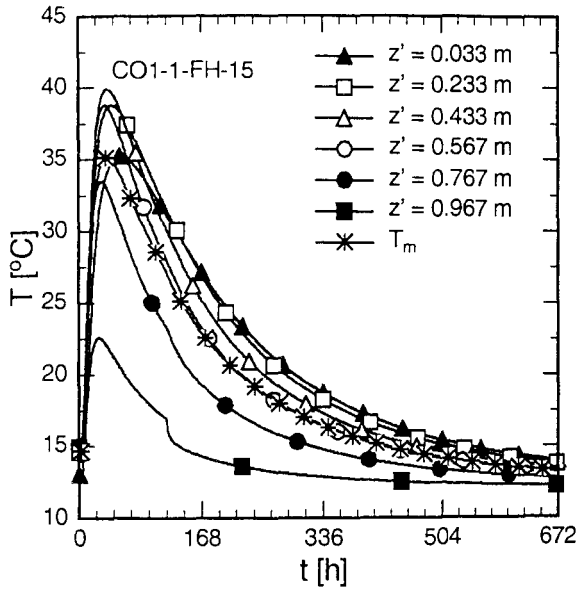

Fig. C.1: Temperature vs. Age. Slab CO1-1-FH-15

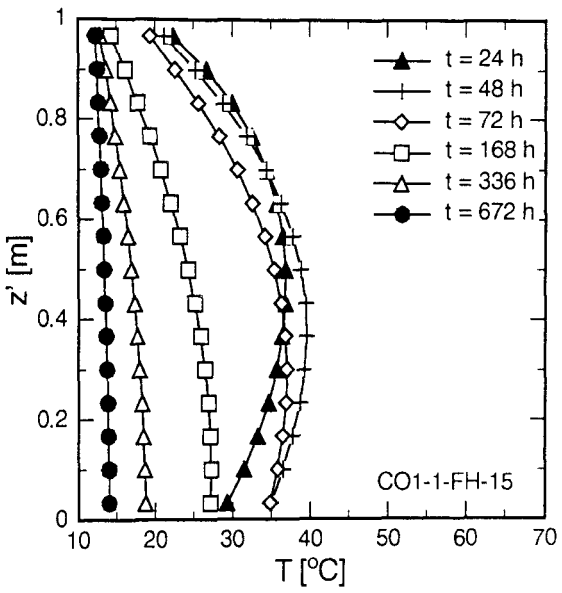

Fig. C.2: Temperature vs. Elevation. Slab CO1-1-FH-15

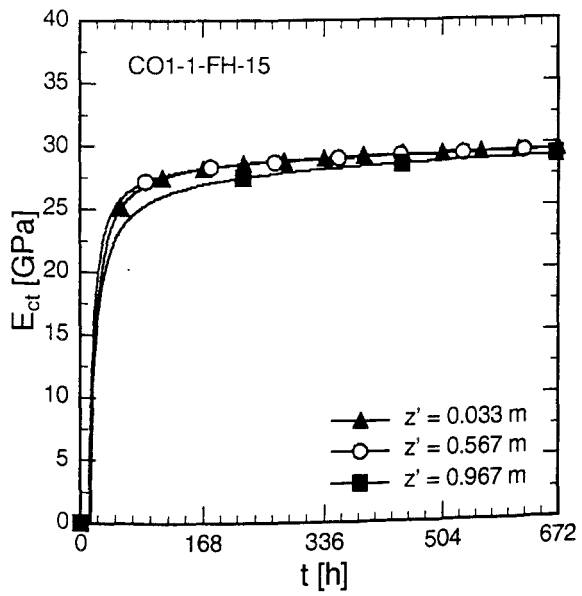

Fig. C.3: E_{ct} vs. Age. Slab CO1-1-FH-15

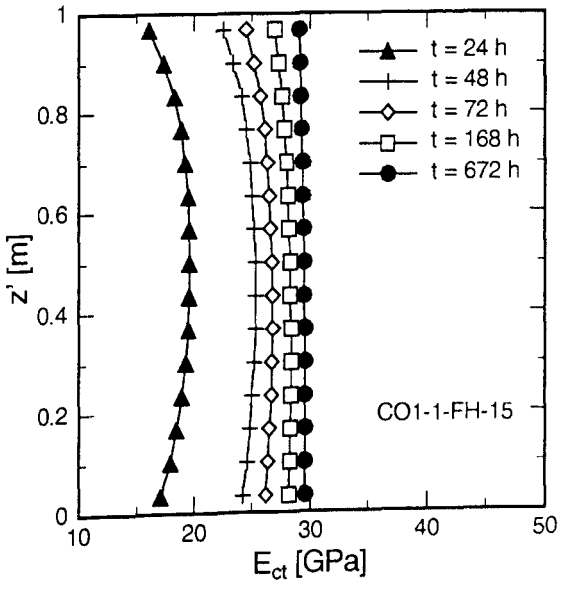

Fig. C.4: E_{ct} vs. Elevation. Slab CO1-1-FH-15

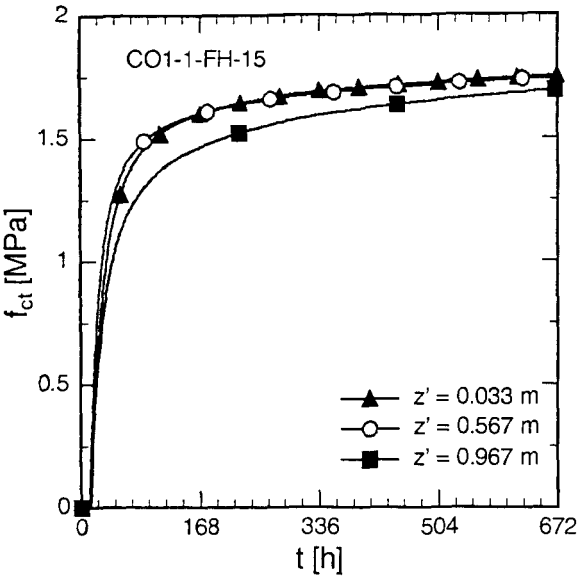

Fig. C.5: f_{ct} vs. Age. Slab CO1-1-FH-15

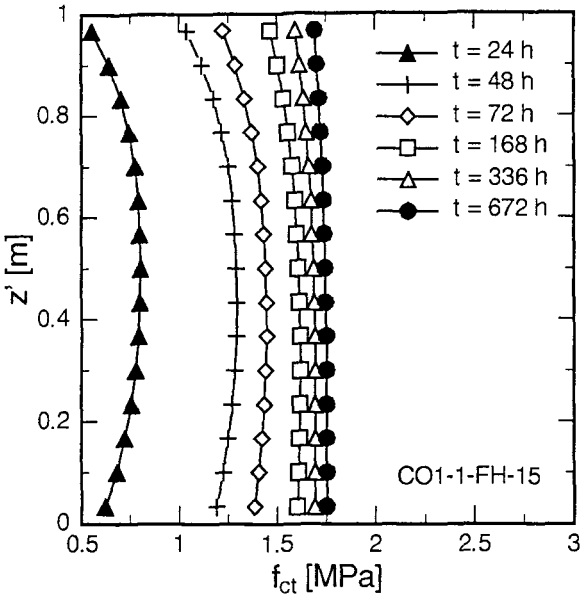

Fig. C.6: f_{ct} vs. Elevation. Slab CO1-1-FH-15

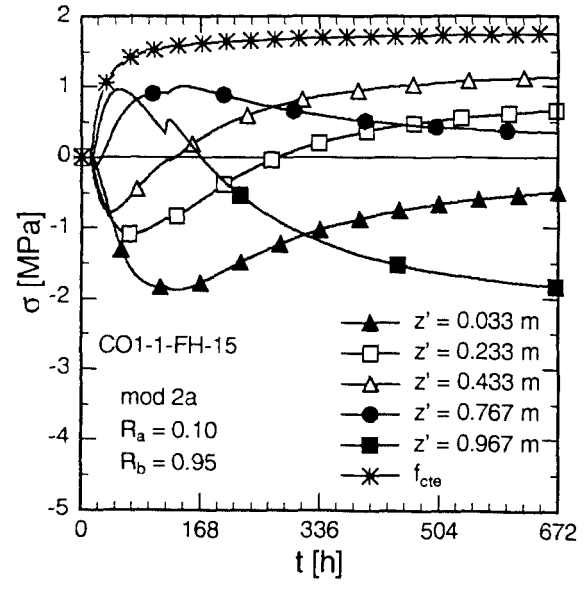

Fig. C.7: Stress vs. Age. Slab CO1-1-FH-15, mod 2 a

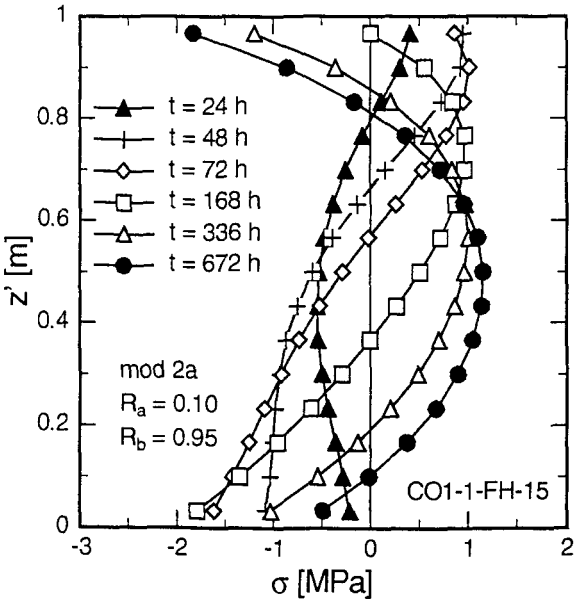

Fig. C.8: Stress vs. Elevation. Slab CO1-1-FH-15, mod 2 a

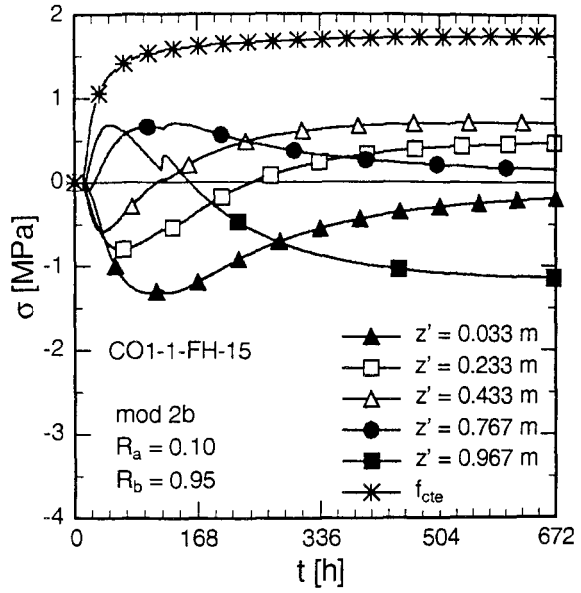

Fig. C.9: Stress vs. Age. Slab CO1-1-FH-15, mod 2 b

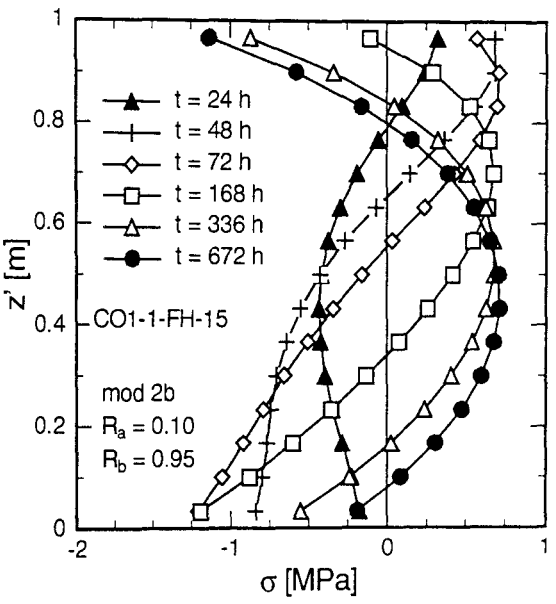

Fig. C.10: Stress vs. Elevation. Slab CO1-1-FH-15, mod 2 b

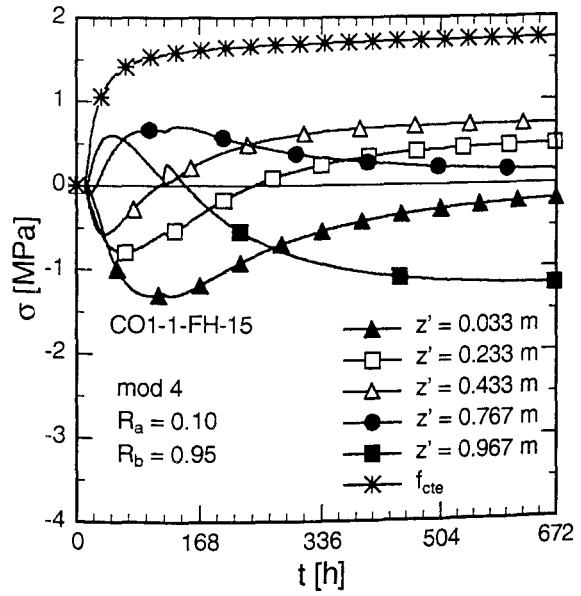

Fig. C.11: Stress vs. Age. Slab CO1-1-FH-15, mod 4

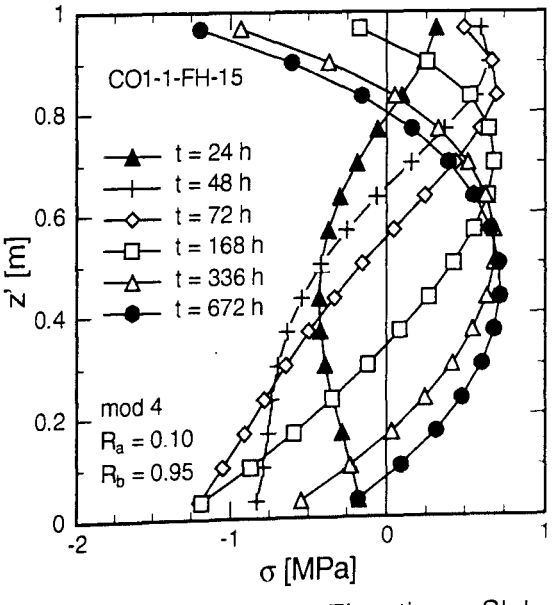

Fig. C.12: Stress vs. Elevation. Slab CO1-1-FH-15, mod 4

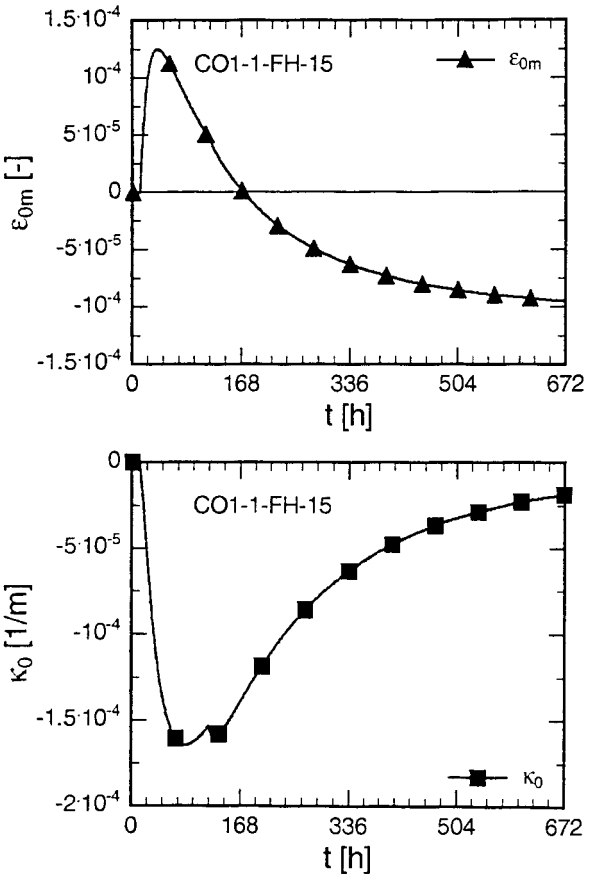

Fig. C.13: Free Thermal Deformation. Slab CO1-1-FH-15

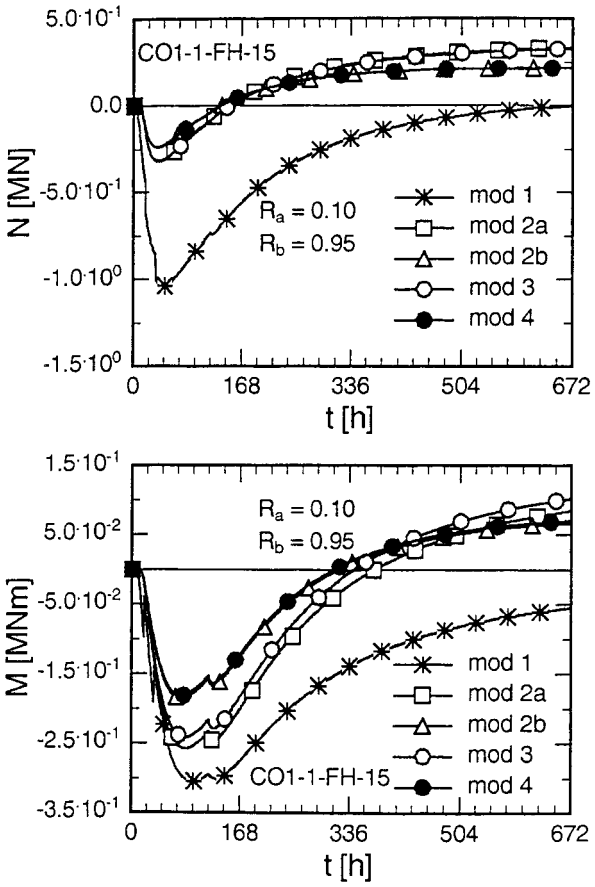

Fig. C.14: Restraint Actions. Slab CO1-1-FH-15, all Models

C.4.2.2 CO1, 1 m, Summer (T_{c0} = 25°C)

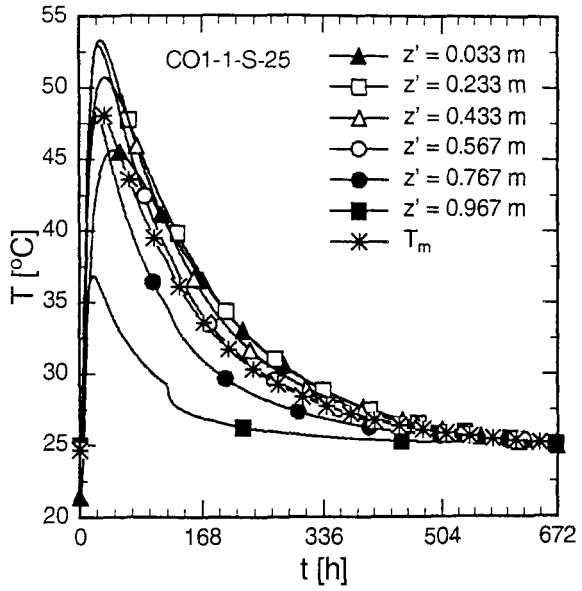

Fig. C.15: Temperature vs. Age. Slab CO1-1-S-25

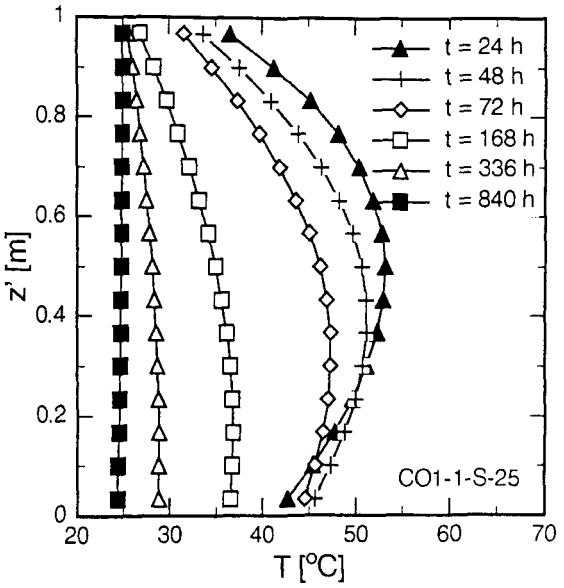

Fig. C.16: Temperature vs. Elevation. Slab CO1-1-S-25

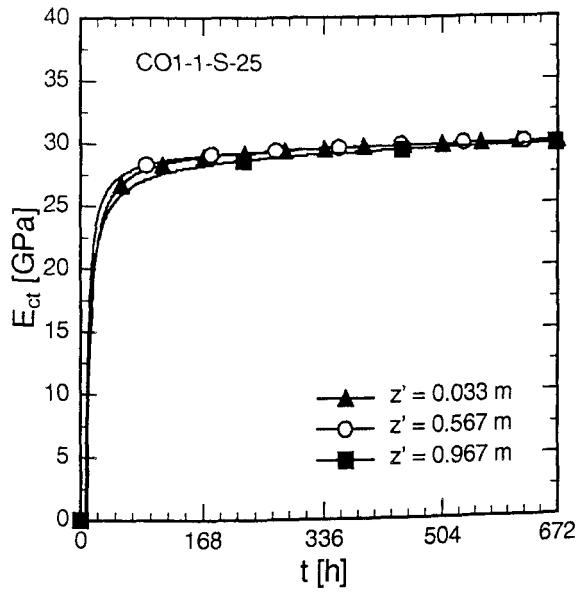

Fig. C.17: E_{ct} vs. Age. Slab CO1-1-S-25

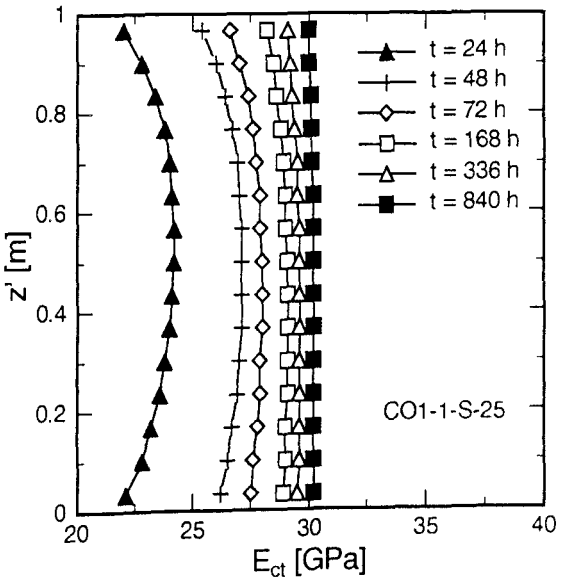

Fig. C.18: E_{ct} vs. Elevation. Slab CO1-1-S-25

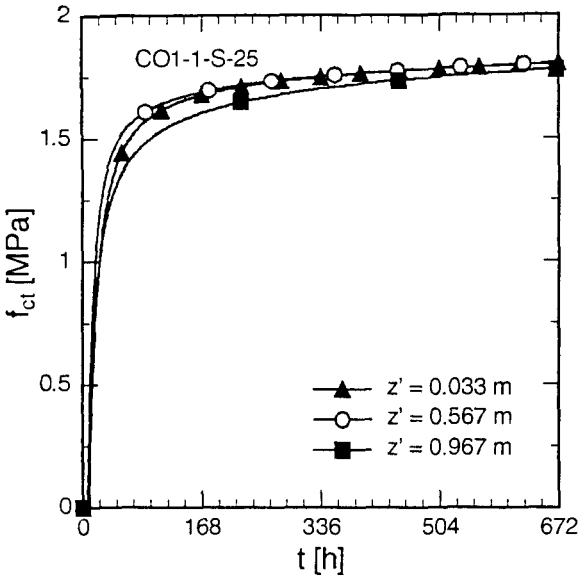

Fig. C.19: f_{ct} vs. Age. Slab CO1-1-S-25

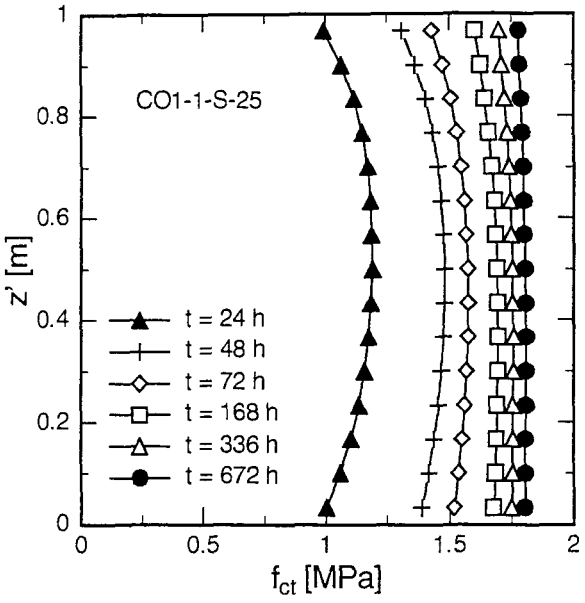

Fig. C.20: f_{ct} vs. Elevation. Slab CO1-1-S-25

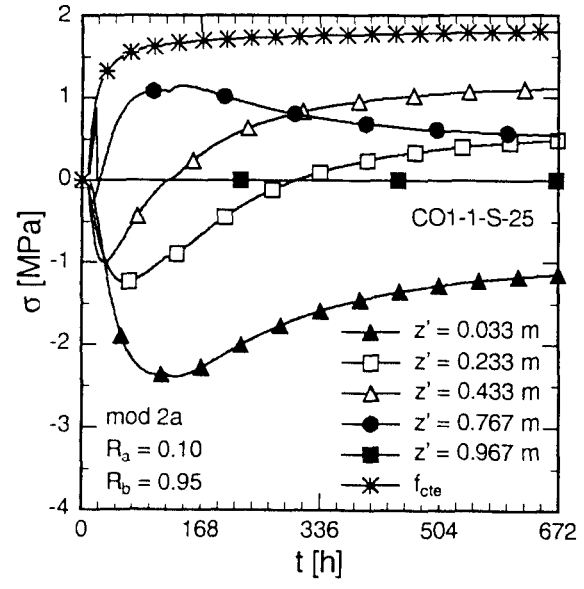

Fig. C.21: Stress vs. Age. Slab CO1-1-S-25, mod 2a

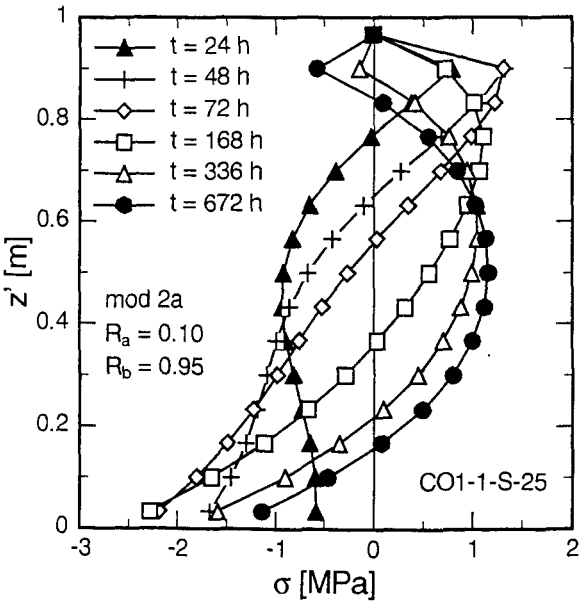

Fig. C.22: Stress vs. Elevation. Slab CO1-1-S-25, mod 2a

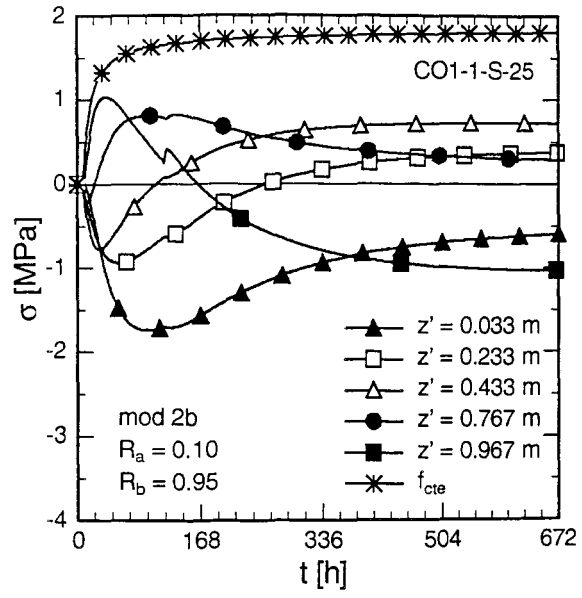

Fig. C.23: Stress vs. Age. Slab CO1-1-S-25, mod 2b

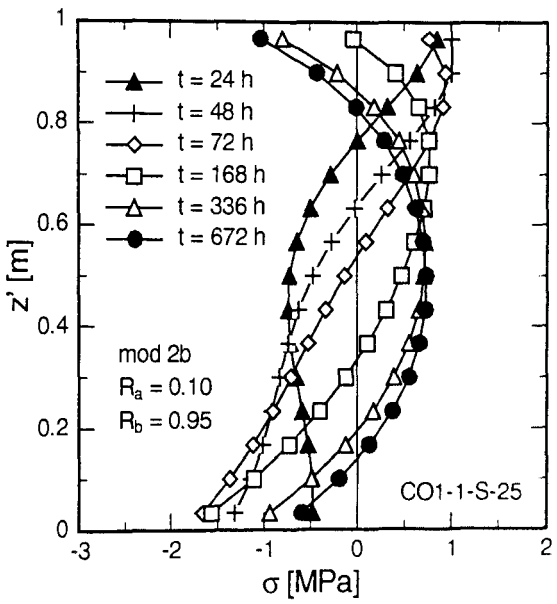

Fig. C.24: Stress vs. Elevation. Slab CO1-1-S-25, mod 2b

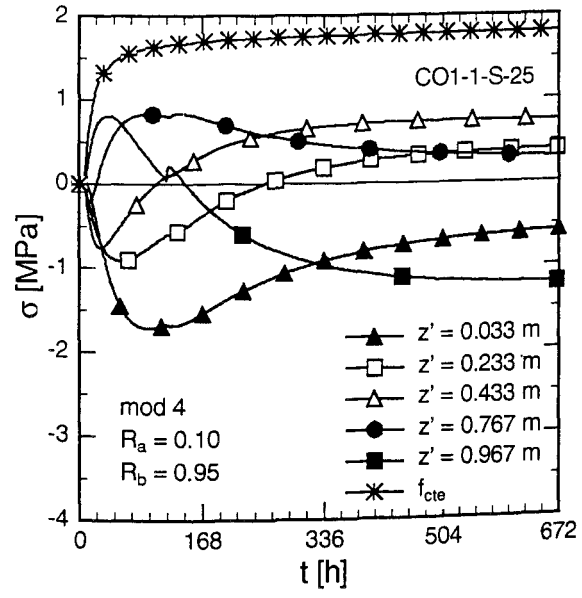

Fig. C.25: Stress vs. Age. Slab CO1-1-S-25, mod 4

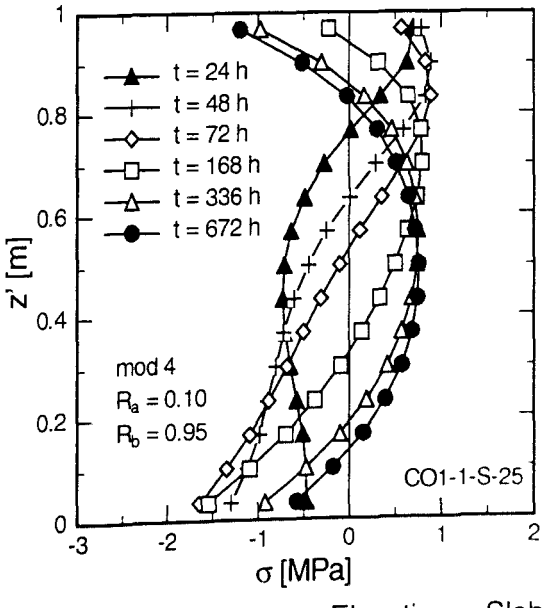

Fig. C.26: Stress vs. Elevation. Slab CO1-1-S-25, mod 4

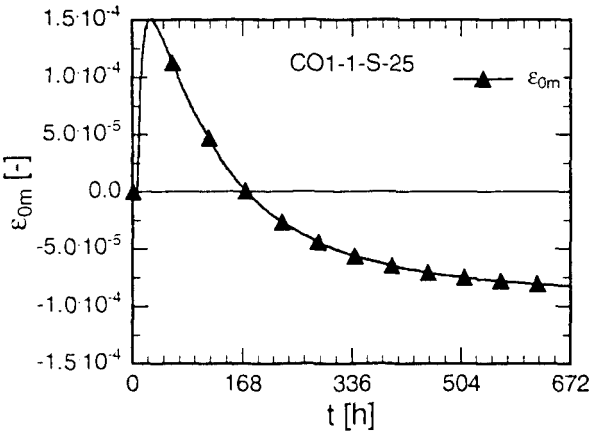

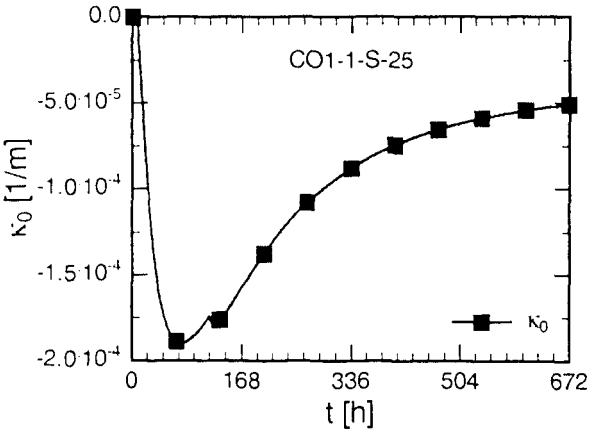

Fig. C.27: Free Thermal Deformation. Slab CO1-1-S-25

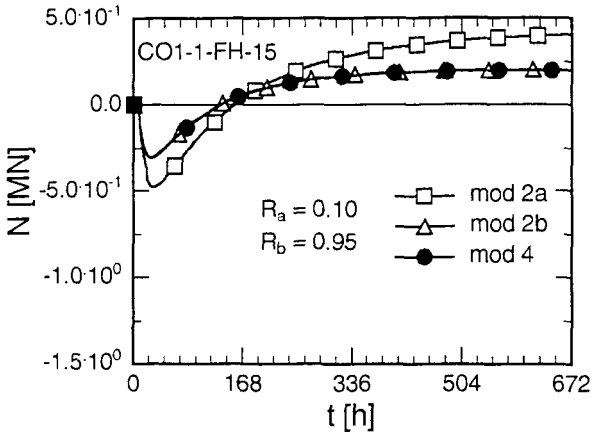

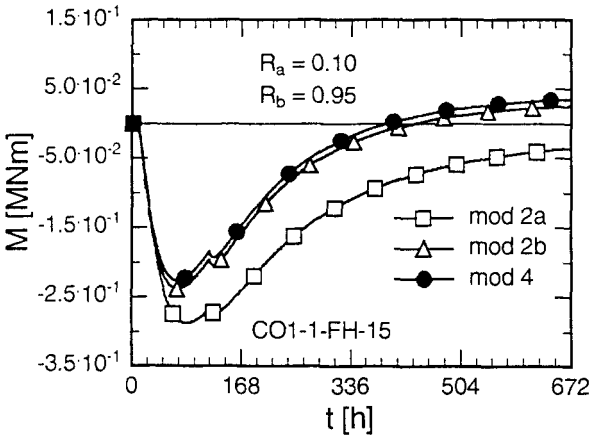

Fig. C.28: Restraint Actions. Slab CO1-1-S-25, all Models

C.4.2.3 CO1, 1 m, Winter (T_{c0} = 10°C)

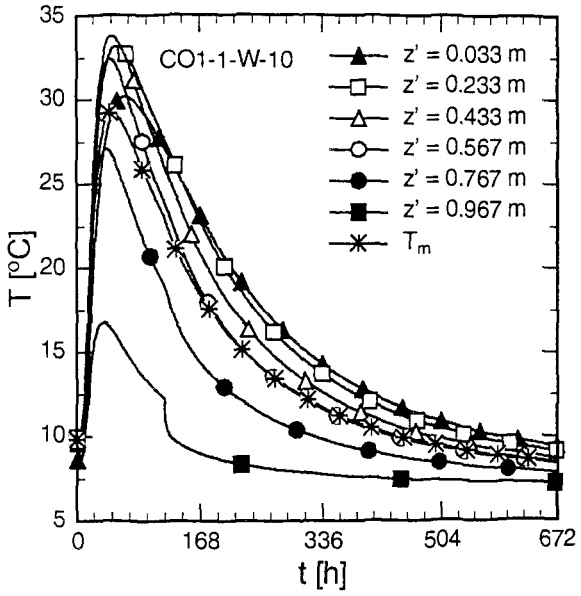

Fig. C.29: Temperature vs. Age. Slab CO1-1-W-10

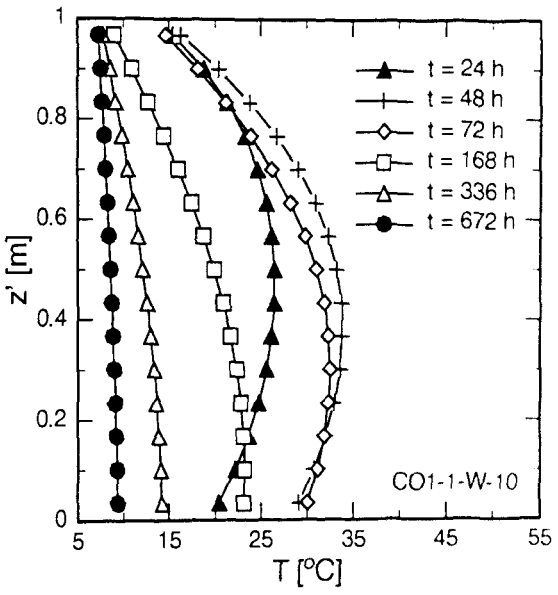

Fig. C.30: Temperature vs. Elevation. Slab CO1-1-W-10

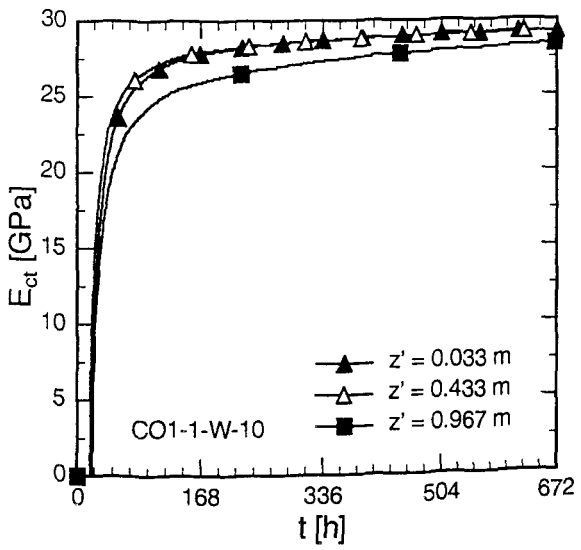

Fig. C.31: E_{ct} vs. Age. Slab CO1-1-W-10

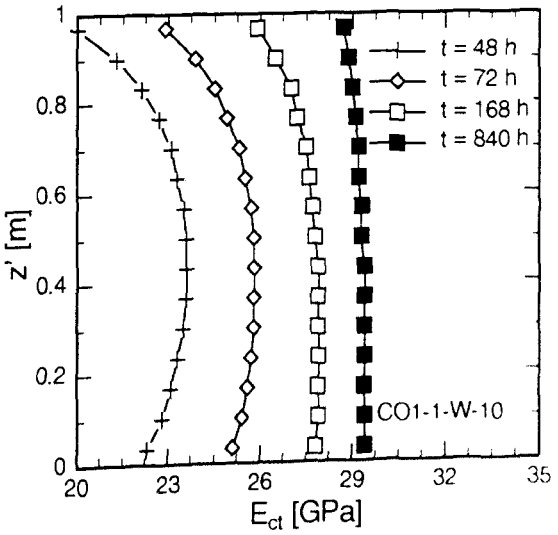

Fig. C.32: E_{ct} vs. Elevation. Slab CO1-1-W-10

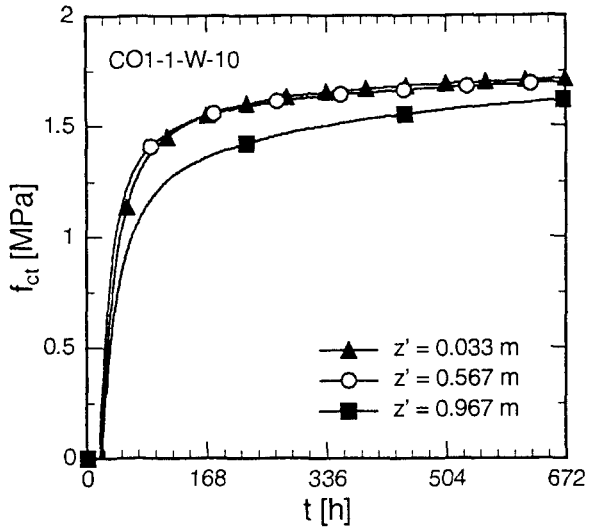

Fig. C.33: f_{ct} vs. Age. Slab CO1-1-W-10

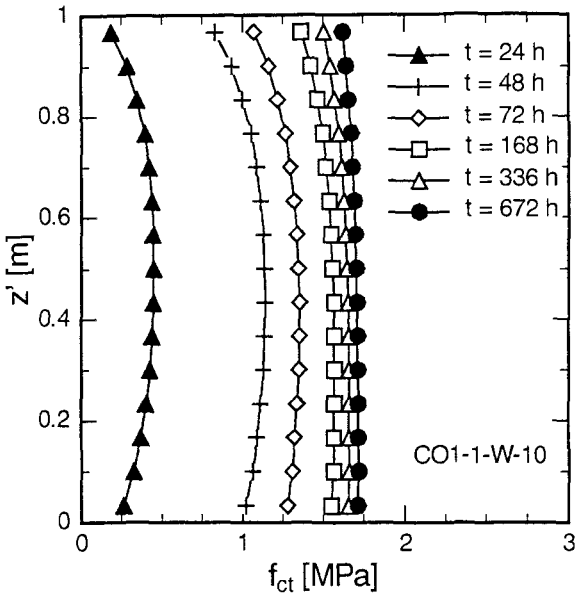

Fig. C.34: f_{ct} vs. Elevation. Slab CO1-1-W-10

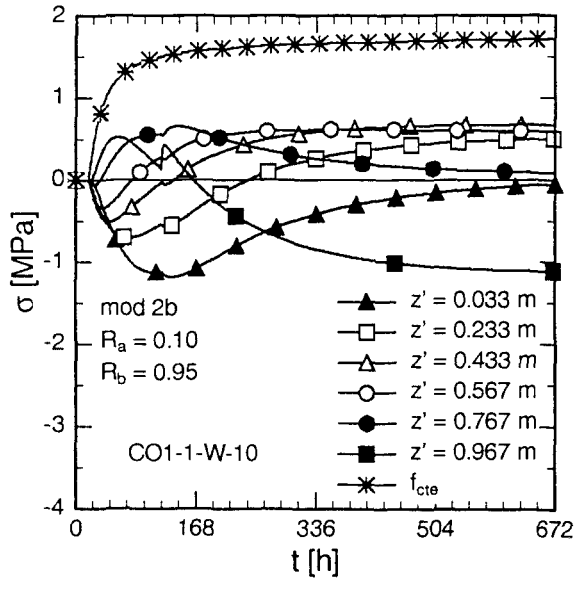

Fig. C.35: Stress vs. Age. Slab CO1-1-W-10, mod 2b

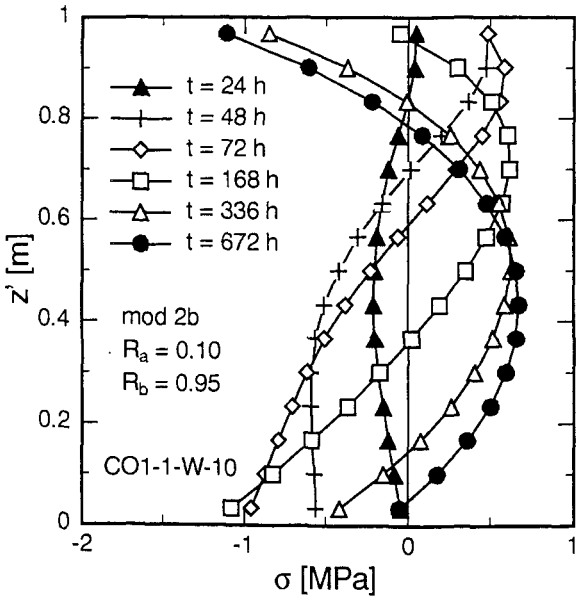

Fig. C.36: Stress vs. Elevation. Slab CO1-1-W-10, mod 2b

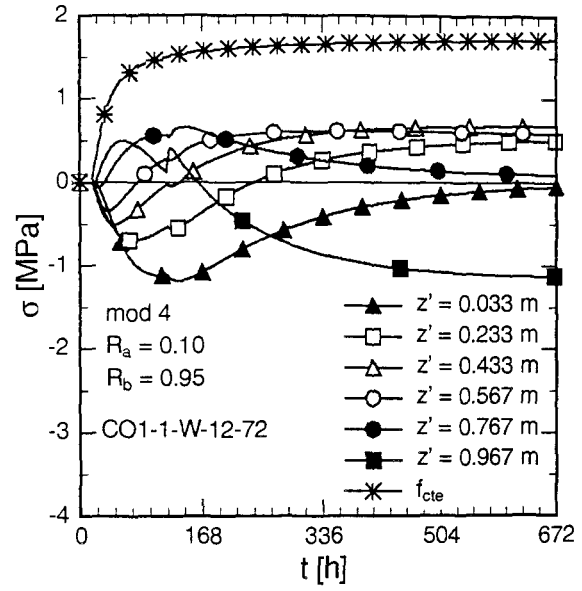

Fig. C.37: Stress vs. Age. Slab CO1-1-W-10, mod 4

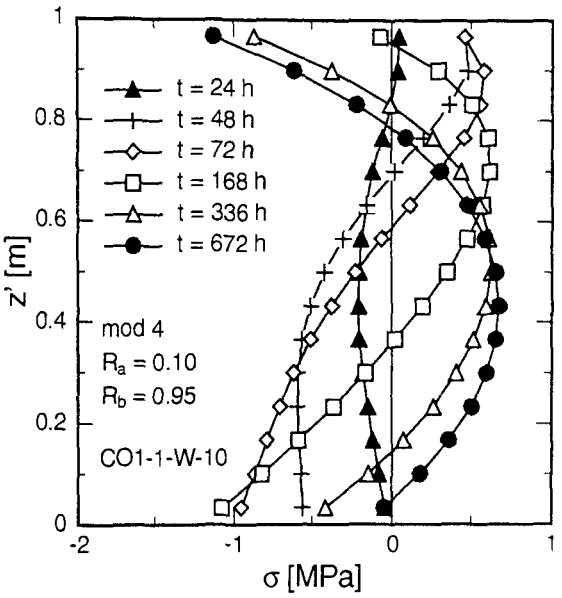

Fig. C.38: Stress vs. Elevation. Slab CO1-1-W-10, mod 4

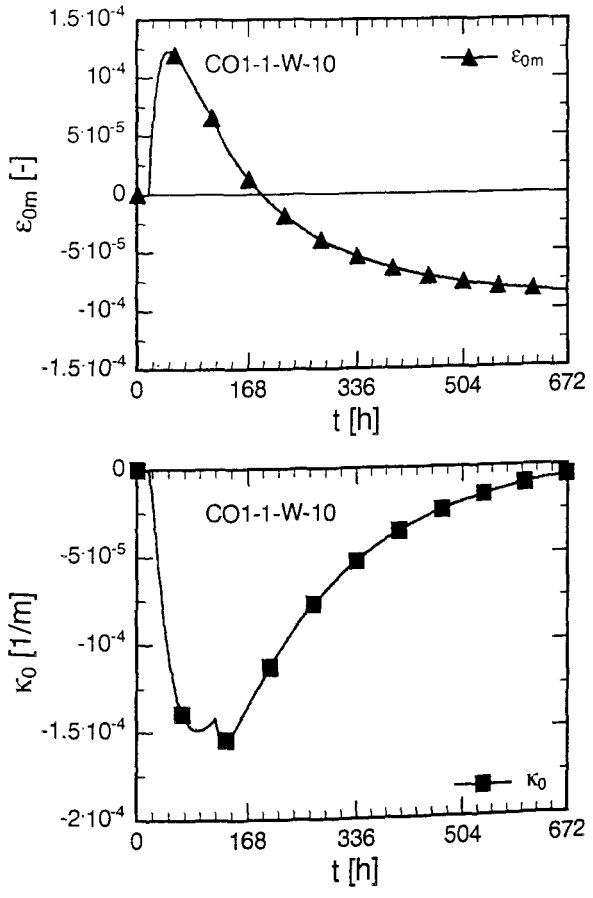

Fig. C.39: Free Thermal Deformation. Slab CO1-1-W-10

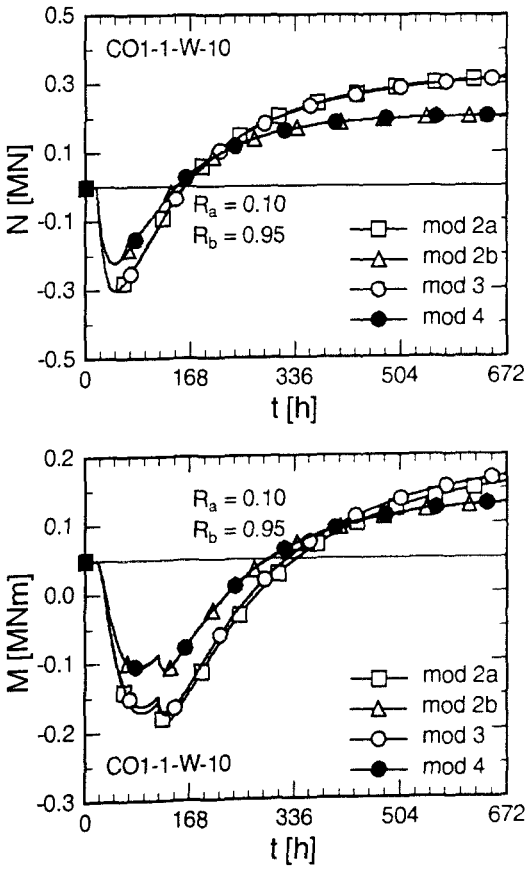

Fig. C.40: Restraint Actions. Slab CO1-1-W-10, all Models

C.4.2.4 CO1, 2 m, Spring/Fall (T_{c0} = 15°C)

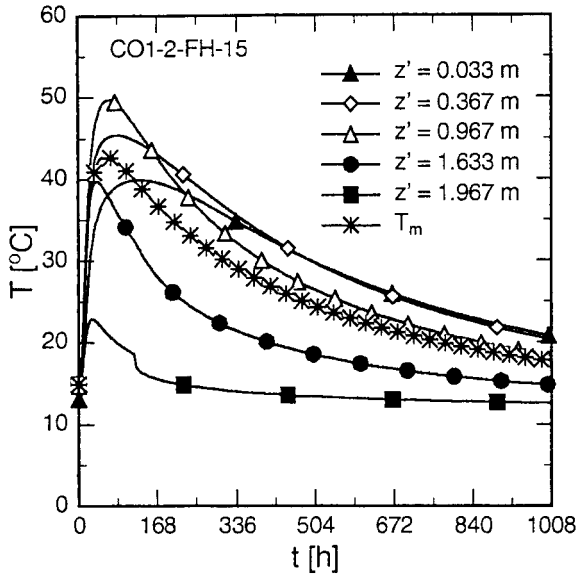

Fig. C.41: Temperature vs. Age. Slab CO1-2-FH-15

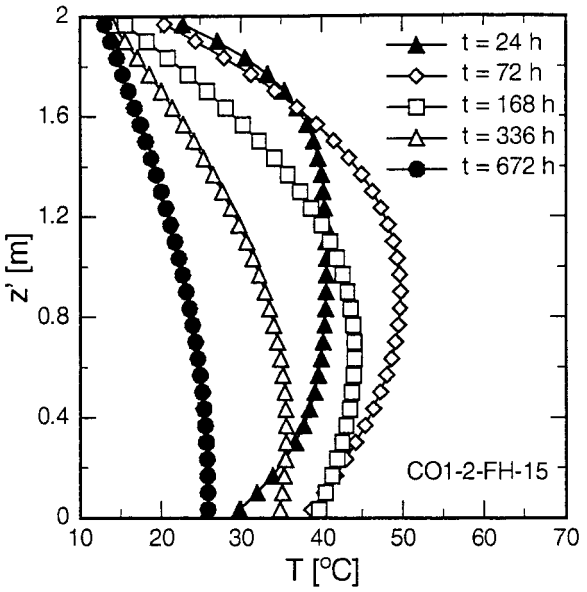

Fig. C.42: Temperature vs. Elevation. Slab CO1-2-FH-15

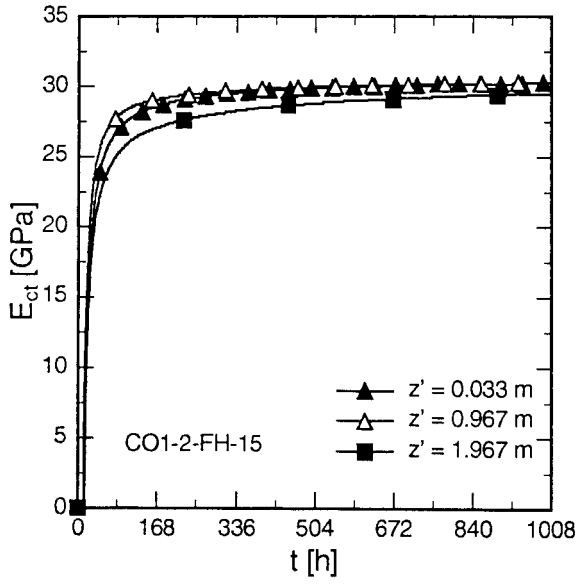

Fig. C.43: E_{ct} vs. Age. Slab CO1-2-FH-15

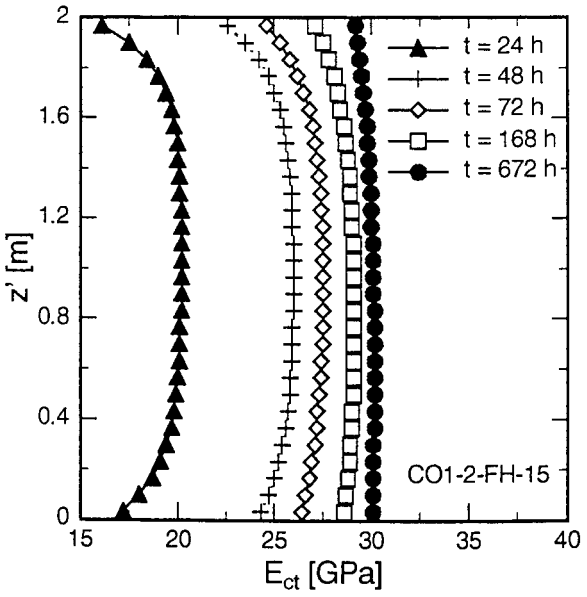

Fig. C.44: E_{ct} vs. Elevation. Slab CO1-2-FH-15

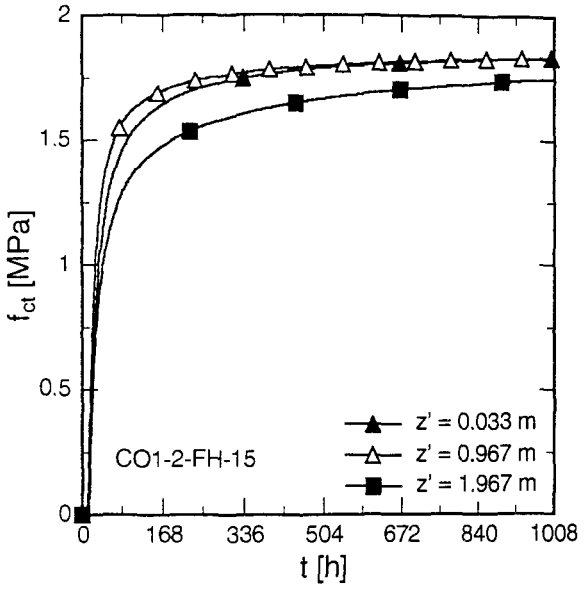

Fig. C.45: f_{ct} vs. Age. Slab CO1-2-FH-15

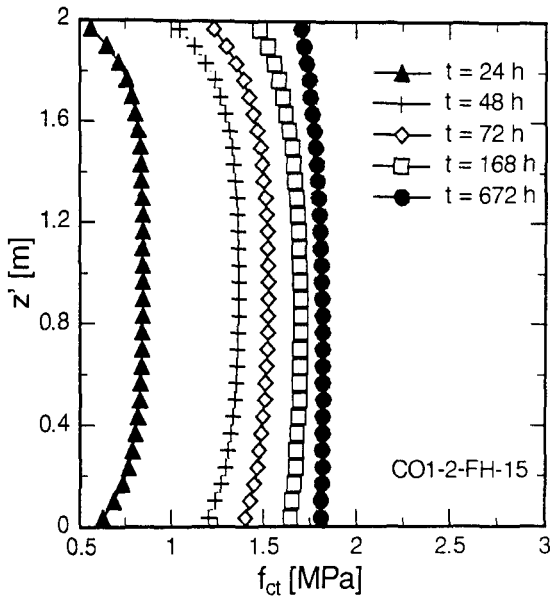

Fig. C.46: f_{ct} vs. Elevation. Slab CO1-2-FH-15

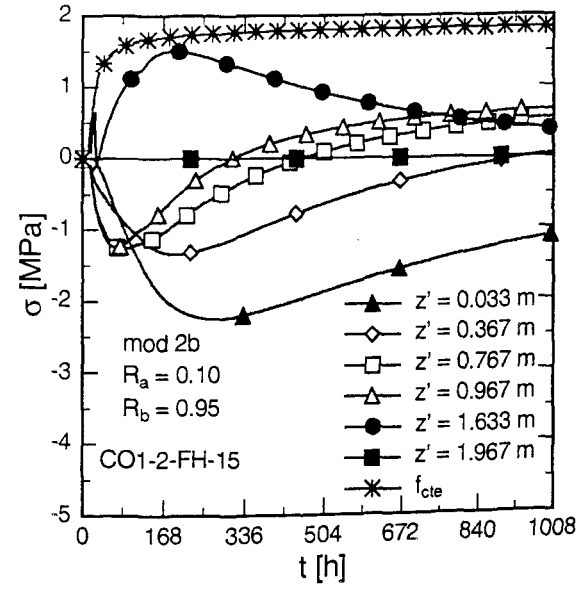

Fig. C.47: Stress vs. Age. Slab CO1-2-FH-15, *mod 2b*

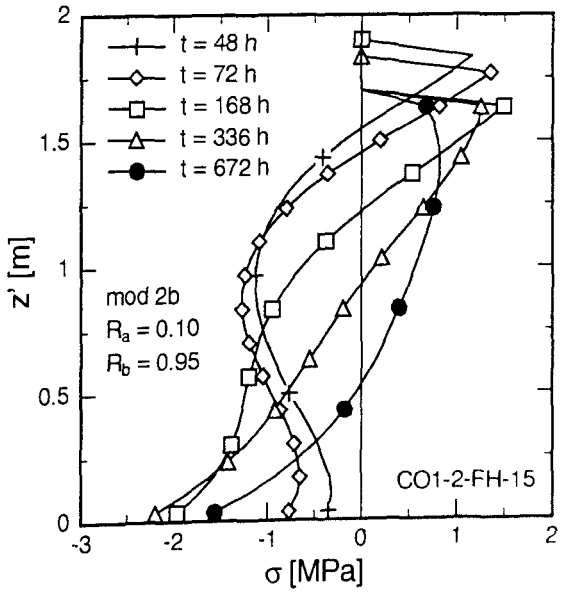

Fig. C.48: Stress vs. Elevation. Slab CO1-2-FH-15, mod 2b

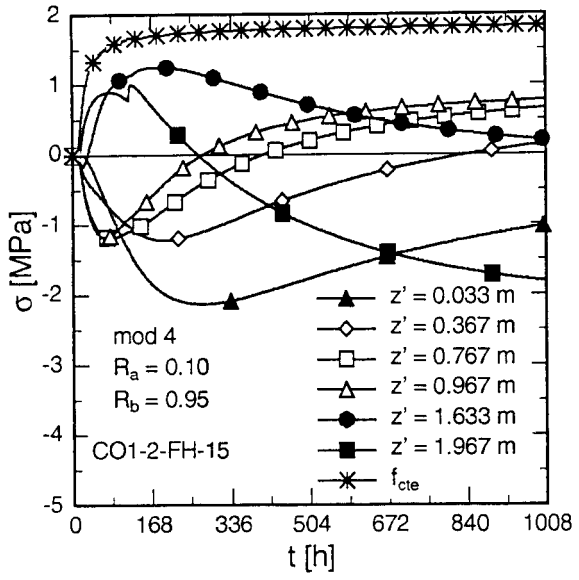

Fig. C.49: Stress vs. Age. Slab CO1-2-FH-15, mod 4

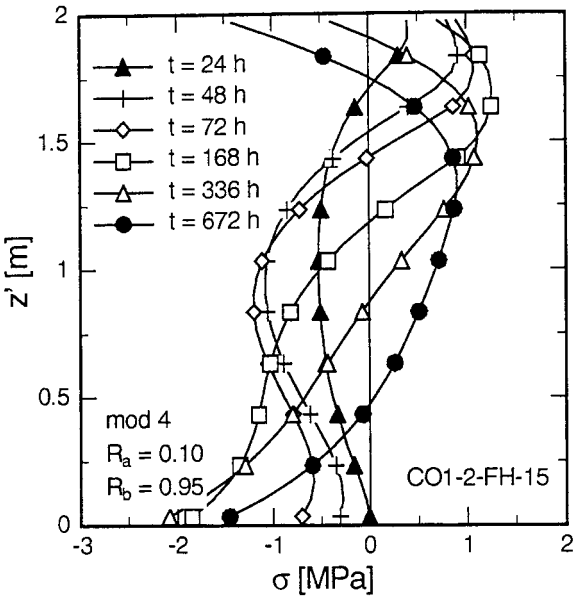

Fig. C.50: Stress vs. Elevation. Slab CO1-2-FH-15, mod 4

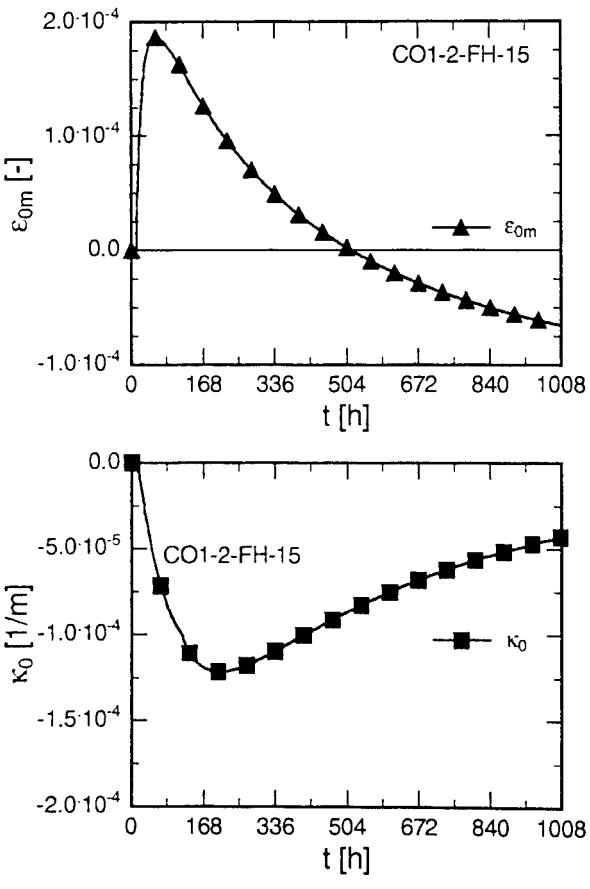

Fig. C.51: Free Thermal Deformation. Slab CO1-2-FH-15

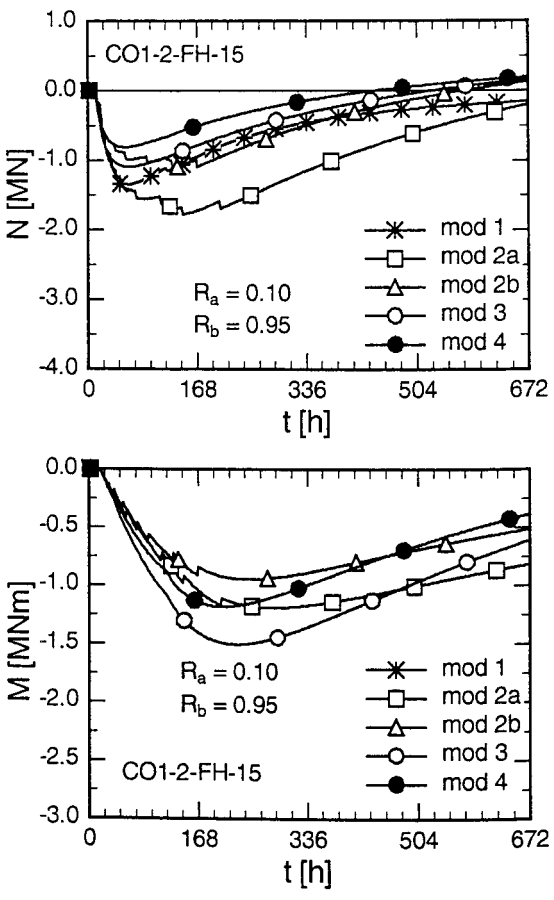

Fig. C.52: Restraint Actions. Slab CO1-2-FH-15, all Models

C.4.2.5 CO1, 3 m, Spring/Fall (T = 15°C)

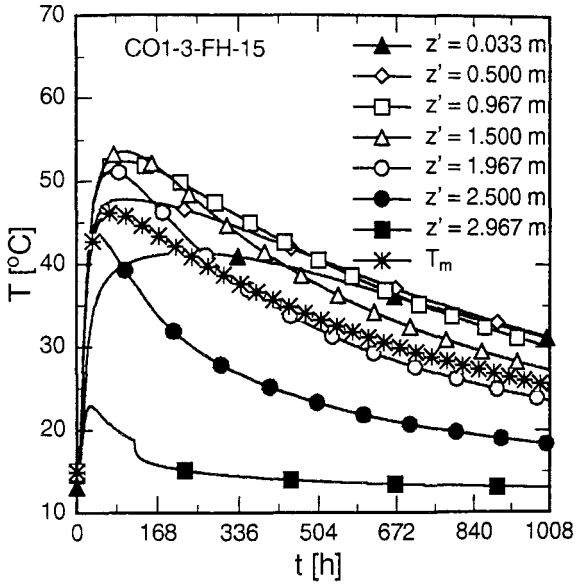

Fig. C.53: Temperature vs. Age. Slab CO1-3-FH-15

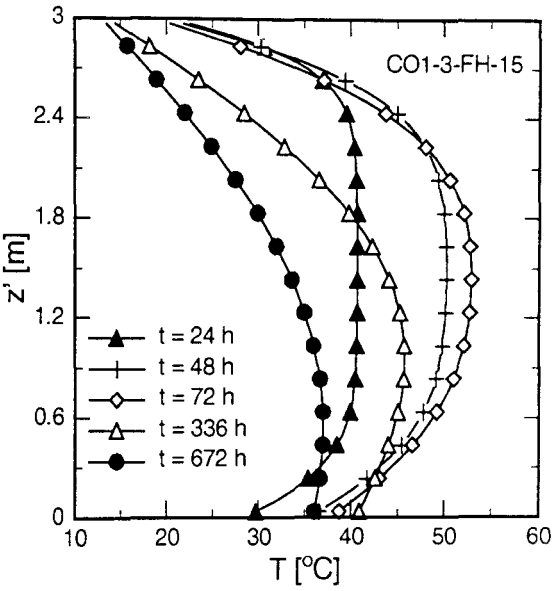

Fig. C.54: Temperature vs. Elevation. Slab CO1-3-FH-15

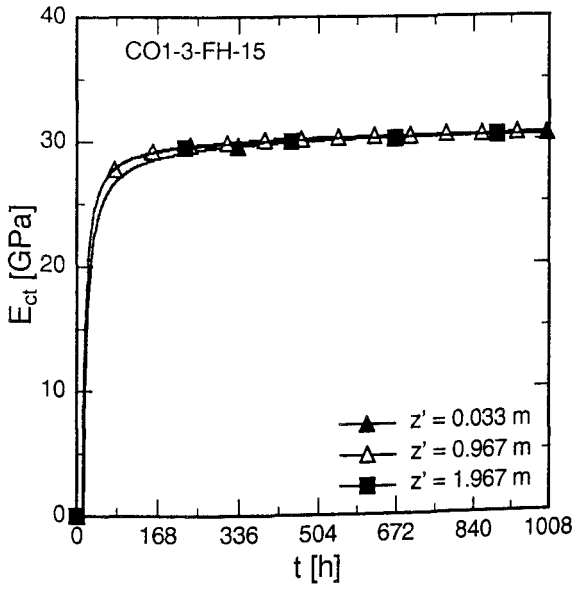

Fig. C.55: E_{ct} vs. Age. Slab CO1-3-FH-15

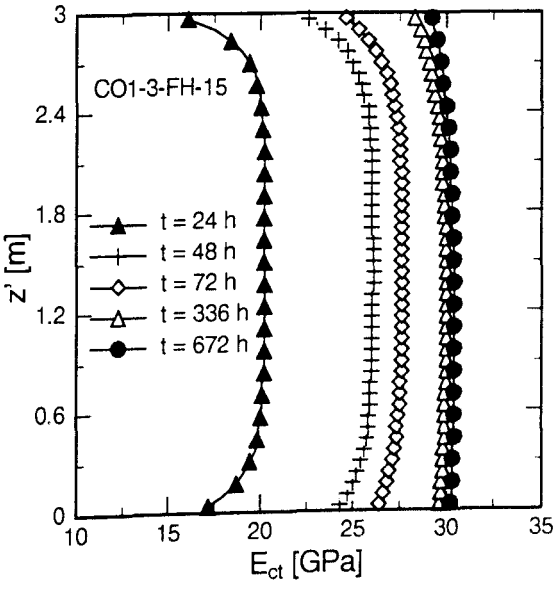

Fig. C.56: E_{ct} vs. Elevation. Slab CO1-3-FH-15

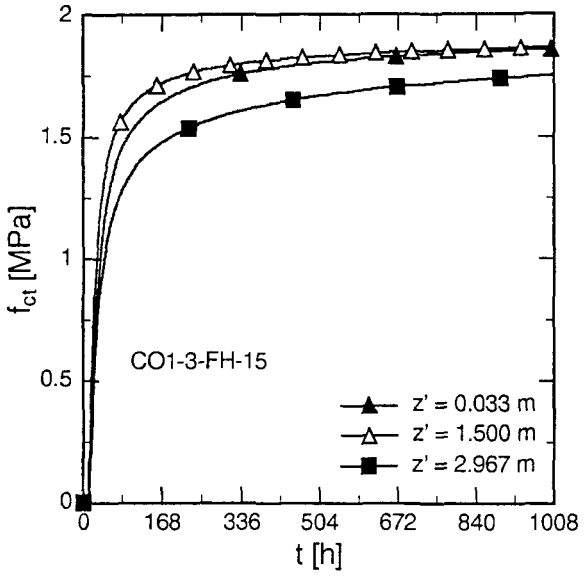

Fig. C.57: f_{ct} vs. Age. Slab CO1-3-FH-15

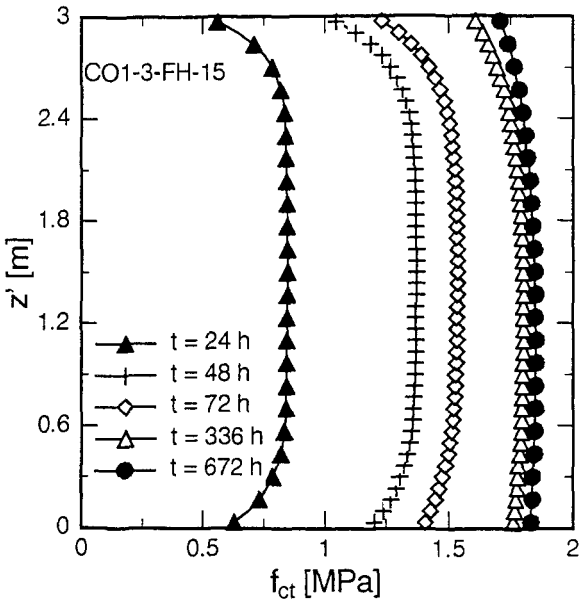

Fig. C.58: f_{ct} vs. Elevation. Slab CO1-3-FH-15

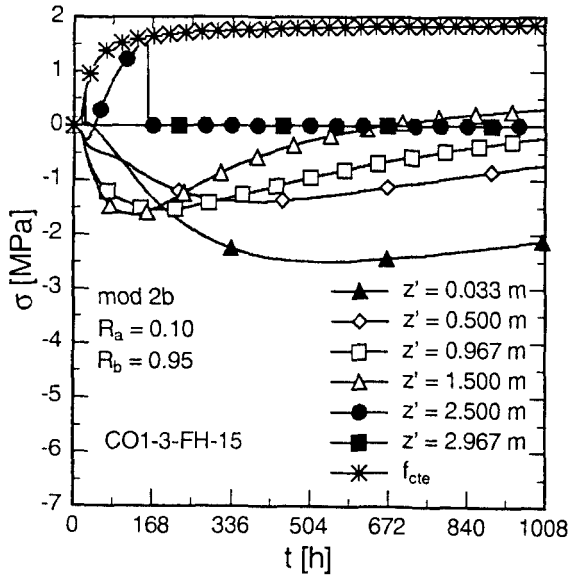

Fig. C.59: Stress vs. Age. Slab CO1-3-FH-15, mod 2b

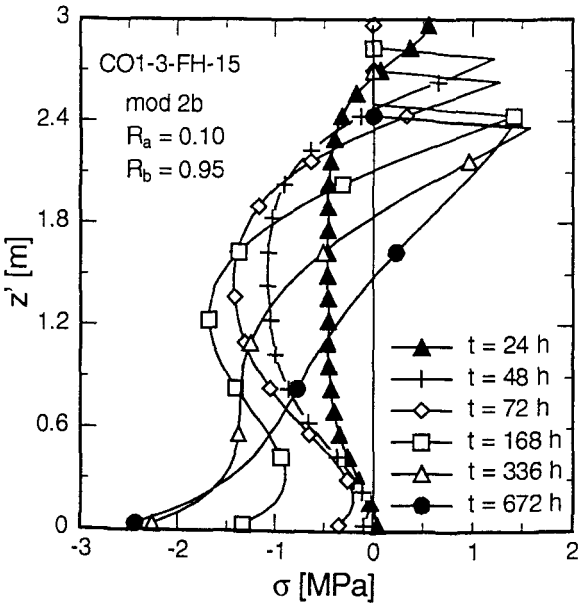

Fig. C.60: Stress vs. Elevation. Slab CO1-3-FH-15, mod 2b

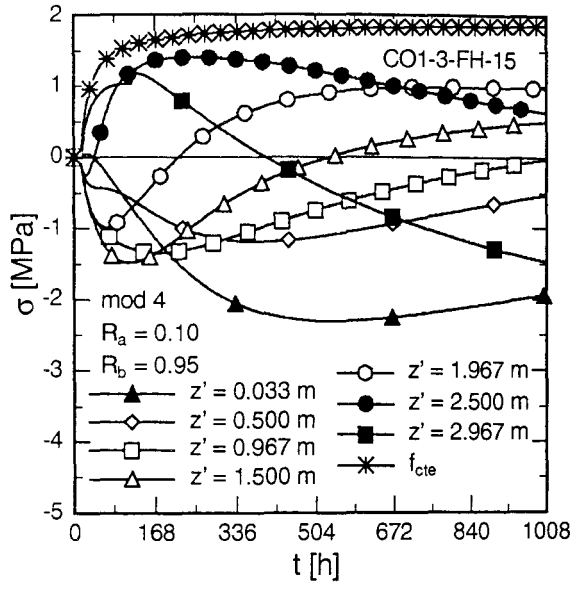

Fig. C.61: Stress vs. Age. Slab CO1-3-FH-15, mod 4

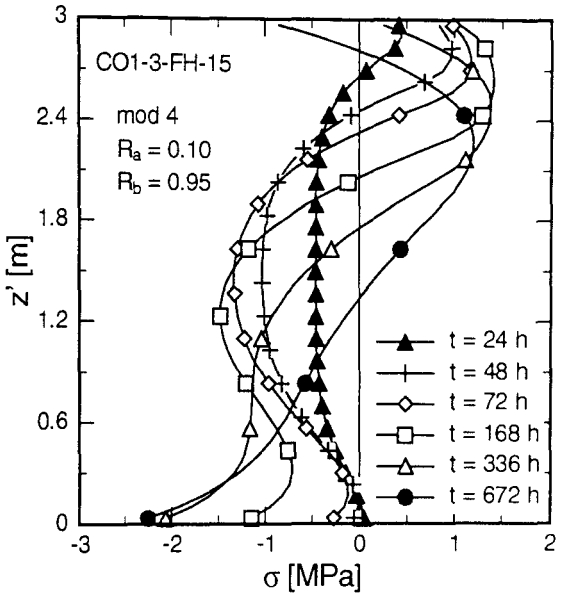

Fig. C.62: Stress vs. Elevation. Slab CO1-3-FH-155, mod 4

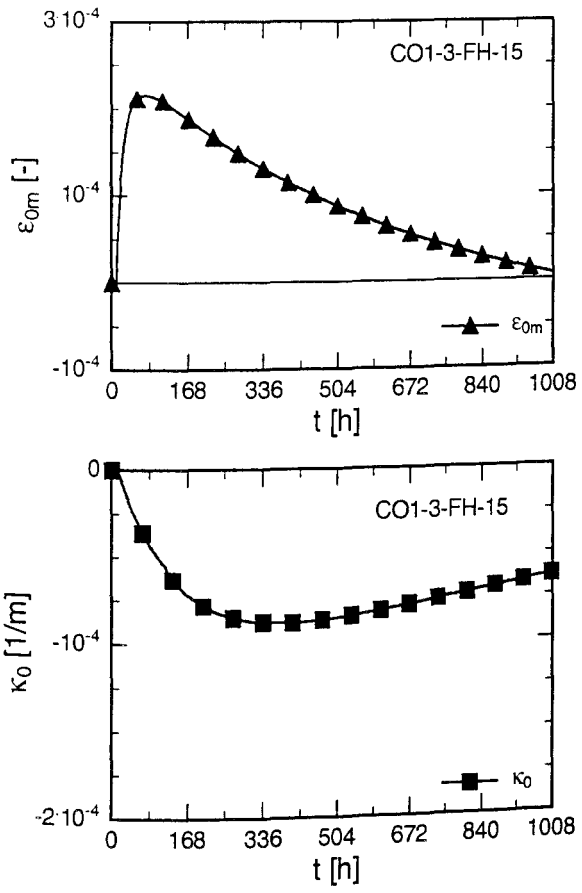

Fig. C.63: Free Thermal Deformation. Slab CO1-3-FH-15

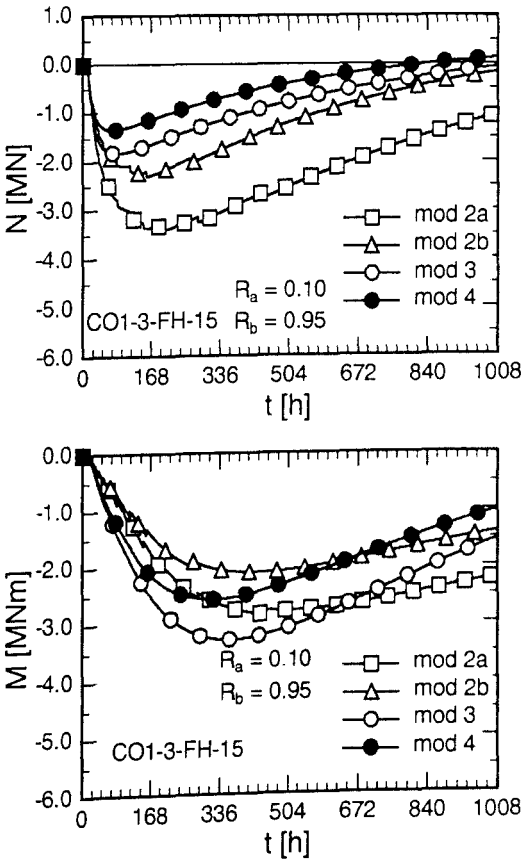

Fig. C.64: Restraint Actions. Slab CO1-3-FH-15, all Models

C.4.2.6 CO23, 1 m, Spring/Fall (T = 15°C)

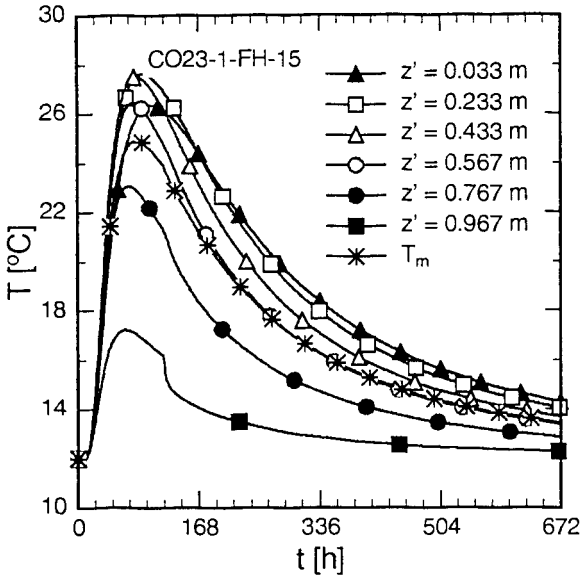

Fig. C.65: Temperature vs. Age. Slab CO23-1-FH-15

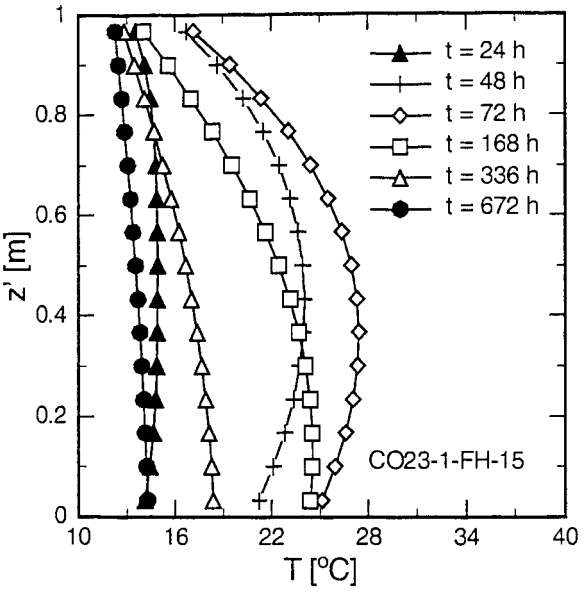

Fig. C.66: Temperature vs. Elevation. Slab CO23-1-FH-15

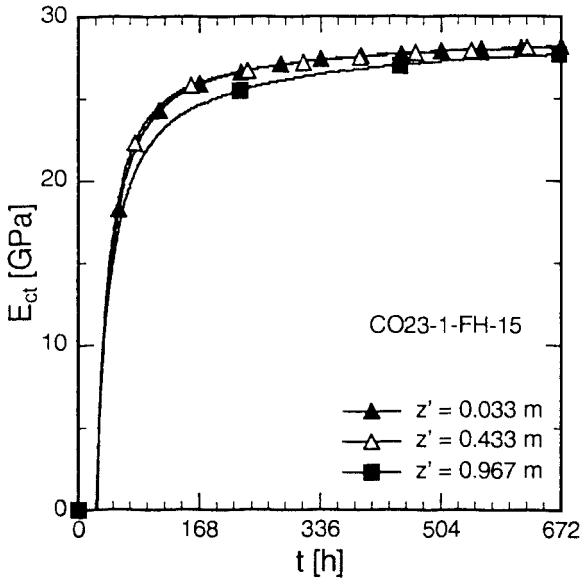

Fig. C.67: E_{ct} vs. Age. Slab CO23-1-FH-15

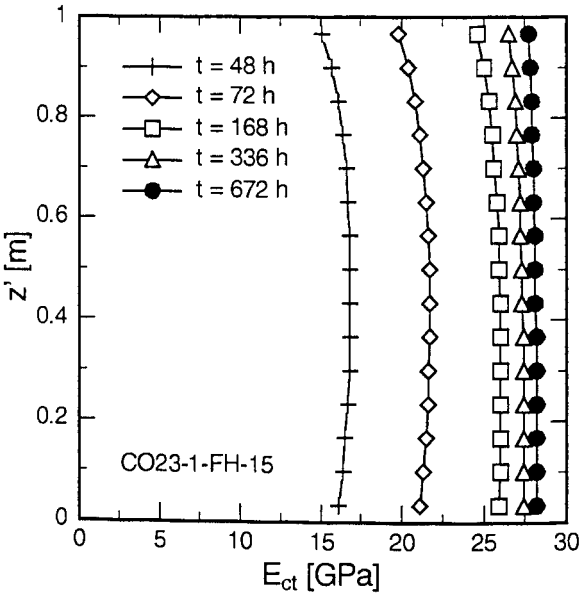

Fig. C.68: E_{ct} vs. Elevation. Slab CO23-1-FH-15

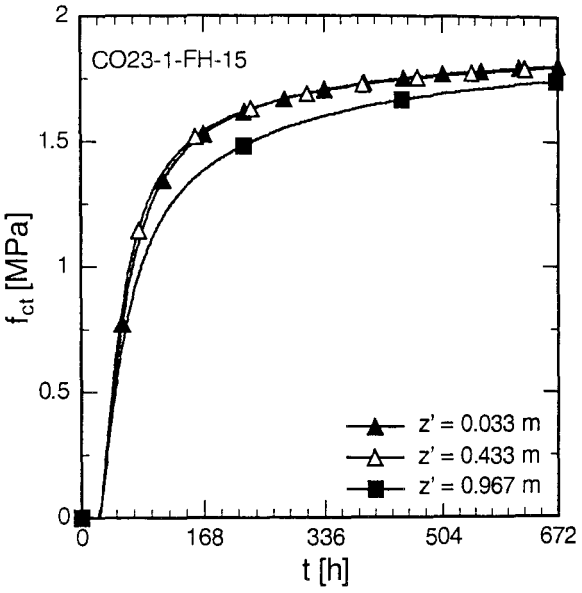

Fig. C.69: f_{ct} vs. Age. Slab CO23-1-FH-15

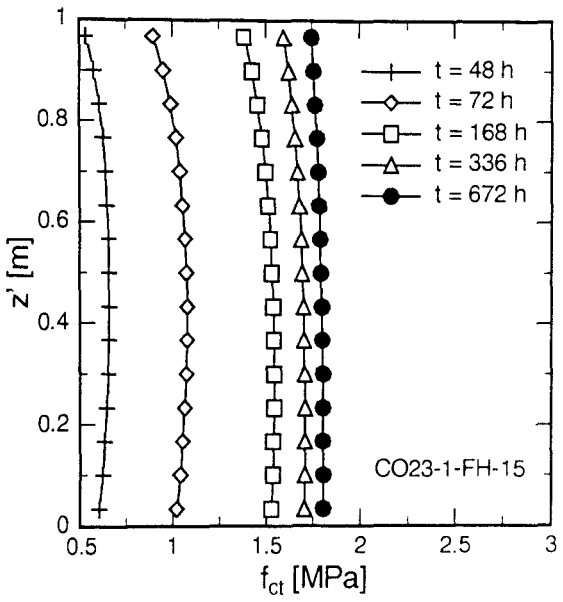

Fig. C.70: f_{ct} vs. Elevation. Slab CO23-1-FH-15

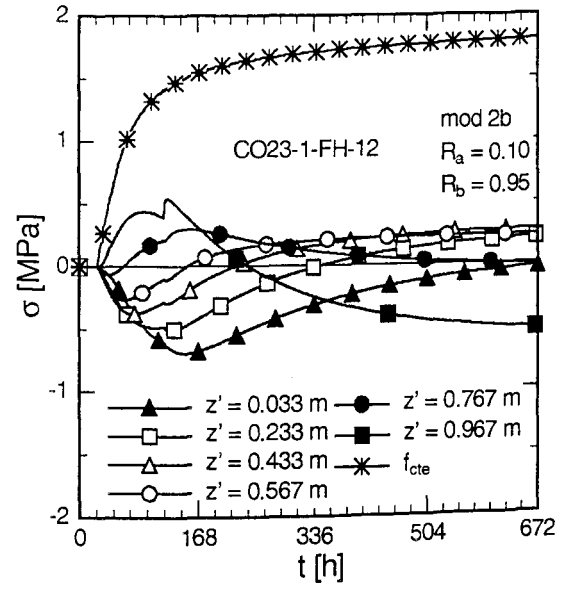

Fig. C.71: Stress vs. Age. Slab CO23-1-FH-15, mod 2b

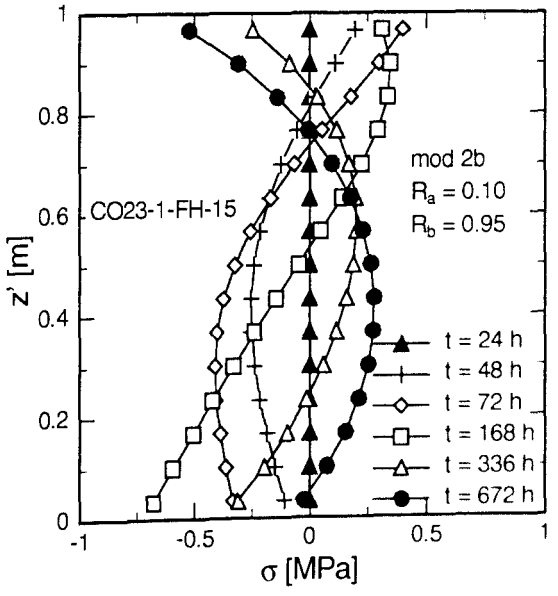

Fig. C.72: Stress vs. Elevation. Slab CO23-1-FH-15, mod 2b

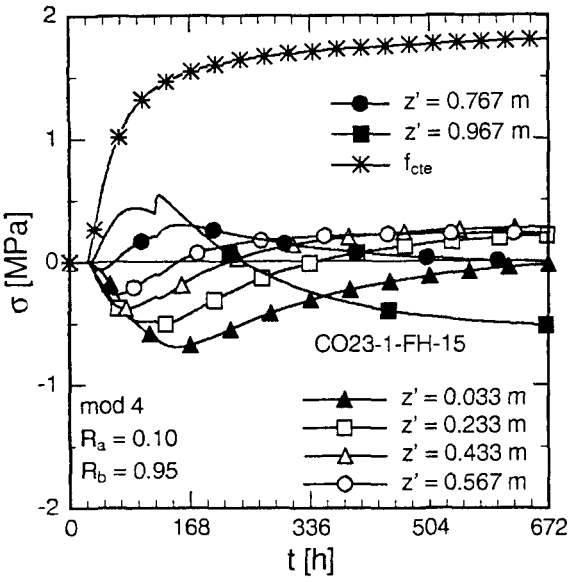

Fig. C.73: Stress vs. Age. Slab CO23-1-FH-15, mod 4

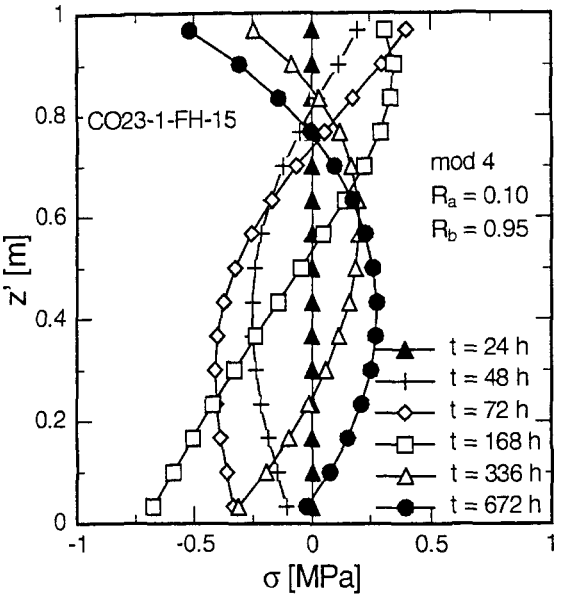

Fig. C.74: Stress vs. Elevation. Slab CO23-1-FH-15, mod 4

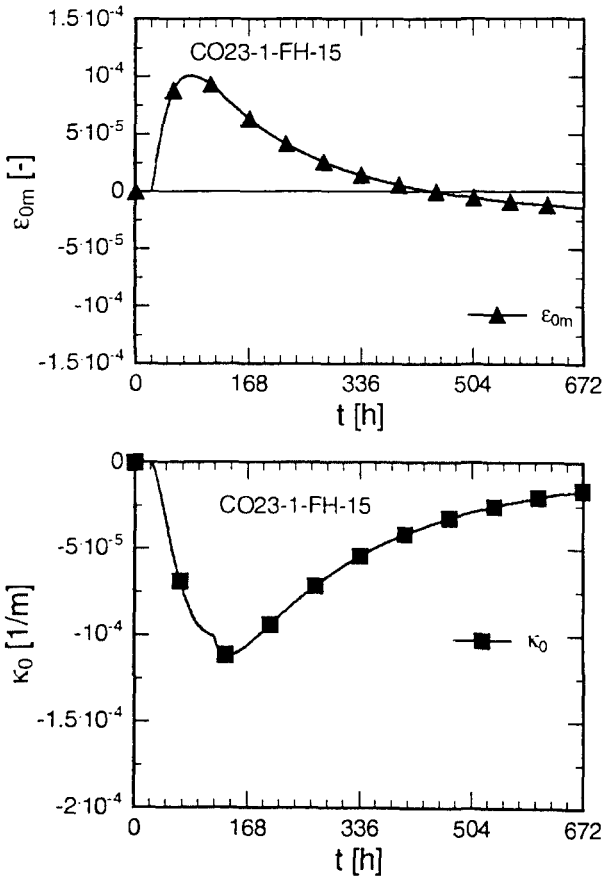

Fig. C.75: Free Thermal Deformation. Slab CO23-1-FH-15

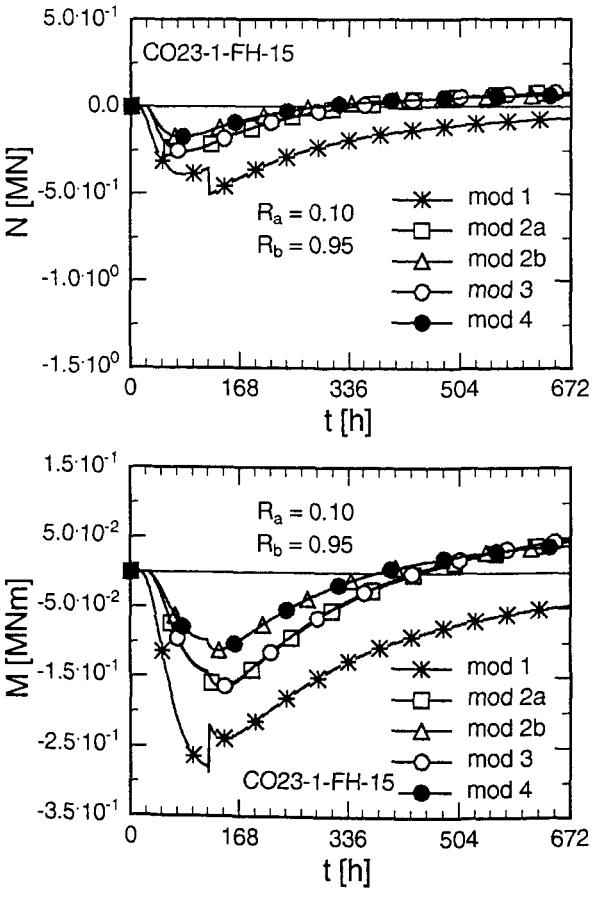

Fig. C.76: Restraint Actions. Slab CO23-1-FH-15, all Models

C.4.2.7 Comparisons

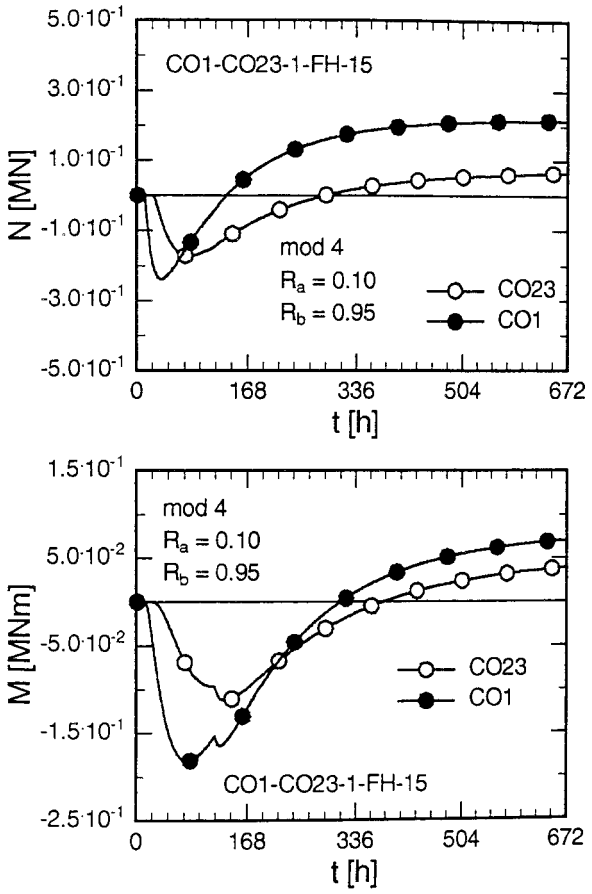

Fig. C.77: Influence of Heat Potential of Concrete on Restraint Actions. Slabs CO1- and CO23-1-FH-15

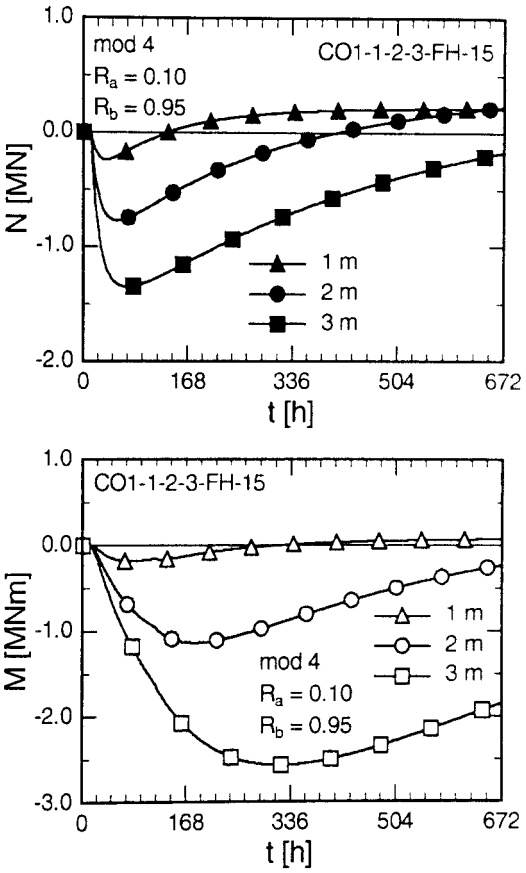

Fig. C.78: Influence of Thickness of Slab on Restraint Actions. Slabs CO1-d_c-FH-15

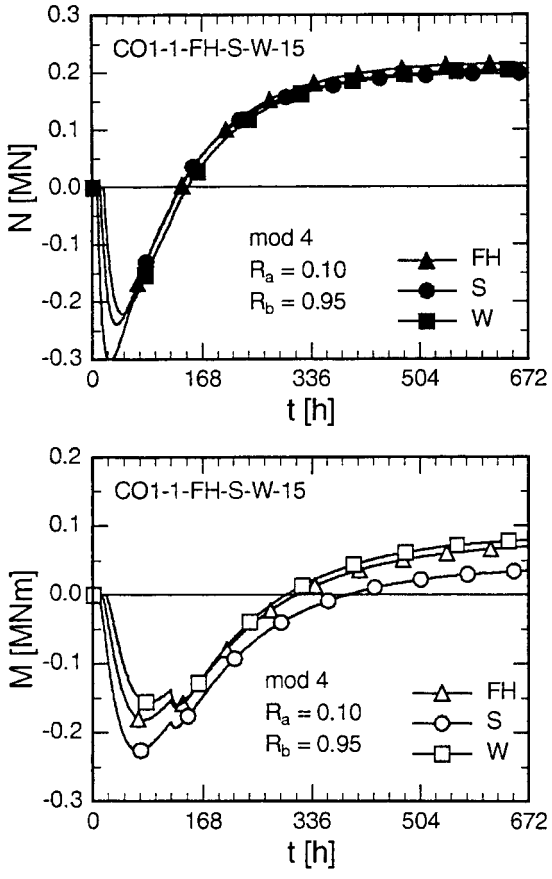

Fig. C.79: Dependence of Restraint Actions on Casting Season. Slab CO1-1-FH/S/W-15

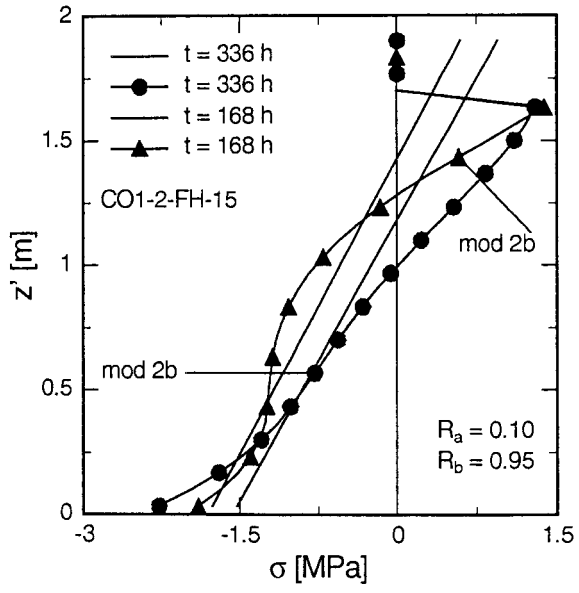

Fig. C.80: Non-Linear vs. Linear Beam Stresses. Slab CO1-2-FH-15, mod 2b

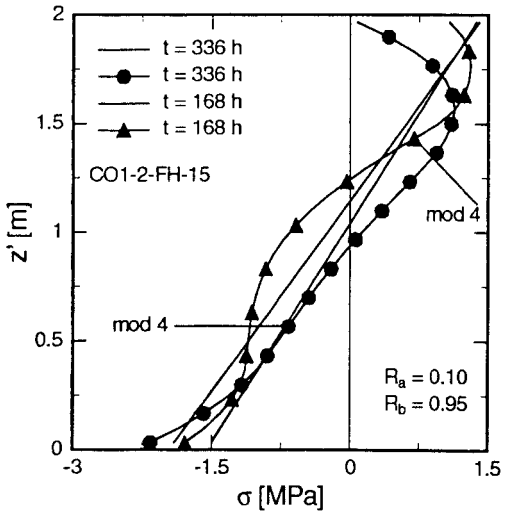

Fig. C.81: Non-Linear vs. Linear Beam Stresses. Slab CO1-2-FH-15, mod 4

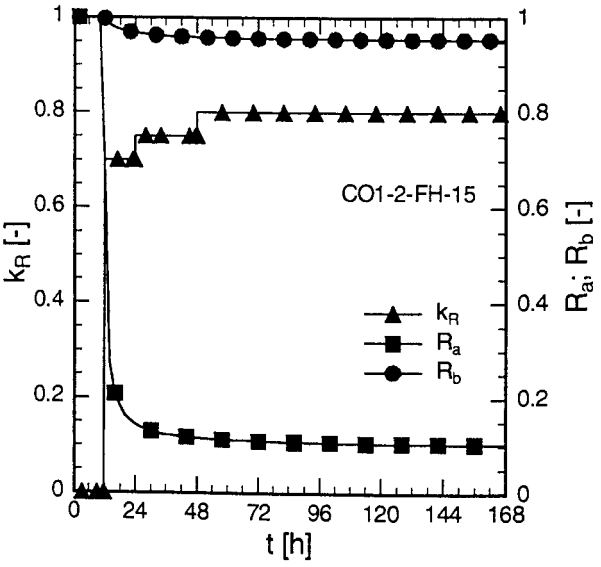

Fig. C.82: Degrees of Restraint and Relaxationfactor k_R Dependent on Age. Slab CO1-2-FH-15

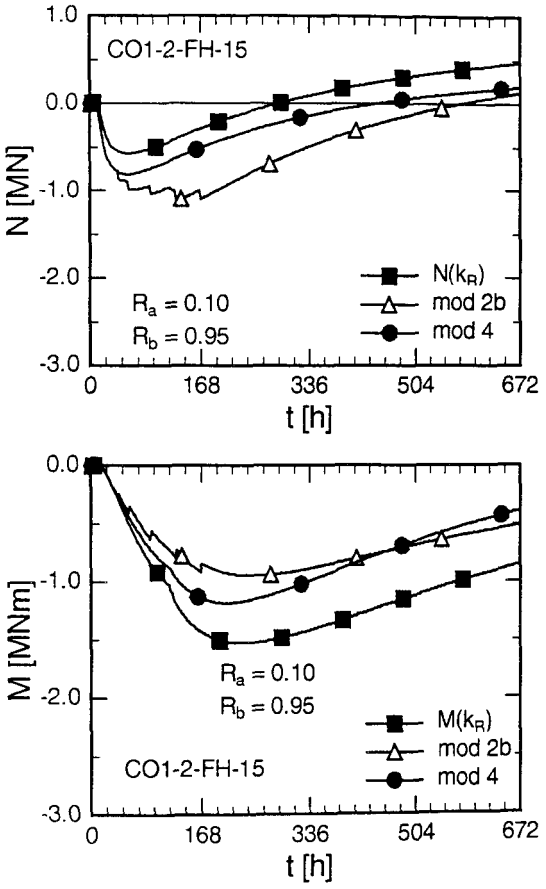

Fig. C.83: Comparison of Restraint Force Acc. Different Models with Effective Age Method

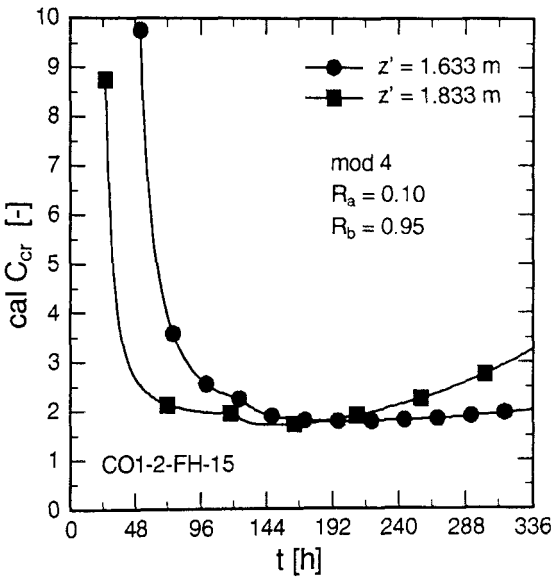

Fig. C.84: Crack Ratio for 2 Elevations vs. Age. Slab CO1-2-FH-15, mod 4

VERZEICHNIS DER BISHER IN DER SCHRIFTENREIHE DES IBMB ERSCHIENENEN HEFTE (ISSN 0178-5796)

In der Schriftenreihe "Institut für Baustoffe, Massivbau und Brandschutz der Technischen Universität Braunschweig - ISSN 0178-5796 (Heft 1 bis 16 als "Institut für Baustoffkunde und Stahlbetonbau der Technischen Hochschule Braunschweig", Heft 17 bis 39 als "Institut für Baustoffkunde und Stahlbetonbau der Technischen Universität Braunschweig") sind bisher die nachfolgend aufgeführten Hefte erschienen.

Sie können bezogen werden von:

Institut für Baustoffe,
Massivbau und Brandschutz
der Technischen Universität Braunschweig
Bibliothek
Beethovenstraße 52
38106 Braunschweig

Tel. (05 31) 3 91-54 54
Fax (05 31) 3 91-45 73
E-Mail o.dienelt@tu-bs.de

oder über jede Buchhandlung.

Kosten:
Je nach Umfang zwischen DM 10,-- und DM 60,--.

Vergriffene Hefte können als Kopien gegen Erstattung der Kopierkosten bezogen werden.

Heft 1:
Deters, R.: Über das Verdunstungsverhalten und den Nachweis öliger Holzschutzmittel. Institut für Baustoffkunde und Stahlbetonbau der Technischen Hochschule Braunschweig, 1962; Zugl.: Dissertation, Technische Hochschule Braunschweig, 1962

Heft 2:
Kordina, K.: Das Verhalten von Stahlbeton- und Spannbetonbauteilen unter Feuerangriff. Institut für Baustoffkunde und Stahlbetonbau der Technischen Hochschule Braunschweig, 1963; Sonderdruck aus: Beton 13(1962), S. 11-18, 81-84

Heft 3:
Eibl, J.: Zur Stabilitätsfrage des Zweigelenkbogens mit biegeweichem Zugband und schlaffen Hängestangen. Institut für Baustoffkunde und Stahlbetonbau der Technischen Hochschule Braunschweig, 1963; Zugl.: Dissertation, Technische Hochschule Braunschweig, 1963

Heft 4:
Kordina, K.; Eibl, J.: Ein Verfahren zur Bestimmung des Vorspannverlustes infolge Schlupf in der Verankerung. Zur Frage der Temperaturbeanspruchung von kreiszylindrischen Stahlbetonsilos. Institut für Baustoffkunde und Stahlbetonbau der Technischen Hochschule Braunschweig, 1964; Sonderdruck aus: Beton- und Stahlbetonbau 58(1963), S. 265-268; 59(1964), S. 1-11

Heft 5:
Ertingshausen, H.: Über den Schalungsdruck von Frischbeton. Institut für Baustoffkunde und Stahlbetonbau der Technischen Hochschule Braunschweig, 1965; Zugl.: Dissertation, Technische Hochschule Hannover, 1965

Heft 6:
Waubke, N.V.: Transportphänomene in Betonporen. Institut für Baustoffkunde und Stahlbetonbau der Technischen Hochschule Braunschweig, 1966; Zugl.: Dissertation, Technische Hochschule Braunschweig, 1968

Heft 7:
Ehm, H.: Ein Beitrag zur rechnerischen Bemessung von brandbeanspruchten balkenartigen Stahlbetonbauteilen. Institut für Baustoffkunde und Stahlbetonbau der Technischen Hochschule Braunschweig, 1967; Zugl.: Dissertation, Technische Hochschule Braunschweig, 1967

Heft 8:
Steinert, J.: Möglichkeiten der Bestimmung der kritischen Last von Stab- und Flächentragwerken mit Hilfe ihrer Eigenfrequenz. Institut für Baustoffkunde und Stahlbetonbau der Technischen Hochschule Braunschweig, 1967; Zugl.: Dissertation, Technische Hochschule Braunschweig, 1967

Heft 9:
Lämmke, A.: Untersuchungen an dämmschichtbildenden Feuerschutzmitteln. Institut für Baustoffkunde und Stahlbetonbau der Technischen Hochschule Braunschweig, 1967; Zugl.: Dissertation, Technische Hochschule Braunschweig, 1967

Heft 10:
Rafla, K.: Beitrag zur Frage der Kippstabilität aufgehängter Träger. Institut für Baustoffkunde und Stahlbetonbau der Technischen Hochschule Braunschweig, 1968; Zugl.: Dissertation, Technische Hochschule Braunschweig, 1968

Heft 11:
Ivanyi, G.: Die Traglast von offenen, kreisförmigen Stahlbetonquerschnitten: Brazier-Effekt. Institut für Baustoffkunde und Stahlbetonbau der Technischen Hochschule Braunschweig, 1968; Zugl.: Dissertation, Technische Hochschule Braunschweig, 1968

Heft 12:
Meyer-Ottens, C.: Brandverhalten verschiedener Bauplatten aus Baustoffen der Klassen A und B. Institut für Baustoffkunde und Stahlbetonbau der Technischen Hochschule Braunschweig, 1969

Heft 13:
Fuchs, G.: Zum Tragverhalten von kreisförmigen Doppelsilos unter Berücksichtigung der Eigensteifigkeit des Füllgutes. Institut für Baustoffkunde und Stahlbetonbau der Technischen Hochschule Braunschweig, 1968; Zugl.: Dissertation, Technische Hochschule Braunschweig, 1968

Heft 14:
Meyer-Ottens, C.: Wände aus Holz und Holzwerkstoffen unter Feuerangriff. Institut für Baustoffkunde und Stahlbetonbau der Technischen Hochschule Braunschweig, 1970; Sonderdruck aus: Mitteilungen der Deutschen Gesellschaft für Holzforschung, H.56(1969)

Heft 15:
Lewandowski, R.: Beurteilung von Bauwerksfestigkeiten anhand von Betongütewürfeln und -bohrproben. Institut für Baustoffkunde und Stahlbetonbau der Technischen Hochschule Braunschweig, 1970; Zugl.: Dissertation, Technische Hochschule Braunschweig, 1970

Heft 16:
Neubauer, F.-J.: Untersuchungen zur Frage der Rissesicherung von leichten Trennwänden aus Gips-Wandbauplatten. Institut für Baustoffkunde und Stahlbetonbau der Tech-nischen Hochschule Braunschweig, 1970; Zugl.: Dissertation, Technische Hochschule Braunschweig, 1969

Heft 17:
Meyer-Ottens, C.; Kordina, K.: Gutachten über das Brandverhalten von Bauteilen aus dampfgehärtetem Gasbeton: aufgestellt für den Fachverband Gasbetonindustrie. Institut für Baustoffkunde und Stahlbetonbau der Technischen Universität Braunschweig, 1970

Heft 17:
Meyer-Ottens, C.; Kordina, K.: Gutachten über das Brandverhalten von Bauteilen aus dampfgehärtetem Gasbeton. Erw. Neuaufl. Institut für Baustoffkunde und Stahlbetonbau der Technischen Universität Braunschweig, 1974

Heft 18:
Bödeker, W.: Die Stahlblech-Holz-Nagelverbindung und ihre Anwendung: Grundlagen und Bemessungsvorschläge. Braunschweig. Institut für Baustoffkunde und Stahlbetonbau der Technischen Universität Braunschweig, 1971; Zugl.: Dissertation, Technische Hochschule Braunschweig, 1971, ISBN 3-89288-057-3

Heft 19:
Meyer-Ottens, C.: Bauaufsichtliche Brandschutzvorschriften: Beispiele für ihre Erfüllung bei Wänden, Brandwänden und Dekken. Institut für Baustoffkunde und Stahlbetonbau der Technischen Universität Braunschweig, 1971

Heft 20:
Liermann, K.: Das Trag- und Verformungsverhalten von Stahlbetonbrückenpfeilern mit Rollenlagern. Institut für Baustoffkunde und Stahlbetonbau der Technischen Universität Braunschweig, 1972; Zugl.: Dissertation, Technische Universität Braunschweig, 1972, ISBN 3-89288-056-5

Heft 22:
Nürnberger, U.: Zur Frage des Spannungsrißkorrosionsverhaltens kohlenstoffarmer Betonstähle in Nitratlösungen unter Berücksichtigung praxisnaher Verhältnisse. Institut für Baustoffkunde und Stahlbetonbau der Technischen Universität Braunschweig, 1972; Zugl.: Dissertation, Technische Universität Braunschweig, 1972, ISBN 3-89288-054-9

Heft 23:
Meyer-Ottens, C.: Zur Frage der Abplatzungen an Betonbauteilen aus Normalbeton bei Brandbeanspruchung. Institut für Baustoffkunde und Stahlbetonbau der Technischen Unversität Braunschweig, 1972; Zugl.: Dissertation, Technische Universität Braunschweig, 1972

Heft 24:
El-Arousy, T.H.: Über die Steinkohlenflugasche und ihre Wirkung auf die Eigenschaften von Leichtbeton mit geschlossenem Gefüge im frischen und festen Zustand. Institut für Baustoffkunde und Stahlbetonbau der Technischen Universität Braunschweig, 1973; Zugl.: Dissertation, Technische Universität Braunschweig, 1973, ISBN 3-89288-053-0

Heft 25:
Rieche, G.: Mechanismen der Spannungskorrosion von Spannstählen im Hinblick auf ihr Verhalten in Spannbetonkonstruktionen. Institut für Baustoffkunde und Stahlbetonbau der Technischen Universität Braunschweig, 1973; Zugl.: Dissertation, Technische Universität Braunschweig, 1973, ISBN 3-89288-052-2

Heft 26:
Tennstedt, E.: Beitrag zur rechnerischen Ermittlung von Zwangschnittgrößen unter Berücksichtigung des wirklichen Verformungsverhaltens des Stahlbetons. Institut für Baustoffkunde und Stahlbetonbau der Technischen Universität Braunschweig, 1974; Zugl.: Dissertation, Technische Universität Braunschweig, 1974, ISBN 3-89288-051-4

Heft 27:
Schneider, U.: Zur Kinetik festigkeitsmindernder Reaktionen in Normalbetonen bei hohen Temperaturen. Institut für Baustoffkunde und Stahlbetonbau der Technischen Universität Braunschweig, 1973; Zugl.: Dissertation, Technische Universität Braunschweig, 1973

Heft 28:
Neisecke, J.: Ein dreiparametriges, komplexes Ultraschall-Prüfverfahren für die zerstörungsfreie Materialprüfung im Bauwesen. Institut für Baustoffkunde und Stahlbetonbau der Technischen Universität Braunschweig, 1974; Zugl.: Dissertation, Technische Universität Braunschweig, 1974, ISBN 3-89288-050-6

Heft 29:
Kordina, K.; Maack, P.; Hjorth, O.: Traglastermittlung an Stahlbeton-Druckgliedern. Schlußbericht (AIF-Nr. 956). Institut für Baustoffkunde und Stahlbetonbau der Technischen Universität Braunschweig, 1974, ISBN 3-89288-048-4

Heft 30:
Eibl, J.; Ivanyi, G.: Berücksichtigung der Torsionssteifigkeit von Randbalken bei Stahlbetondecken. Schlußbericht, Institut für Baustoffkunde und Stahlbetonbau der Technischen Universität Braunschweig, 1974

Heft 31:
Kordina, K.; Janko, B.: Stabilitätsnachweise von Rahmensystemen im Stahlbetonbau. Schlußbericht (AIF-Nr. 1388), Institut für Baustoffkunde und Stahlbetonbau der Technischen Universität Braunschweig, 1974, ISBN 3-89288-049-2

Heft 32:
Hjorth, O.: Ein Beitrag zur Frage der Festigkeiten und des Verbundverhaltens von Stahl und Beton bei hohen Beanspruchungsgeschwindigkeiten. Institut für Baustoffkunde und Stahlbetonbau der Technischen Universität Braunschweig, 1976; Zugl.: Dissertation, Technische Universität Braunschweig, 1975

Heft 33:
Klingsch, W.: Traglastberechnung instationär thermisch belasteter schlanker Stahlbetondruckglieder mittels zwei- und dreidimensionaler Diskretisierung. Institut für Baustoffkunde und Stahlbetonbau der Technischen Universität Braunschweig, 1976; Zugl.: Dissertation, Technische Universität Braunschweig, 1976

Heft 34:
Djamous, F.: Thermische Zerstörung natürlicher Zuschlagstoffe im Beton. Institut für Baustoffkunde und Stahlbetonbau der Technischen Universität Braunschweig, 1977; Zugl.: Dissertation, Technische Universität Braunschweig, 1977

Heft 35:
Haksever, A.: Zur Frage des Trag- und Verformungsverhaltens ebener Stahlbetonrahmen im Brandfall. Braunschweig. Institut für Baustoffkunde und Stahlbetonbau der Technischen Universität Braunschweig, 1977; Zugl.: Dissertation, Technische Universität Braunschweig, 1977

Heft 36:
Storkebaum, K.-H.: Ein Beitrag zur Traglastermittlung von vierseitig gelagerten Stahlbetonwänden. Institut für Baustoffkunde und Stahlbetonbau der Technischen Universität Braunschweig, 1977; Zugl.: Dissertation, Technische Universität Braunschweig, 1977, ISBN 3-89288-045-X

Heft 37:
Bechtold, R.: Zur thermischen Beanspruchung von Außenstützen im Brandfall. Institut für Baustoffkunde und Stahlbetonbau der Technischen Universität Braunschweig, 1977; Zugl.: Dissertation, Technische Universität Braunschweig, 1977, ISBN 3-89288-046-8

Heft 38:
Steinert, J.: Bestimmung der Wasserdurchlässigkeit von Kiesbeton aus dem Wassereindringverhalten. Institut für Baustoffkunde und Stahlbetonbau der Technischen Universität Braunschweig, 1977; Unveränderter Nachdruck der Erstveröffentlichung Bad Honnef, Osang, 1977 (Zivilschutzforschung, Bd. 7)

Heft 39:
Weiß, R.: Ein haufwerkstheoretisches Modell der Restfestigkeit geschädigter Betone. Institut für Baustoffkunde und Stahlbetonbau der Technischen Universität Braunschweig, 1978; Zugl.: Dissertation, Technische Universität Braunschweig, 1978, ISBN 3-89288-047-6

Heft 40:
Alda, W.: Zum Schwingkriechen von Beton. Institut für Baustoffe, Massivbau und Brandschutz der Technischen Universität Braunschweig, 1978; Zugl.: Dissertation, Technische Universität Braunschweig, 1978, ISBN 3-89288-035-2

Heft 41:
Teutsch, M.: Trag- und Verformungsverhalten von Stahlbeton- und Spannbetonbalken mit rechteckigem Querschnitt unter kombinierter Beanspruchung aus Biegung, Querkraft und Torsion. Institut für Baustoffe, Massivbau und Brandschutz der Technischen Universität Braunschweig, 1979; Zugl.: Dissertation, Technische Universität Braunschweig, 1979, ISBN 3-89288-036-0

Heft 42:
Schneider, U.: Ein Beitrag zur Frage des Kriechens und der Relaxation von Beton unter hohen Temperaturen. Institut für Baustoffe, Massivbau und Brandschutz der Technischen Universität Braunschweig, 1979; Zugl.: Dissertation, Technische Universität Braunschweig, 1979

Heft 43:
Institut für Baustoffe, Massivbau und Brandschutz: Veröffentlichungen 1967 bis 1979. Institut für Baustoffe, Massivbau und Brandschutz der Technischen Universität Braunschweig, 1979, ISBN 3-89288-037-9

Heft 44:
Kordina, K.; Fröning, H.: Druckmessungen in Silozellen mit einer neu entwickelten Sonde. Abschlußbericht, Institut für Baustoffe, Massivbau und Brandschutz der Technischen Universität Braunschweig, 1979, ISBN 3-89288-038-7

Heft 45:
Henke, V.: Ein Beitrag zur Zuverlässigkeit frei gelagerter Stahlbetonstützen unter genormter Brandeinwirkung. Institut für Baustoffe, Massivbau und Brandschutz der Technischen Universität Braunschweig, 1980; Zugl.: Dissertation, Technische Universität Braunschweig, 1980

Heft 46:
Schneider, U.; Haksever, A.: Wärmebilanzrechnungen für Brandräume mit unterschiedlichen Randbedingungen (Teil 1). Institut für Baustoffe, Massivbau und Brandschutz der Technischen Universität Braunschweig, 1980

Heft 47:
Walter, R.: Partiell brandbeanspruchte Stahlbetondecken: Berechnung des inneren Zwanges mit einem Scheibenmodell. Institut für Baustoffe, Massivbau und Brandschutz der Technischen Universität Braunschweig, 1981; Zugl.: Dissertation, Technische Universität Braunschweig, 1981, ISBN 3-89288-039-5

Heft 48:
Svensvik, B.: Zum Verformungsverhalten gerissener Stahlbetonbalken unter Einschluß der Mitwirkung des Betons auf Zug in Abhängigkeit von Last und Zeit. Institut für Baustoffe, Massivbau und Brandschutz der Technischen Universität Braunschweig, 1981; Zugl.: Dissertation, Technische Universität Braunschweig, 1981, ISBN 3-89288-040-9

Heft 49:
Institut für Baustoffe, Massivbau und Brandschutz: Veröffentlichungen 1967 bis 1981. Institut für Baustoffe, Massivbau und Brandschutz der Technischen Universität Braunschweig, 1981, ISBN 3-89288-041-7

Heft 50:
Ojha, S.K.: Die Steifigkeit und das Verformungsverhalten von Stahlbeton- und Spannbetonbalken unter kombinierter Beanspruchung aus Torsion, Biegemoment, Querkraft und Axialkraft. Institut für Baustoffe, Massivbau und Brandschutz der Technischen Universität Braunschweig, 1982, ISBN 3-89288-042-5

Heft 51:
Henke, V.: Zusammenstellung und Anwendung Bayes'scher Verfahren bei der Stichprobenbeurteilung. Projekt D1 des SFB 148. Institut für Baustoffe, Massivbau und Brandschutz der Technischen Universität Braunschweig, 1982, ISBN 3-89288-043-3

Heft 52:
Haksever, A.: Stahlbetonstützen mit Rechteckquerschnitten bei natürlichen Bränden. Institut für Baustoffe, Massivbau und Brandschutz der Technischen Universität Braunschweig, 1982; Zugl.: Habil.-Schr., Technische Universität Istanbul, 1982, ISBN 3-89288-044-1

Heft 53:
Weber, V.: Untersuchung des Riß- und Verformungsverhaltens segmentärer Spannbetonbauteile. Braunschweig. Institut für Baustoffe, Massivbau und Brandschutz der Technischen Universität Braunschweig, 1982; Zugl.: Dissertation, Technische Universität Braunschweig, 1982, ISBN 3-89288-017-4

Heft 54:
Ranisch, E.-H.: Zur Tragfähigkeit von Verklebungen zwischen Baustahl und Beton: geklebte Bewehrung. Institut für Baustoffe, Massivbau und Brandschutz der Technischen Universität Braunschweig, 1982; Zugl.: Dissertation, Technische Universität Braunschweig, 1982

Heft 54:
Ranisch, E.-H.: Zur Tragfähigkeit von Verklebungen zwischen Baustahl und Beton: geklebte Bewehrung. Unveränderter Nachdruck der Ausgabe 1982. Institut für Baustoffe, Massivbau und Brandschutz der Technischen Universität Braunschweig, 1986; Zugl.: Dissertation, Technische Universität Braunschweig, 1982, ISBN 3-89288-010-7

Heft 55:
Wiedemann, G.: Zum Einfluß tiefer Temperaturen auf Festigkeit und Verformung von Beton. Institut für Baustoffe, Massivbau und Brandschutz der Technischen Universität Braunschweig, 1982; Zugl.: Dissertation, Technische Universität Braunschweig, 1982

Heft 56:
Timm, R.: Ein geometrisch und physikalisch nichtlineares Rechenmodell zur optimalen Biegebemessung ebener Stahlbetonrahmen. Institut für Baustoffe, Massivbau und Brandschutz der Technischen Universität Braunschweig, 1982; Zugl.: Dissertation, Technische Universität Braunschweig, 1982, ISBN 3-89288-018-2

Heft 57:
Diederichs, U.: Untersuchungen über den Verbund zwischen Stahl und Beton bei hohen Temperaturen. Institut für Baustoffe, Massivbau und Brandschutz der Technischen Universität Braunschweig, 1983; Zugl.: Dissertation, Technische Universität Braunschweig, 1983, ISBN 3-89288-019-0

Heft 58:
Schneider, U.: Wärmebilanzrechnungen in Verbindung mit Versuchen in Brandräumen (Teil 2). Institut für Baustoffe, Massivbau und Brandschutz der Technischen Universität Braunschweig, 1983, ISBN 3-89288-020-4

Heft 59:
Dobbernack, R.: Wärmebilanzrechnungen in Brandräumen unter Berücksichtigung der Mehrzonenmodellbildung (Teil 3). Institut für Baustoffe, Massivbau und Brandschutz der Technischen Universität Braunschweig, 1983, ISBN 3-89288-021-2

Heft 60:
Hillger, W.: Verbesserungen und Erweiterungen von Ultraschallprüfverfahren zur zerstörungsfreien Fehlstellen- und Qualitätskontrolle von Betonbauteilen. Institut für Baustoffe, Massivbau und Brandschutz der Technischen Universität Braunschweig, 1983; Zugl.: Dissertation, Technische Universität Braunschweig, 1983, ISBN 3-89288-014-X

Heft 61:
Blume, F.: Zur Wirklichkeitsnähe der Lastannahmen in Silovorschriften für Zellen aus Stahlbeton und Spannbeton. Institut für Baustoffe, Massivbau und Brandschutz der Technischen Universität Braunschweig, 1984; Zugl.: Dissertation, Technische Universität Braunschweig, 1984, ISBN 3-89288-013-1

Heft 62:
Nölting, D.: Das Durchstanzen von Platten aus Stahlbeton : Tragverhalten, Berechnung, Bemessung. Institut für Baustoffe, Massivbau und Brandschutz der Technischen Universität Braunschweig, 1984; Zugl.: Dissertation, Technische Universität Braunschweig, 1984, ISBN 3-89288-012-3

Heft 63:
Wesche, J.: Brandverhalten von Stahlbetonplatten im baupraktischen Einbauzustand. Institut für Baustoffe, Massivbau und Brandschutz der Technischen Universität Braunschweig, 1985; Zugl.: Dissertation, Technische Universität Braunschweig, 1985, ISBN 3-89288-009-3

Heft 64:
Droese, S.: Untersuchungen zur Technologie des Gleitschalungsbaus. Institut für Baustoffe, Massivbau und Brandschutz der Technischen Universität Braunschweig, 1985; Zugl.: Dissertation, Technische Universität Braunschweig, 1985, ISBN 3-89288-000-X

Heft 65:
Institut für Baustoffe, Massivbau und Brandschutz: Forschungsarbeiten 1978 - 1983. Institut für Baustoffe, Massivbau und Brandschutz der Technischen Universität Braunschweig, 1984, ISBN 3-89288-001-8

Heft 66:
Hegger, J.: Einfluß der Verbundart auf die Grenztragfähigkeit von Spannbetonbalken. Institut für Baustoffe, Massivbau und Brandschutz der Technischen Universität Braunschweig, 1985; Zugl.: Dissertation, Technische Universität Braunschweig, 1985, ISBN 3-89288-002-6

Heft 67:
Kepp, B.: Zum Tragverhalten von Verankerungen für hochfeste Stäbe aus Glasfaserverbundwerkstoff als Bewehrung im Spannbetonbau. Institut für Baustoffe, Massivbau und Brandschutz der Technischen Universität Braunschweig, 1985; Zugl.: Dissertation, Technische Universität Braunschweig, 1985, ISBN 3-89288-003-4

Heft 68:
Sager, H.: Zum Einfluß hoher Temperaturen auf das Verbundverhalten von einbetonierten Bewehrungsstäben. Institut für Baustoffe, Massivbau und Brandschutz der Technischen Universität Braunschweig, 1985; Zugl.: Dissertation, Technische Universität Braunschweig, 1985, ISBN 3-89288-004-2

Heft 69:
Haß, R.: Zur praxisgerechten brandschutztechnischen Beurteilung von Stützen aus Stahl und Beton. Institut für Baustoffe, Massivbau und Brandschutz der Technischen Universität Braunschweig, 1986; Zugl.: Dissertation, Technische Universität Braunschweig, 1986, ISBN 3-89288-005-0

Heft 70:
Institut für Baustoffe, Massivbau und Brandschutz: 17. Forschungskolloquium des Deutschen Ausschusses für Stahlbeton, März 1986, Kurzfassungen der Beiträge. Institut für Baustoffe, Massivbau und Brandschutz der Technischen Universität Braunschweig, 1986, ISBN 3-89288-006-9

Heft 71:
Ehm, C.: Versuche zur Festigkeit und Verformung von Beton unter zweiaxialer Beanspruchung und hohen Temperaturen. Institut für Baustoffe, Massivbau und Brandschutz der Technischen Universität Braunschweig, 1986; Zugl.: Dissertation, Technische Universität Braunschweig, 1986, ISBN 3-89288-007-7

Heft 72:
Hartwich, K.: Zum Riß- und Verformungsverhalten von Stahlfaserverstärkten Stahlbetonstäben unter Längszug. Institut für Baustoffe, Massivbau und Brandschutz der Technischen Universität Braunschweig, 1986; Zugl.: Dissertation, Technische Universität Braunschweig, 1986, ISBN 3-89288-008-5

Heft 73:
Scheuermann, J.: Zum Einfluß tiefer Temperaturen auf Verbund und Rißbildung von Stahlbetonbauteilen. Institut für Baustoffe, Massivbau und Brandschutz der Technischen Universität Braunschweig, 1987; Zugl.: Dissertation, Technische Universität Braunschweig, 1987, ISBN 3-89288-011-5

Heft 74:
Hinrichsmeyer, K.: Strukturorientierte Analyse und Modellbeschreibung der thermischen Schädigung von Beton. Institut für Baustoffe, Massivbau und Brandschutz der Technischen Universität Braunschweig, 1987; Zugl.: Dissertation, Technische Universität Braunschweig, 1987, ISBN 3-89288-015-8

Heft 75:
Institut für Baustoffe, Massivbau und Brandschutz: Fachseminar Neue Bemessungsregeln durch Änderung der Stahlbeton- und Spannbetonvorschriften DIN 1045, DIN 4227, Juni 1986, Kurzfassungen der Beiträge. Institut für Baustoffe, Massivbau und Brandschutz der Technischen Universität Braun-schweig, 1986, ISBN 3-89288-022-0

Heft 76:
Budelmann, H.: Zum Einfluß erhöhter Temperaturen auf Festigkeit und Verformung von Beton mit unterschiedlichen Feuchtegehalten. Institut für Baustoffe, Massivbau und Brandschutz der Technischen Universität Braunschweig, 1987; Zugl.: Dissertation, Technische Universität Braunschweig, 1987, ISBN 3-89288-016-6

Heft 77:
Großmann, F.: Spannungen und bruchmechanische Vorgänge im Normelbeton unter Zugbeanspruchung. Institut für Baustoffe, Massivbau und Brandschutz der Technischen Universität Braunschweig, 1987; Zugl.: Dissertation, Technische Universität Braunschweig, 1987, ISBN 3-89288-023-9

Heft 78:
Rohling, A.: Zum Einfluß des Verbundkriechens auf die Rißbreitenentwicklung sowie auf die Mitwirkung des Betons zwischen den Rissen. Institut für Baustoffe, Massivbau und Brandschutz der Technischen Universität Braunschweig, 1987; Zugl.: Dissertation, Technische Universität Braunschweig, 1987, ISBN 3-89288-024-7

Heft 79:
Henning, W.: Zwangrißbildung und Bewehrung von Stahlbetonwänden auf steifen Unterbauten. Institut für Baustoffe, Massivbau und Brandschutz der Technischen Universität Braunschweig, 1987; Zugl.: Dissertation, Technische Universität Braunschweig, 1987, ISBN 3-89288-025-5

Heft 80:
Richter, E.: Zur Berechnung der Biegetragfähigkeit brandbeanspruchter Spannbetonbauteile unter Berücksichtigung geeigneter Vereinfachungen für die Materialgesetze. Institut für Baustoffe, Massivbau und Brandschutz der Technischen Universität Braunschweig, 1987; Zugl.: Dissertation, Technische Universität Braunschweig, 1987, ISBN 3-89288-026-3

Heft 81:
Kiel, M.: Nichtlineare Berechnung ebener Stahlbetonflächentragwerke unter Einschluß von Brandbeanspruchung. Institut für Baustoffe, Massivbau und Brandschutz der Technischen Universität Braunschweig, 1987; Zugl.: Dissertation, Technische Universität Braunschweig, 1987, ISBN 3-89288-027-1

Heft 82:
Konietzko, A.: Polymerspezifische Auswirkungen auf das Tragverhalten modifizierter zementgebundener Betone (PCC). Institut für Baustoffe, Massivbau und Brandschutz der Technischen Universität Braunschweig, 1988; Zugl.: Dissertation, Technische Universität Braunschweig, 1988, ISBN 3-89288-028-X

Heft 83:
Grzeschkowitz, R.: Zum Trag- und Verformungsverhalten schlanker Stahlbetonstützen unter besonderer Berücksichtigung der schiefen Biegung. Institut für Baustoffe, Massivbau und Brandschutz der Technischen Universität Braunschweig, 1988; Zugl.: Dissertation, Technische Universität Braunschweig, 1988, ISBN 3-89288-030-1

Heft 84:
Wiese, J.: Zum Trag- und Verformungsverhalten von Stahlbetonplatten unter partieller Brandbeanspruchung. Institut für Baustoffe, Massivbau und Brandschutz der Technischen Universität Braunschweig, 1988; Zugl.: Dissertation, Technische Universität Braunschweig, 1988, ISBN 3-89288-031-X

Heft 85:
Rudolph, K.: Traglastberechnung zweiachsig biegebeanspruchter Stahlbetonstützen unter Brandeinwirkung. Institut für Baustoffe, Massivbau und Brandschutz der Technischen Universität Braunschweig, 1988; Zugl.: Dissertation, Technische Universität Braunschweig, 1988, ISBN 3-89288-032-8

Heft 86:
Kordina, K.; Meyer-Ottens, C.; Noack, I.: Einfluß der Eigenbrandlast auf das Brandverhalten von Bauteilen aus brennbaren Baustoffen. Institut für Baustoffe, Massivbau und Brandschutz der Technischen Universität Braunschweig, 1989, in Vorbereitung, ISBN 3-89288-058-1

Heft 87:
Institut für Baustoffe, Massivbau und Brandschutz: Forschungsarbeiten 1984 - 1989. Institut für Baustoffe, Massivbau und Brandschutz der Technischen Universität Braunschweig, 1989, ISBN 3-89288-034-4

Heft 88:
Grossert, E.: Untersuchungen zum Tragverhalten von Massivbrücken mit zweizelligem Kastenquerschnitt. Institut für Baustoffe, Massivbau und Brandschutz der Technischen Universität Braunschweig, 1989; Zugl.: Dissertation, Technische Universität Braunschweig, 1989, ISBN 3-89288-059-X

Heft 89:
Falkner, H.; Teutsch, M. [Hrsg.]: Weiterbildungsseminar "Bauen in Europa", 15.-16. November 1990 in Braunschweig, Kurzreferate, ISBN 3-89288-063-8

Heft 90:
Falkner, H.; Teutsch, M.; Claußen, T.; Voß, K.-U.: Vorspannung im Hochbau. Institut für Baustoffe, Massivbau und Brandschutz der Technischen Universität Braunschweig, 1991, ISBN 3-89288-064-6

Heft 91:
Falkner, H.; Teutsch, M. [Hrsg.]: Fachtagung Spannbeton im Hoch- und Industriebau, Kurzreferate, 1991, ISBN 3-89288-065-4

Heft 92:
Heins, T.: Simulationsmodell zur sicherheitstechnischen Beurteilung der Rauchausbreitung in ausgedehnten Räumen. Institut für Baustoffe, Massivbau und Brandschutz der Technischen Universität Braunschweig, 1991; Zugl.: Dissertation, Technische Universität Braunschweig, ISBN 3-89288-066-2

Heft 93:
Hagen, E.: Zur Prognose des Gefährdungspotentials von Raumbränden. Institut für Baustoffe, Massivbau und Brandschutz der Technischen Universität Braunschweig, 1992; Zugl.: Dissertation, Technische Universität Braunschweig, 1991, ISBN 3-89288-072-7

Heft 94:
Falkner, H.; Teutsch, M. [Hrsg.]: Fachseminar "Instandsetzung und Ertüchtigung von Massivbauten", 14.-15. November 1991 in Braunschweig, Kurzreferate, ISBN 3-89288-068-9

Heft 95:
Qualitätssicherung im Bauwesen, VMPA-Tagung 1992, 25.-26.06.1992, Tagungsbericht, ISBN 3-89288-071-9

Heft 96:
Weiterbildungsseminar "Brandschutz im Industriebau", 30.09.1992 in Braunschweig, Kurzreferate, ISBN 3-89288-070-0

Heft 97:
Falkner, H.; Teutsch, M. [Hrsg.]: Fachseminar "Neue Technologien im Bauwesen", 12.-13.11.1992 in Braunschweig, Kurzreferate, ISBN 3-89288-073-5

Heft 98:
Gunkler, E.: Verstärkung biegebeanspruchter Mauerwerkswände durch bewehrte Ergänzungsschichten. Institut für Baustoffe, Massivbau und Brandschutz der Technischen Universität Braunschweig, 1993; Zugl.: Dissertation, Technische Universität Braunschweig, 1992, ISBN 3-89288-074-3

Heft 99:
Dorn, T.: Zur Berechnung des Tragverhaltens brandbeanspruchter Tragwerke in Verbundbauweise unter besonderer Berücksichtigung der Träger-Stützen-Anschlüsse. Institut für Baustoffe, Massivbau und Brandschutz der Technischen Universität Braunschweig, 1993; Zugl.: Dissertation, Technische Universität Braunschweig, 1992, ISBN 3-89288-075-1

Heft 100:
Falkner, H.; Teutsch, M. [Hrsg.]: Fachseminar "Stahlfaserbeton", 04.03.1993 in Braunschweig, Kurzreferate, ISBN 3-89288-076-X

Heft 101:
Falkner, H.; Teutsch, M.: Vergleichende Untersuchungen an unbewehrten und stahlfaserbewehrten Industriefußböden. Forschungsbericht, Institut für Baustoffe, Massivbau und Brandschutz der Technischen Universität Braunschweig, 1993, ISBN 3-89288-077-8

Heft 102:
Falkner, H.; Teutsch, M.: Comperative studies of plain and steel fiber reinforced concrete industrial ground slabs. Forschungsbericht, Institut für Baustoffe, Massivbau und Brandschutz der Technischen Universität Braunschweig, 1993, ISBN 3-89288-078-6

Heft 103:
Braunschweiger Brandschutz-Tage 1993: Fachseminar Brandschutz - Forschung und Praxis. 06.-07.10.1993, Kurzreferate, ISBN 3-89288-079-4

Heft 104:
Thienel, K.-C.: Festigkeit und Verformung von Beton bei hoher Temperatur und biaxialer Beanspruchung. Institut für Baustoffe, Massivbau und Brandschutz der Technischen Universität Braunschweig, 1993
Zugl.: Dissertation, Technische Universität Braunschweig, 1993, ISBN 3-89288-080-8

Heft 105:
Falkner, H.; Teutsch, M. [Hrsg.]: Braunschweiger Bauseminar 1993 "Dauerhafte Bauwerke aus Faserbeton", 11.-12.11.1993 in Braunschweig, Kurzreferate, ISBN 3-89288-081-6

Heft 106:
Neuentwicklungen im baulichen Brandschutz. Dr. Meyer-Ottens 60 Jahre; Fachseminar 18.03.1994 in Braunschweig, ISBN 3-89288-085-9

Heft 107:
Bunte, D.: Zum karbonatisierungsbedingten Verlust der Dauerhaftigkeit von Außenbauteilen aus Stahlbeton. Institut für Baustoffe, Massivbau und Brandschutz der Technischen Universität Braunschweig, 1994
Zugl.: Dissertation, Technische Universität Braunschweig, 1993, ISBN 3-89288-086-7

Heft 108:
Holzenkämpfer, P.: Ingenieurmodell des Verbundes geklebter Bewehrung für Betonbauteile. Institut für Baustoffe, Massivbau und Brandschutz der Technischen Universität Braunschweig, 1994
Zugl.: Dissertation, Technische Universität Braunschweig, 1994, ISBN 3-89288-087-5

Heft 109:
Forschungsarbeiten 1990 - 1994. Institut für Baustoffe, Massivbau und Brandschutz der Technischen Universität Braunschweig, 1994, ISBN 3-89288-088-3

Heft 110:
Falkner, H.; Teutsch, M.; Rohde, S.: Untersuchung der Schubtragfähigkeit und der Wasserundurchlässigkeit von Arbeitsfugen unter Verwendung von Stremaform-Abschalelementen.
Falkner, H.; Teutsch, M.; Claußen, T.: Schubtragfähigkeit des Vergußbetons zwischen Köcher-, Block oder Hülsenfundamenten und Stützenfuß bei unterschiedlich profilierten Betonoberflächen.
Institut für Baustoffe, Massivbau und Brandschutz der Technischen Universität Braunschweig, 1994, ISBN 3-89288-089-1

Heft 111:
Voß, K.-U.: Zum Trag- und Verformungsverhalten bei Schwellbeanspruchung. Institut für Baustoffe, Massivbau und Brandschutz der Technischen Universität Braunschweig, 1994
Zugl.: Dissertation, Technische Universität Braunschweig, 1993, ISBN 3-89288-090-5

Heft 112:
Weiterbildungsseminar Brandschutz bei Sonderbauten: 05./06.10.1994 in Braunschweig; Kurzreferate, 1994, ISBN 3-89288-092-1

Heft 113:
Falkner, H.; Teutsch, M. [Hrsg.]: Aus der Forschung in die Praxis: 10./11.11.1994; Braunschweiger Bauseminar 1994, ISBN 3-89288-091-3

Heft 114:
Warnecke, P.: Tragverhalten und Konsolidierung von historischem Natursteinmauerwerk, 1995
Zugl.: Dissertation, Technische Universität Braunschweig, 1995, ISBN 3-89288-094-8

Heft 115:
Braunschweiger Brandschutz-Tage 1995: 6. Fachseminar Brandschutz - Forschung und Praxis: 04.-05.10.1995, Kurzreferate, ISBN 3-89288-093-X

Heft 116:
Huang, Z.: Grenzbeanspruchung gebetteter Stahlfaserbetonplatten, 1995
Zugl.: Dissertation, Technische Universität Braunschweig, 1995, ISBN 3-89288-095-6

Heft 117:
Falkner, H.; Teutsch, M.; Huang, Z.: Untersuchung des Trag- und Verformungsverhaltens von Industriefußböden aus Stahlfaserbeton. Institut für Baustoffe, Massivbau und Brandschutz der Technischen Universität Braunschweig, 1995, ISBN 3-89288-096-4

Heft 118:
Kubat, B.: Durchstanzverhalten von vorgespannten, punktförmig gestützten Platten aus Stahlfaserbeton, 1995
Zugl.: Dissertation, Technische Universität Braunschweig, 1995, ISBN 3-89288-097-2

Heft 119:
Falkner, H.; Teutsch, M. [Hrsg.]: Dichte Bauwerke: 09./10.11.1995; Braunschweiger Bauseminar 1995, ISBN 3-89288-091-3

Heft 120:
Steinert, C.: Bestimmung der Wärmeübergangsbedingungen auf Bauteile im Brandfall, Abschlußbericht, 1995, ISBN 3-89288-099-9

Heft 121:
Schütte, J.; Teutsch, M.; Falkner, H.: Fugenlose Betonbodenplatten, Forschungsbericht, 1996, ISBN 3-89288-100-6

Heft 122:
Weiterbildungsseminar Brandschutz bei Sonderbauten: 24./25.09.1996 in Braunschweig, Kurzreferate, 1996, ISBN 3-89288-101-4

Heft 123:
Droese, S.; Riese, A.: Belastungsversuche an zwei Durchlauf-Plattenstreifen aus Elementplatten mit Aufbeton aus Stahlfaserbeton, 1996, ISBN 3-89288-102-4

Heft 124:
Hankers, C.: Zum Verbundtragverhalten laschenverstärkter Betonbauteile unter nicht vorwiegend ruhender Beanspruchung, 1996
Zugl.: Dissertation, Technische Universität Braunschweig, 1996, ISBN 3-89288-103-0

Heft 125:
Schmidt-Döhl, F.: Ein Modell zur Berechnung von kombinierten chemischen Reaktions- und Transportprozessen und seine Anwendung auf die Korrosion mineralischer Baustoffe, 1996
Zugl.: Dissertation, Technische Universität Braunschweig, 1996, ISBN 3-89288-104-9

Heft 126:
Falkner, H.; Teutsch, M. [Hrsg.]: Ingenieurbauwerke mit neuen Konzepten: 14./15.11.1996, Braunschweiger Bauseminar 1996, ISBN 3-89288-105-7

Heft 127:
Forschung über Baudenkmalpflege - Arbeitsberichte: 1990 - 1993, 1996, ISBN 3-89288-106-5

Heft 128:
Festschrift zum 65. Geburtstag von Prof. Dr.-Ing. F. S. Rostásy: Baustoffe in Praxis, Lehre und Forschung, 1997, ISBN 3-89288-107-3

Heft 129:
Forschung über Baudenkmalpflege - Arbeitsberichte: 1994, 1997, ISBN 3-89288-108-1

Heft 130:
Forschung über Baudenkmalpflege - Arbeitsberichte: 1995, 1997,
ISBN 3-89288-109-X

Heft 131:
Falkner, H.; Teutsch, M.; Klinkert H.: Trag- und Verformungsverhalten dynamisch beanspruchter Fahrbahnen aus Beton- und Stahlfaserbeton, Forschungsbericht, 1997, ISBN 3-89288-110-3

Heft 132:
Schütte, J.: Einfluß der Lagerungsbedingungen auf Zwang in Betonbodenplatten, 1997
Zugl.: Dissertation, Technische Universität Braunschweig, 1997, ISBN 3-89288-111-1

Heft 133:
Braunschweiger Brandschutz-Tage 1997: 7. Fachseminar Brandschutz - Forschung und Praxis: 01.-02.10.1997, Kurzreferate,
ISBN 3-89288-112-X

Heft 134:
Ameler, J.: Betonverhalten bei hohen Temperaturen und triaxialer Beanspruchung - FE-Modell auf der Basis der Betonstruktur, 1997
Zugl.: Dissertation, Technische Universität Braunschweig, 1997, ISBN 3-89288-113-8

Heft 135:
Tagung Konsolidierung von historischem Natursteinmauerwerk: 06./07.11.1997 in Braunschweig, ISBN 3-89288-114-6

Heft 136:
Falkner, H.; Teutsch, M. [Hrsg.]: Innovatives Bauen: 13./14.11.1997, Braunschweiger Bauseminar 1997, ISBN 3-89288-115-4

Heft 137:
Forschung über Baudenkmalpflege - Arbeitsberichte: 1996 - 1997. 1998.
ISBN 3-89288-116-2

Heft 138:
Scheibe, M.: Vorhersage des Zeitstandverhaltens unidirektionaler Aramidfaserverbundstäbe in alkalischer Umgebung. 1998.
Zugl.: Braunschweig, TU, Diss., 1998.
ISBN 3-89288-117-0

Heft 139:
Weiterbildungsseminar Brandschutz bei Sonderbauten : 29./30.9.1998 in Braunschweig ; Kurzreferate. 1998.
ISBN 3-89288-118-9

Heft 140:
Gutsch, A.: Stoffeigenschaften jungen Betons - Versuche und Modelle. 1998. Zugl.: Braunschweig, TU, Diss.
ISBN 3-89288-119-7

Heft 141:
Falkner, H. ; Teutsch, M. [Hrsg.]
Beton auf neuen Wegen : 12.-13.11.1998 ; Braunschweiger Bauseminar 1998.
ISBN 3-89288-120-0

Heft 142:
Betonbau - Forschung, Entwicklung und Anwendung : Festschrift zum 60. Geburtstag von Univ.-Prof. Dr.-Ing Horst Falkner am 20.4.1999. 1999.
ISBN 3-89288-121-9

Heft 143:
Teutsch, M ; Klinkert, H.
Leistungsklassen von Stahlfaserbeton. 1999.
ISBN 3-89288-122-7

Heft 144:
Forschungsarbeiten 1995 - 1999. 1999.
ISBN 3-89288-123-5

Heft 145:
Braunschweiger Brandschutztage 1999: 8. Fachseminar Brandschutz - Forschung und Praxis ; 4.-5. Oktober 1999 in Braunschweig., Kurzreferate. 1999.
ISBN 3-89288-124-3

Heft 146:
Falkner, H. ; Teutsch, M. [Hrsg.]
Bauen im nächsten Jahrtausend : 11.11.-12.11.1999 ; Braunschweiger Bauseminar 1999.
ISBN 3-89288-125-1

Heft 147:
Weiterbildungsseminar Brandschutz bei Sonderbauten: 28./29.3.2000 in Braunschweig; Kurzreferate, 2000.
ISBN 3-89288-126-X

Heft 148:
Hariri, K.: Bruchmechanisches Verhalten jungen Betons - Laser-Speckle-Interferometrie und Modellierung der Rißprozeßzone. 2000.
Zugl.: Braunschweig, TU, Diss., 2000.
ISBN 3-89288-127-8

Heft 149:
Wigger, H.: Rissbildung in historischem Natursteinmauerwerk : Beobachtung, Versuche und Berechnungsmodelle. 2000.
Zugl.: Braunschweig, TU, Diss., 2000.
ISBN 3-89288-128-6

Heft 150:
Neubauer, U.: Verbundtragverhalten geklebter Lamellen aus Kohlenstoffaser – Verbundwerkstoff zur Verstärkung von Betonbauteilen. 2000
Zugl.: Braunschweig, TU, Diss., 2000.
ISBN 3-89288-129-4.

Heft 151:
Brandschutz in Chemikalienlagern. 2000.
ISBN 3-89288-130-8

Heft 152:
Falkner, H. ; Teutsch, M. [Hrsg.]
Trends und Entwicklungen im Bauwesen : 9.-10.11.2000 ; Braunschweiger Bauseminar 2000.
ISBN 3-89288-131-6

Heft 153:
Rostásy, F.S. ; Budelmann, H. [Hrsg.]
Rissbeherrschung massiger Betonbauteile : Bauwerk, Werkstoff, Simulation ; Braunschweig, 20.3.2001.
ISBN 3-89288-132-4

Heft 154:
Krauß, M. ; Hariri, K. ; Rostásy, F.S.
Hydratationsgrad, Ultraschall-Technik zur Beschreibung der Erhärtung, bruchmechanisches Verhalten jungen Betons : Berichte ; Forschungsprojekt der EU (Brite Euram BE96-3843), IPACS. 2001.
ISBN 3-89288-135-9.

Heft 155:
Gutsch, A. ; Rostásy, F.S.
Spannungs-Dehnungslinie, viskoelastisches Verhalten und autogenes Schwinden jungen Betons : Berichte ; Forschungsprojekt der EU (Brite Euram BE96-3843), IPACS. 2001.
ISBN 3-89288-136-7

Heft 156:
Rostásy, F.S. ; Krauß, M. ; Gutsch, A.
Spannungsberechnung und Risskriterien für jungen Beton – Methoden des iBMB : Bericht ; Forschungsprojekt der EU (Brite Euram BE96-3843), IPACS. 2001.
ISBN 3-89288-137-5

Heft 157:
Rostásy, F.S. ; Krauß, M. ; Gutsch, A.
Früher Zwang in massigen Sohlplatten : Bericht ; Forschungsprojekt der EU (Brite Euram BE96-3843), IPACS. 2001.
ISBN 4-89288-138-3

Heft 158:
Braunschweiger Brandschutztage 2001: 9. Fachseminar Brandschutz - Forschung und Praxis ; 1.-2. Oktober 2001 in Braunschweig., Kurzreferate. 2001.
ISBN 3-89288-139-1

Heft 159:
Falkner, H. ; Teutsch, M. [Hrsg.]
Bauen im Wandel der Zeit : 8.-9.11.2001 ; Braunschweiger Bauseminar 2001. 2001.
ISBN 3-89288-140-5.

Heft 160:
Beiträge zum 40. Forschungskolloquium des Deutschen Ausschusses für Stahlbeton : 11.-12.10.2001 in Braunschweig. 2001.
ISBN 3-89288-141-3

Druck und Einband
Druckerei & Buchbinderei Wolfram Schmidt
38114 Braunschweig · Hamburger Str. 267
Telefon: 0531/ 33 75 89 · Fax: 0531/ 34 44 49
E-Mail: Schmidt.Druck.BS@t-online.de